Sapienza University of Rome

Department of Mechanical and Aerospace Engineering
PhD in Theoretical and Applied Mechanics

THESIS FOR THE DEGREE OF DOCTOR OF PHILOSOPHY

Self-propelled fish locomotion in an otherwise quiescent fluid

Advisors
Prof. Giorgio Graziani
Prof. Renzo Piva
Dr. Claudio Lugni

Candidate
Damiano Paniccia
1405708

Academic Year 2022-2023 (XXXV cycle)

Acknowledgements

Abstract

Since the deep observations by Leonardo da Vinci, understanding fish locomotion in water has always attracted the attention of scientists in many fields, from fluid mechanics to other disciplines concerning environmental sciences. The complexity of this problem is mainly given by the non-linear interaction between the fish body and the surrounding fluid otherwise at rest, leading to the desired forward locomotion and to the unavoidable angular and lateral recoil reactions, which are essential for a correct evaluation of the swimming performance. Despite many advances have been obtained for the study of fish self-propulsion in recent years, from simple mathematical models up to complex numerical solutions, the main mechanisms underlying fish locomotion are not fully clarified and still require further investigations.

In this thesis free swimming conditions is deeply analyzed for both steady swimming and fast maneuvers by a theoretical approach which considers the full body-fluid system to obtain the exchanged internal forces. The focus is on the added mass and the vortex shedding contributions to the locomotion performance and on the role of recoil motions which, together with the prescribed body deformation, define the free swimming behavior.

To this purpose, the impulse formulation allows for an easy isolation of the potential contribution, related to the added mass, and of the vortical contribution related to bound and released vorticity and a simple two-dimensional numerical model with concentrated vorticity is adopted for the numerical simulations to generate meaningful results able to clarify these physical phenomena. The aim is a unified procedure for both undulatory and oscillatory swimming to obtain valid answers for cruising speed, expended energy and kinematics, hence for the swimming performance in terms of the cost of transport and propulsive efficiency. The same model is also able to give new insights on the impressive performance characterizing fish fast maneuvers. The extreme turning capability and the large acceleration, so essential to fish survival along pray-predator encounters, are studied by highlighting the potential and the vortical impulses and their interplay induced by recoil motions, to show their relevance for the realization of the maneuver.

Keywords: fish swimming, self propulsion, aquatic locomotion, recoil motions, C-start, undulatory swimming, oscillatory swimming.

Contents

Chapter 1

Outline of the research work

Every living being, whether walking on land or soaring the sky, has its roots within the seas and oceans. The earliest forms of life exploited water to move and interact, and even today thousands of living species spend their lives underwater interacting with the aquatic environment in ways that constantly leave us in awe and wonder. From the smallest organisms to the largest cetaceans, the amazing adaptation of aquatic life is surely a topic of enormous interest, as it opens the door to a world that is still little known and explored. Specifically, understanding aquatic locomotion has always attracted the attention of scientists, since the deep observations that Leonardo da Vinci described in his notes (e.g. Atlanticus Codex folio 571 A recto) more than five centuries ago. At the beginning of the last century, to unveil the secrets behind fish incredible skills, a large number of zoologists, biologists and fluid dynamicists started to systematically investigate fish swimming with the aim to discover and understand the physical mechanisms behind fish capabilities[13, 28, 42, 68, 77]. Given the genuine scientific interest in such an intriguing subject, the aim is to define novel concepts of underwater bioinspired vehicles with high efficiency, long-term endurance and improved maneuverability. This requires a strong multidisciplinary approach combining competencies coming from biology, structural mechanics, fluid dynamics and cybernetics to empower the design of energetically and fluidynamically efficient robots which may provide innovative and sustainable forms of exploration and exploitation of aquatic environments. From a fluid mechanics perspective, fish locomotion represents a particular case of the more general problem of the self-locomotion of a deformable body which sets in motion the fluid about it through its own deformation to obtain the desired advancement motion. The study of this problem is extremely complex and its treatment is generally simplified by some hypothesis depending on the subject. For example, the body is often assumed to be placed under a uniform stream and its unsteady motion, whether it is a rigid motion or a deformation, is imposed to evaluate the loads on the body surface due to the generated flow field. However, in reality, the fish motion is strongly dependent on the surrounding fluid, more precisely, it relies on the fluid pushed by fish movements. This means that further unknowns in a self-propelled problem, in addition to the flow field and to the hydrodynamic forces, are the locomotion, i.e. the advancement motion obtained by the interaction with the surrounding fluid, and the unavoidable lateral and angular recoil motions. The search for the unknown locomotion speed also requires a different perspective than the fixed-swimming approach usually adopted in the literature. For instance, parameters such as the Strouhal number or the reduced frequency can no longer be used as inputs of the problem since their definition contains the unknown locomotion speed. The

selection of new parameters not depending on the problem unknowns is then necessary to allow for a clear results analysis, which adds further complexity to the comparison with the existing literature. Examples are the phase velocity and the tail oscillation amplitude which, identifying in a way the body deformation, are given only in terms of the assigned data.

In recent years, computational fluid dynamics has made great strides and is now able to provide very accurate estimates of the fluid and pressure fields generated by a self-propelled body immersed in a fluid domain. Actually, nowadays it is possible to obtain, although with a huge computational effort, solutions of the complete Navier-Stokes equations, so to be able to estimate the hydrodynamic forces acting on the body and its consequent motion with a sufficient accuracy. However, such accurate models may hide the essence of the self-propulsion problem due to its entangled nature. For instance, a lot of attention is often given to the geometry of the vortical structures released into the wake, already recognized as not reliable indicator of swimming performance[21], or to the resulting pressure field which, due to its integral nature, hides within it the effects of different physical phenomena not easy to be identified.

"In order to go on, you have to know what to leave out: this is the essence of effective thinking." These words, attributed to the logician, mathematician and philosopher Kurt Gödel, in a way reflect the line of reasoning followed in the present PhD research, where the adopted mathematical and numerical model has been selected by laying aside everything which is not essential for the specific aims. Actually, the suggested simple impulse model is build to provide everything necessary for a thorough analysis of the physics behind the self-propulsion of a body by means of the surrounding fluid. The model is constructed by combining the impulse formulation with a simple two-dimensional model so to obtain neat results as firmly suggested by several authors (e.g. Schultz and Webb [63], Akoz et al.[2, 3]) and successively encouraged by the matching between the two-dimensional flow field and the midbody plane flow in three-dimensions (see Wolfgang et al.[73]). A non-diffusive flow solution procedure is also used so to isolate the potential contribution associated with added mass from the circulatory contribution associated with vortex shedding in the wake, and so to finally give insight on the role of the lateral and angular recoil reactions which are always accompanying the advancement motion of the fish and are of major importance for the evaluation of the swimming performance. This model is accurate enough to give reliable measures of swimming speed and energy consumption, and is mainly applied for both the study of undulatory and oscillatory free swimming and the study of typical impulsive fish maneuvers observed during prey-predator interactions.

The present thesis consists of the collection of five already published (paper 1, 2, 3 and 5) or submitted (paper 4) papers resulted from the research activity. The articles are introduced by an opening chapter presenting a general and comprehensive survey of the research by providing a common background for the following papers. The first section presents a complete description of the mathematical and numerical model, while the next three sections present an overview of the results obtained for the three main subjects deepened in the reported papers, namely undulatory swimming, oscillatory swimming and fast maneuvers. For instance, the role of recoil motion in defining the swimming performance is highlighted in the case of undulatory and oscillatory swimming to show its relevance on locomotion speed and on energy consumption once free-swimming gait is considered. The phase velocity, known to drive the locomotion velocity in undulatory swimming, is also modified by recoil motions and is identified in the case of oscillatory swimming by some specific geometrical

characteristics of the tail flapping motion. Moreover, the contemporary observation of the Froude efficiency and the cost of transport allowed for the understanding of their validity for different swimming demands to overcome the conflicting opinions appearing in the literature about the best procedure to evaluate swimming performance.

1.1 A unified simple model

After some early studies[12, 58], fish swimming started to be experimentally investigated by biologists by analyzing fish motion in water tunnels or towed in water tanks to keep them in the most suitable position for easy measurements[13, 28–30, 39]. By following the same idea, the associated theoretical models were developed to predict the thrust force obtained by the fish as a consequence of a prescribed deformation under a prescribed uniform stream. The thrust, often associated exclusively with the fish's caudal fin, was supposed to counterbalance the unavoidable body resistance and to provide the Froude efficiency as the natural way to evaluate the swimming performance[42, 76, 77]. More recently, self-propulsion was recognized as a more appropriate way to investigate the optimal conditions for swimming bodies[14, 19, 36, 70, 78]. In this case, at steady state, the proper unknown of the problem is the locomotion speed achieved by the fish when the total force vanishes for thrust and drag balancing each other. As a consequence, the Froude efficiency looses its meaning and the swimming performance are better measured by the cost of transport, i.e. by the energy consumption per covered distance[7, 25]. However, fish propulsion is characterized by many different styles related to different goals and requirements. As anticipated above, the present PhD research tries to explore these different swimming gaits by means of a suitable impulse model able to neatly highlight, due to its simplicity, the essence of the problem. The model is presented below in a comprehensive and detailed way with the aim to treat all the steps needed to construct the solution methodology while a model description focusing on the most relevant issues for the specific application is presented in each reported paper.

1.1.1 The impulse formulation

The motion of a deformable body within an infinite volume of initially quiescent fluid with constant density is studied by considering a fluid-body domain with no external forces or moments applied. In other words the total linear and angular momenta are conserved for the whole domain, while the forces and moments exchanged between fluid and body appear as internal actions. The equations describing the dynamics of the body centre of mass are obtained directly from the momentum balance expressed through the time derivative of the fluid impulse (linear $\boldsymbol{p}$ and angular $\boldsymbol{\pi}$). This impulse formulation has been extensively discussed by several authors[32, 45, 46, 51, 60, 75] and allows for the separation of potential and vortical impulses so to highlight the contributions due to both added mass and release of vorticity, respectively. Moreover, the impulse formulation does not show the conditional convergence properties that the momentum has in an infinite domain[15, 38] and even more it is linear with respect to the vorticity. By using classic vector identities, the linear and angular impulses are expressed by means of two terms concerning the vorticity concentrated on the contour of the body and shed within the field.

As anticipated above, we consider an impermeable and flexible body with bounding surface $\partial\mathcal{B}$ in an infinite dimensional volume $\mathcal{V}$ with zero velocity at infinity and we assume a Newtonian,

incompressible fluid with density ρ. The outer surface is stationary in an absolute reference frame and the fluid velocity is assumed to vanish on the far field boundary. In an isolated fluid-body system ($\mathcal{V} + \mathcal{B}$), the sum of the forces (and moments) acting on the body and on the fluid is zero, as given by

$$\frac{d}{dt}\left[\int_{\mathcal{B}} \rho_b \boldsymbol{u}_b \, dV + \int_{\mathcal{V}} \rho \boldsymbol{u} \, dV\right] = 0 \tag{1.1}$$

where ρ_b and $\boldsymbol{u}_b$ are respectively the density and the velocity of the body and $\boldsymbol{u}$ is the flow velocity in fluid field.

The conservation of the total impulse[19, 35, 61] allows to avoid the calculation of the time derivative, necessary when evaluating the forces, and the subsequent time integration for the body motion. In this way, a more accurate and simpler numerical computation is obtained. So, we remove the time derivative in eq.(1.1) and, by assuming null initial condition, the momentum balance gives

$$\int_{\mathcal{B}} \rho_b \boldsymbol{u}_b \, dV + \rho \boldsymbol{p} = 0 \tag{1.2}$$

By using a vectory identity for the unbounded fluid volume[52, 75], the fluid impulse $\boldsymbol{p}$ is expressed as

$$\boldsymbol{p} = \frac{1}{N-1}\left[\int_{\mathcal{V}} \boldsymbol{x} \times \boldsymbol{\omega} \, dV + \int_{\partial\mathcal{B}} \boldsymbol{x} \times (\boldsymbol{n} \times \boldsymbol{u}) \, dS\right] \tag{1.3}$$

where N is the dimension (here $N = 2$ will be assumed), $\boldsymbol{x}$ is the position vector in the inertial frame and $\boldsymbol{\omega}$ is the field vorticity. In the second term in eq.(1.3), $\boldsymbol{u}$ stays for the limiting value of the fluid velocity on $\partial\mathcal{B}$ and the integral over the external boundary receding to infinity has been proven to exactly vanish[52, 74]. The normal $\boldsymbol{n}$ points out of the flow domain and all the vorticity is enclosed within the fluid volume $\mathcal{V}$ which extends to infinity. The right-hand side of eq.(1.3) is independent of the choice of the reference frame origin[32, 52, 75].

A similar approach for the angular momentum (positive anticlockwise) balance yields

$$\int_{\mathcal{B}} \rho_b \boldsymbol{x} \times \boldsymbol{u}_b \, dV + \rho \boldsymbol{\pi} = 0 \tag{1.4}$$

where the angular impulse $\boldsymbol{\pi}$ is

$$\boldsymbol{\pi} = \frac{1}{2}\left[\int_{\mathcal{V}} |\boldsymbol{x}|^2 \times \boldsymbol{\omega} \, dV + \int_{\partial\mathcal{B}} |\boldsymbol{x}|^2 (\boldsymbol{n} \times \boldsymbol{u}) \, dS\right] \tag{1.5}$$

The velocity field $\boldsymbol{u}$ can be expressed, through the Helmholtz decomposition, as the sum of both the acyclic component and that related to circulation and vortices:

$$\boldsymbol{u} = \boldsymbol{\nabla}\phi + \boldsymbol{\nabla} \times \boldsymbol{\psi} = \boldsymbol{\nabla}\phi + \boldsymbol{u}_w \tag{1.6}$$

where ϕ and ψ are referred to as scalar and vector potential, respectively, and are given by the solution of the Laplace/Poisson equation, subject to the impermeability boundary condition on $\partial\mathcal{B}$ and to the related velocity vanishing at infinity.

The velocity decomposition (1.6) can be used to recast the total impulse (1.3) as the sum of the

potential and of the vortical ones: $\boldsymbol{p} = \boldsymbol{p}_\phi + \boldsymbol{p}_v$. The potential impulse is given by

$$\boldsymbol{p}_\phi = -\int_{\partial \mathcal{B}} \phi \boldsymbol{n} \, dS \tag{1.7}$$

where a vector identity for a scalar quantity has been used and the unit normal $\boldsymbol{n}$ to the body surface is now pointing into the fluid. The vortical impulse $\boldsymbol{p}_v$ is given by:

$$\boldsymbol{p}_v = \int_{\mathcal{V}} \boldsymbol{x} \times \boldsymbol{\omega} \, dV + \int_{\partial \mathcal{B}} \boldsymbol{x} \times (\boldsymbol{n} \times \boldsymbol{u}_w) \, dS \tag{1.8}$$

The expression for the angular momentum can be similarly obtained by separating the vortical and the potential contributions using another vector identity[75] and the generalized Stokes' theorem. By considering eq.(1.5), we can define the angular potential impulse as

$$\boldsymbol{\pi}_\phi = -\int_{\partial \mathcal{B}} \boldsymbol{x} \times \phi \boldsymbol{n} \, dS \tag{1.9}$$

$$\boldsymbol{\pi}_v = -\frac{1}{2} \int_{\mathcal{V}} |\boldsymbol{x}|^2 \boldsymbol{\omega} \, dV - \frac{1}{2} \int_{\partial \mathcal{B}} |\boldsymbol{x}|^2 (\boldsymbol{n} \times \boldsymbol{u}_w) \, dS \tag{1.10}$$

1.1.2 Locomotion procedure

Let's now consider the two-dimensional motion of the deformable body $\mathcal{B}$ within a Cartesian inertial frame $(\boldsymbol{e}_1, \boldsymbol{e}_2, \boldsymbol{e}_3)$. The body motion occurs in the plane $(\boldsymbol{e}_1, \boldsymbol{e}_2)$ and an angular velocity $\boldsymbol{\Omega}$ about the axis $\boldsymbol{e}_3$ may be present as well. The total motion of the body $\boldsymbol{u}_b$ can be expressed as the sum of the prescribed shape deformation with velocity $\boldsymbol{u}_{sh}$ plus the centre of mass (CM) linear velocity $\boldsymbol{u}_{cm}$ which, combined with the angular velocity Ω, gives the total locomotion velocity $\boldsymbol{u}_{loc}$. Thus we can split the body motion as:

$$\boldsymbol{u}_b = \boldsymbol{u}_{sh} + \boldsymbol{u}_{cm} + \boldsymbol{\Omega} \times (\boldsymbol{x} - \boldsymbol{x}_{cm}) = \boldsymbol{u}_{sh} + \boldsymbol{u}_{loc} \tag{1.11}$$

where $\boldsymbol{x}_{cm}$ is the position of the body center of mass. As a mandatory requirement for eq.(1.11) to be valid, since no rigid motions are allowed for an isolated body, the body deformation velocity has to satisfy the following two conditions

$$\int_{\mathcal{B}} \rho_b \boldsymbol{u}_{sh} \, dV = 0 \qquad \int_{\mathcal{B}} \rho_b \boldsymbol{x}' \times \boldsymbol{u}_{sh} \, dV = 0 \tag{1.12}$$

so as the net linear and angular momenta of the imposed kinematics are equal to zero.

Finally, by combining eq.(1.11) with eq.(1.2) and eq.(1.4), we obtain:

$$m_b \boldsymbol{u}_{cm} + \rho \boldsymbol{p} = 0 \tag{1.13}$$

$$J\Omega - \rho \pi' = 0 \tag{1.14}$$

where m_b and J are the body mass and the moment of inertia of the body respectively and the angular impulse is recast in terms of the distance with respect to the center of mass as $\pi' =$

$(\boldsymbol{\pi} - \boldsymbol{x}_{cm} \times \boldsymbol{p}) \cdot \boldsymbol{e}_3$.

Let us now express the locomotion equations eq.(1.13) and eq.(1.14) in a coordinate frame attached to the body $\boldsymbol{b}_1, \boldsymbol{b}_2, \boldsymbol{b}_3$ with origin in CM and with $\boldsymbol{b}_3$ parallel to $\boldsymbol{e}_3$. The angular and the linear velocity of the center of mass are rewritten in the new body frame as $\boldsymbol{\Omega} = \Omega \boldsymbol{b}_3$ and $\boldsymbol{V}_{cm} = V_1 \boldsymbol{b}_1 + V_2 \boldsymbol{b}_2$ respectively, while the angular and linear fluid impulses are $\boldsymbol{\Pi} = \Pi \boldsymbol{b}_3$ and $\boldsymbol{P} = P_1 \boldsymbol{b}_1 + P_2 \boldsymbol{b}_2$, leading to

$$m_b \boldsymbol{V}_{cm} + \rho \boldsymbol{P} = 0 \qquad (1.15)$$

$$J\Omega - \rho\Pi = 0 \qquad (1.16)$$

The velocity field is represented through the previously introduced Helmholtz decomposition and the acyclic term is also split into the contribution given by shape deformation and locomotion

$$\boldsymbol{u} = \boldsymbol{\nabla}\phi_{sh} + \boldsymbol{\nabla}\phi_{loc} + \boldsymbol{\nabla} \times \boldsymbol{\psi} = \boldsymbol{u}_{sh} + \boldsymbol{u}_{loc} + \boldsymbol{u}_w \qquad (1.17)$$

The locomotion potential is expressed through the three Kirchhoff base potentials $(\phi_1, \phi_2, \phi_\Omega)$ related to unit linear motions in $\boldsymbol{b}_1$ and $\boldsymbol{b}_2$ directions as well as to unit angular rotation about $\boldsymbol{b}_3$, respectively. It follows that the total acyclic potential is

$$\phi = \phi_{sh} + \phi_{loc} = \phi_{sh} + V_1\phi_1 + V_2\phi_2 + \Omega\phi_\Omega \qquad (1.18)$$

Each scalar potential is harmonic with the prescribed decay at infinity while the boundary conditions on $\partial\mathcal{B}$ accounts for the impermeability condition:

$$\frac{\partial\phi}{\partial n} = [\boldsymbol{u}_{sh} + V_1\boldsymbol{b}_1 + V_2\boldsymbol{b}_2 + \Omega(\boldsymbol{b}_3 \times \boldsymbol{X})] \cdot \boldsymbol{N} \qquad on \partial\mathcal{B} \qquad (1.19)$$

where $\boldsymbol{X}$ and $\boldsymbol{N}$ stay for the position vector and the body surface normal direction in the body fixed frame. The vector potential $\boldsymbol{\psi}$ satisfies $\boldsymbol{\nabla}^2\boldsymbol{\psi} = -\boldsymbol{\omega}$ together with the boundary condition $(\boldsymbol{\nabla} \times \boldsymbol{\psi}) \cdot \boldsymbol{n} = 0$ on $\partial\mathcal{B}$ and $\boldsymbol{\nabla} \times \boldsymbol{\psi} = 0$ at infinity.

By combining eq.(1.15) and eq.(1.16) and using the velocity decomposition, we obtain

$$\int_{\partial\mathcal{B}} \phi\boldsymbol{N}\,dS - \frac{m_b}{\rho}\boldsymbol{V}_b = \boldsymbol{P}_{sh} + \boldsymbol{P}_v \qquad (1.20)$$

$$\frac{J}{\rho}\Omega - \int_{\partial\mathcal{B}} (\boldsymbol{X} \times \phi\boldsymbol{N}) \cdot \boldsymbol{b}_3\,dS = \Pi_{sh} + \Pi_v \qquad (1.21)$$

Finally, let us now express the locomotion impulses in terms of the added mass coefficients reported in the classical literature[9, 37, 50] by combining eq.(1.20) and eq.(1.21) with the decomposition of ϕ_{loc} appearing in eq.(1.18). Upon inserting the relevant added mass coefficients m_{ij} in the equations, we obtain the final form of the system as

$$\begin{cases} V_1\,(m_{11} - m_b) + V_2\,m_{12} + \Omega\,m_{13} = P_{sh1} + P_{v1} \\ V_1\,m_{21} + V_2\,(m_{22} - m_b) + \Omega\,m_{23} = P_{sh2} + P_{v2} \\ V_1\,m_{31} + V_2\,m_{32} + \Omega\,(m_{33} - J) = \Pi_{sh} + \Pi_v \end{cases} \qquad (1.22)$$

We may appreciate that the added mass terms which multiply the unknowns now appear directly in the l.h.s with a major advantage in terms of stability of the integration procedure. Let us notice that the above system of equations provides the evaluation of the body velocities without considering time derivatives as required when using the standard formulation in terms of forces and moments.

1.1.3 Flow solution procedure

The numerical solution of the above system is obtained by considering a potential flow with concentrated vorticity on the body surface and its subsequent shedding behind the body into the vortex wake. The flow solution at each time step is obtained by using an unsteady potential panel code which is based on the Hess and Smith[33] approach while the unsteadiness of the problem, i.e. the wake release, is taken into account following the Basu and Hancock procedure[8]. Specifically, the swimming fish at rest is represented by a shape corresponding to a NACA airfoil with a chord length c equal to 1 and a surface perimeter l. The deformable body surface is approximated by a finite number of straight-lines called panels, each with a local, uniform, distributed source strength σ and all with a global (i.e. equal for each panel), uniform, distributed vortex strength γ. The n panels are identified by $n + 1$ points called nodes and by their mid-points called collocation point so to give a total of $n + 1$ unknowns. It follows that $n + 1$ equations are required to find the source and vortex strengths on the body surface. Specifically, the impermeability condition is imposed on each panel to give first n equations, while last one is given by an unsteady Kutta condition which ensures that the pressure on the upper and lower surface at the trailing edge is equal. However, given the unsteadiness of the problem under analysis, these $n + 1$ unknowns are obviously time dependent so that it is reasonable to introduce a subscript k which will indicate the time-step of reference.

For instance at each time-step $t_k (k = 1, 2..., \infty)$ the singularities on the airfoil, i.e. the sources and the uniform circulation density, will be indicated as:

- $(\sigma_j)_k \quad (j = 1, 2..., n)$

- γ_k

According to the well known Kelvin theorem, if the total circulation in the flow field is equal to zero at the starting time, it will stay equal to zero, hence any changes in the circulation on the body must be followed by equal and opposite changes in the circulation in the wake. Consequently, the vortex shedding process and the wake formation are modelled by assuming that a vortex is shed into the wake at each time-step, taking place as straight line wake element which is essentially an additional panel attached to the body trailing edge with a uniform vortex distribution $(\gamma_w)_k$ on it. This panel will be indicated as shed panel and is numerated as $n + 1$ and is defined by the introduction of two additional unknowns, i.e. its length $(\Delta_w)_k$ and its inclination $(\theta_w)_k$ with respect to the axial direction in the body fixed frame. The strength of the vortex distribution on the shed panel can be obtained as a simple application of Kelvin Theorem:

$$\Gamma_k - \Gamma_{k-1} = (\Delta_w)_k (\gamma_w)_k \tag{1.23}$$

where the left-hand side is the change in the total circulation on the airfoil between the actual time-step t_k and the previous time-step t_{k-1} and Γ_k is obtained as the product between γ_k and the airfoil perimeter l.

The introduction of the above mentioned two unknowns associated to the wake panel requires two additional conditions to be specified:

1. the shed panel is oriented as the velocity at the panel's collocation point

2. the length of the shed panel is equal to the velocity at the panel's collocation point multiplied by the time-step size $dt = t_k - t_{k-1}$

Finally, at the end of each time step, the vortex distribution on the shed panel is lumped in a point vortex, indicated as core vortex, and is advected downstream with the flow for every $t > t_k$.

It's worth to be noticed that the shed panel and the resultant wake core vortices are definitely going to influence the upstream flow and the singularities on the body surface $(\sigma_j)_k$ and γ_k which, in turn, are also going to influence the shed panel distribution $(\gamma_w)_k$ and the motion of the vortices in the wake. It follows that this vortex shedding procedure is clearly non-linear and thus an iterative solution scheme must be used which is here summurized:

1. the shed panel vortex distribution at the previous time-step $k-1$ is concentrated in a lumped-vortex and moved according to the velocity calculated at the point-vortex itself (always at the time-step $k-1$)

2. all the other shed core vortices generated before are moved with the flow velocity at their location

3. the body is moved according to the computed rigid motion velocity and deformed according to the shape deformation velocity, both at the previous time-step $k-1$

4. a new shed panel is generated at the actual time-step t_k and first-attempt values are chosen for $(\Delta_w)_k$ and $(\theta_w)_k$ based on the flow velocity on the shed panel in the previous time-step

5. all the singularity distributions on the body surface are evaluated by applying the impermeability condition and the Kutta condition

6. the velocity at the shed panel collocation point is calculated and it is used to update the values of $(\Delta_w)_k$ and $(\theta_w)_k$

7. point 5 and 6 are repeated until the updated values of $(\Delta_w)_k$ and $(\theta_w)_k$ are essentially the same as the previous iteration

In principle, the method just described is plenty sufficient to find the solution of the flow in the case of a deformable body undergoing a fully prescribed rigid motion. In the present case of self-propulsion, however, the body rigid motion is an additional unknown and is going to be determined at each time-step as described in the previous paragraph. In fact, in this case, a double iterative cycle is required to simultaneously determine both the flow solution with the relative singularities distributions and the self-propulsion velocity, either linear and angular. To this purpose, the following steps are added to the solution procedure:

8 the locomotion problem is solved to find the three components of the unknown rigid body velocity $(V_1)_k$, $(V_2)_k$ and $(\Omega)_k$

9 point 4, 5, 6, 7 and 8 are repeated until the values of the $(V_1)_k$, $(V_2)_k$ and $(\Omega)_k$ are essentially the same as the previous iteration

1.2   Undulatory swimming

To obtain the desired locomotion by keeping as low as possible the energy consumption, many fishes undulate a large part of their body, if not the whole body, by generating a travelling wave along their body or fins to push fluid backwards. Examples of undulatory swimmers include eels, lampreys, mackerels and some rays. As brightly explained by Gray[31] and successively assumed by many others, the main feature of undulatory propulsion is the phase velocity of the traveling wave which has to be slightly larger than the forward fish locomotion velocity but sufficiently close to ensure good swimming performance. The most famous analytical model introduced by Lighthill and Wu[42, 77], based on the elongated body theory under a prescribed stream, finds direct expressions for thrust and expended energy which influenced all the subsequent research on the subject. However, the wave-like deformation travelling from head to tail is involving a significant part or the whole body consistently with the fish's shape and swimming style (e.g. anguilliform, carangiform, etc.) so to prevent a clear identification of the propulsive forces[7, 28, 48]. To overcome this issue, a self-propulsion approach started to take place in the following years[11, 14, 36, 78] to obtain the locomotion velocity by leaving the fish completely free to swim according to the forces exchanged with the surrounding fluid. In this condition, the motion of the deformable body in an unbounded fluid domain is characterized by the absence of external forces hence the total momentum is conserved for the fluid-body system. As a consequence, the forces exchanged by the deformable body with the surrounding fluid are necessarily internal forces, which are strongly entangled due to the coupling between the forward motion and the recoil motions, i.e. the lateral and angular ones as clearly shown by the system (1.22). Once a certain given deformation is applied, after an initial transient, the steady state self-propulsion condition is obtained when thrust and drag are exactly balanced. It follows that the Froude efficiency, so important when studying an isolated propulsor, loses its meaning at steady swimming when the mean total force experienced by the body is equal to zero and a proper measure of the performance like the cost of transport, i.e. the inverse of the well-known miles per gallon introduced by von Kármán and Gabrielli[25], becomes a mandatory choice[6, 64]. As explained in
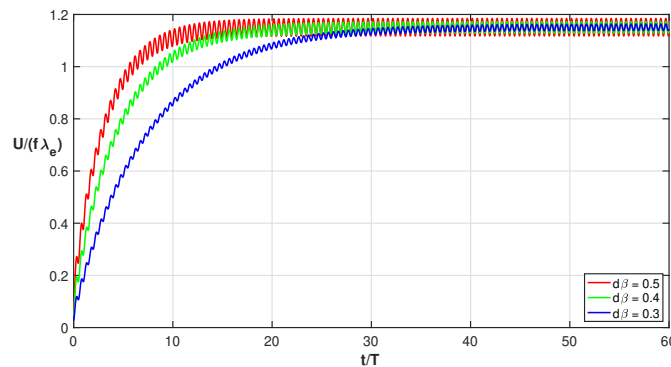
Figure 1.1: Time history of the forward velocity component divided by the equivalent phase velocity $f\lambda_e$ for different deformation amplitudes $\delta\beta$.

the mathematical model and in the related solution procedure, the numerical results are obtained for two-dimensional flow with non-diffusing vorticity. In these conditions, based on momentum conservation, the steady-state swimming speed is fully dictated by the velocity of the fluid pushed backward by the body, i.e. by the phase velocity given by the product between the undulation

frequency and its wavelength. The numerical results reported in fig.1.1 confirm this theoretical prediction to show how the swimming speed is substantially driven by a proper phase velocity accounting for the whole motion of the body in free-swimming condition. Actually, by dividing the forward velocity component by the phase velocity associated to the complete body kinematics ($f\lambda_e$, where f is the frequency and λ_e is the wavelength), the asymptotic locomotion velocity is essentially constant for different deformation amplitudes $\delta\beta$. The constant value of the asymptotic velocity is


(a)

(b)
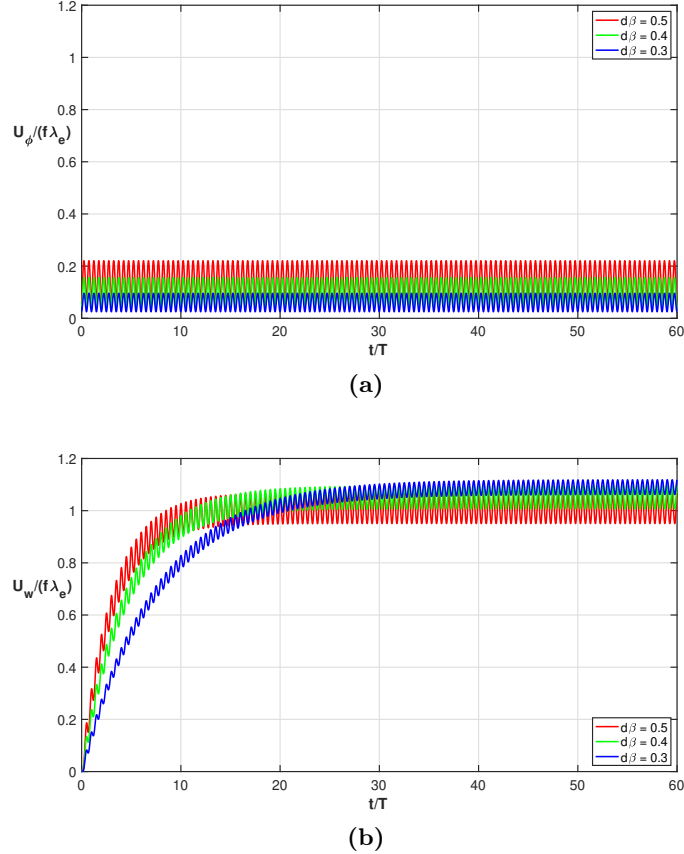
Figure 1.2: Potential contributions 1.2a and vorticity contributions 1.2b of the forward velocity component divided by the equivalent phase velocity $f\lambda_e$ for different deformation amplitudes $\delta\beta$.

given by the sum of potential and vortical contributions of different amount which may be isolated and analyzed through the present model. In particular, they are reported in fig.1.2a and fig.1.2b, respectively. For growing amplitude, the potential contribution $U_\phi/(f\lambda_e)$ increases and the vortical contribution $U_w/(f\lambda_e)$ decreases while their sum remains constant, as reported in fig.1.1, to show how the pure potential contribution associated with the added mass and the vortical contribution associated with vortex shedding are going to combine to obtain the phase velocity relative to body kinematics. It is also worth to notice that the potential contribution reaches instantaneously a steady state value while the vortical one grows in time with a certain delay suggesting that added mass is going to play a crucial role in fast maneuvers such as the C-start that will be analyzed later.

Once a steady state swimming condition has been obtained, a change in the undulation frequency is always going to consistently modify the phase velocity driving the asymptotic swimming speed and the body may experience either a thrust or drag depending on the specific condition. For instance, an abrupt increase in the undulation frequency is always followed by an acceleration phase since
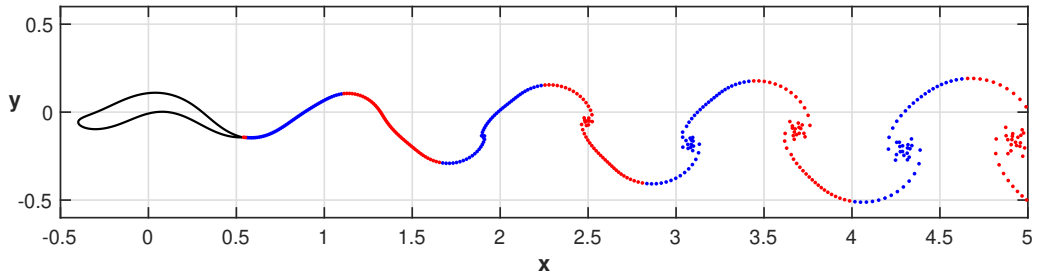
(a)
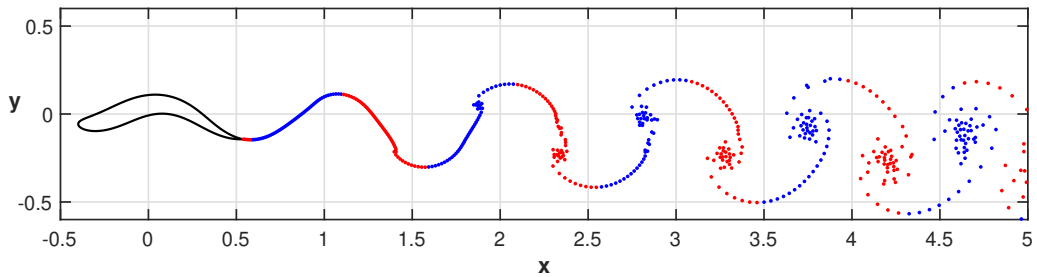
(b)

Figure 1.3: 1.3a Deceleration phase *direct Kármán street* wake pattern. 1.3b Acceleration phase *reverse Kármán street* wake pattern.

the body will suddenly be at a swimming speed lower than the new phase velocity. On the other hand a drag force, hence a deceleration, is always experienced by the body as the phase velocity decreases, according to an eventual drop in the undulation frequency. These two conditions are represented from a qualitative point of view in fig.1.3a and fig.1.3b by the wake patterns which are usually identifying the drag or thrust force experienced by the swimmer, respectively. Specifically, the renown *Kármán vortex street* in fig.1.3a, where the clockwise vortex eddies are positioned above the counterclockwise ones giving a velocity defect in the wake, is usually associated to a drag[71], while the *reverse Kármán street* in fig.1.3b characterized by the opposite vortices arrangement is usually associated to a thrust.

More details are given in paper 1[53] together with the theoretical support for the selection of the proper phase velocity accounting for the whole motion including the recoil components.

1.2.1 The role of recoil motions and the effects of constraints

A great deal of the studies about swimming fish do not take care of lateral and angular fish kinematics and the body is usually constrained or tethered along the horizontal direction. These procedures, both very convenient for experimental and numerical investigations, are unable to account for the actual motion of the fishlike body in free-swimming mode and for its presumed impact on the overall

performance. Actually, in the early 1960s, Lighthill was the first one to emphasize the importance of the lateral and angular recoil motions induced by the fluid–body interactions by identifying them as a required correction to satisfy the equilibrium equations in the framework of his elongated body theory. Subsequently, some authors followed the same fixed-swimming approach and tried to determine, by several numerical investigations, the effects of the recoil motion on the overall performance[40, 49, 54, 59, 65]. However, the free-swimming approach adopted here is the proper way to give a clear insight on the role of recoil motions. To this purpose, it is convenient to consider
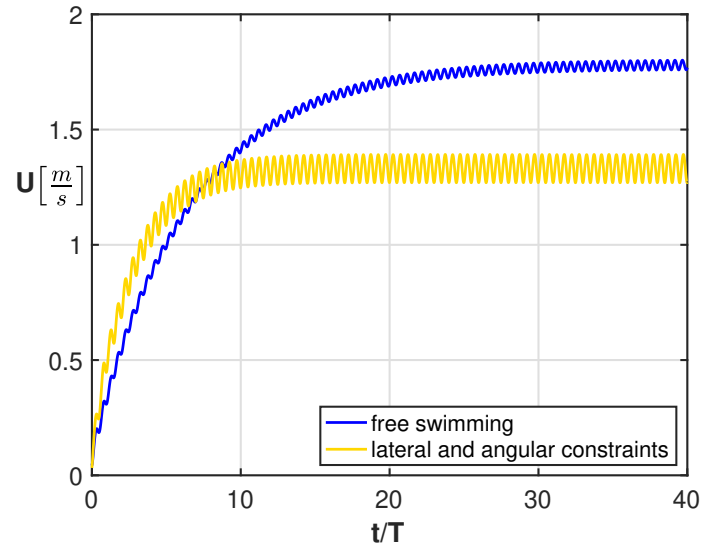
(a)
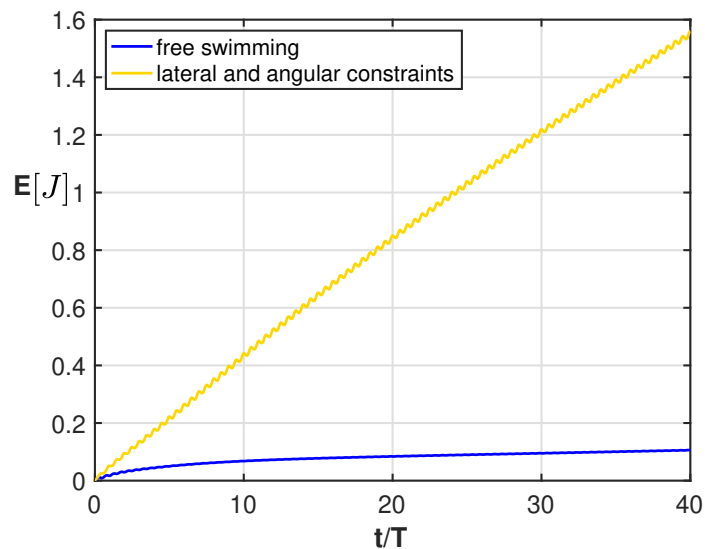
(b)

Figure 1.4: Time history of 1.4a the forward velocity and 1.4b the kinetic energy for free swimming (blue) and lateral and angular constrained swimming (yellow).

the comparison between a free-swimming fish and a fish whose lateral and angular recoil motions are prevented. This constrained swimming gait implies that the center of mass of the fish is able to move exclusively along the forward direction as it occurs in many experimental or numerical

investigations. From the results reported in fig.1.4a it is possible to appreciate that the locomotion velocity obtained by the constrained fish (yellow curve) is smaller than the one obtained by the free-swimming fish (blue curve). In addition, the constrained gait is also unfavorable in terms of expended energy which is essentially given by the released vorticity, as shown by its expression in terms of the excess energy

$$E = \frac{1}{2} \int_{\mathcal{V}} \boldsymbol{\psi} \cdot \boldsymbol{\omega} \, dV \tag{1.24}$$

which is reported in fig.1.4b where the curves slope, i.e. the energy rate of change, is representative of the injected power. To have an intuitive idea of the differences between these two different swimming gaits, it is convenient to have a look to the animation given in paper 2[54] and accessible online at https://doi.org/10.1016/j.jfluidstructs.2021.103290. At a first glance, the animation clearly show that the kinematics of the free-swimming fish (blue) is much more graceful than the one of the constrained fish (yellow) which is not able to follow the surrounding fluid flow. The natural consequence is a much more intense vortex shedding into the wake, indicative of the higher energy consumption. For the sake of convenience, only one frame of the animation is reported here in fig.1.5. The paper also focuses on the interesting analysis of partial constraints which involve either
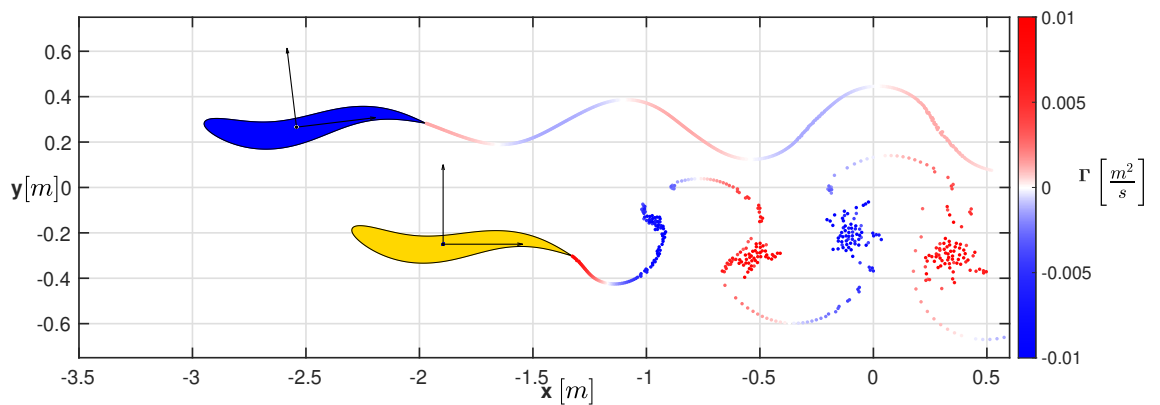
Figure 1.5: Comparison at steady-state of the fully constrained (yellow) and the free swimming case (blue). The full animation is accessible online at https://doi.org/10.1016/j.jfluidstructs.2021.103290.

the lateral or the angular motion to show that the angular recoil motion is much more critical for the swimming performance with respect to the lateral one, both in terms of expended energy and locomotion speed. However, as observed in nature, an intentional reduction of recoil motions might be desirable under certain conditions. For example, the sailfish, is well known to exploit its dorsal fin (sail) raising to optimize the performance during hunting by a substantial reduction in lateral oscillations and rotations[18]. Thus, in this case, the recoil motions reduction is obtained by the fish for a specific task by the use of its dorsal fin, whose raising causes an increase in the lateral and angular coefficients of added mass. Actually, as shown by further results in paper 2[54], a proper modification of these coefficients causes exactly the expected behaviour leading to a reduction in angular and lateral oscillations, followed by higher energy consumption and lower swimming speed.

1.3 Oscillatory swimming

Unlike undulatory swimming where the whole fish body is involved in the generation of the propulsive force, several fish species propel mainly by oscillating their tail, while the remaining part of the body essentially contributes to the overall drag. Examples are tunas, dolphins and cetaceans which use their caudal fin to generate the thrust which is going to counterbalance the viscous drag of the anterior body. In these cases since it is possible, as a first approximation, to separate drag and thrust, most of the attention was focused in the past on the flapping tail represented by an airfoil undergoing a combined heave and pitch motion. By considering the airfoil as immersed in a free uniform stream, the aim was to evaluate the thrust and the Froude efficiency to measure the performance of the propulsion system, as repeatedly provided in many contributions either analytical[22, 26], numerical[34, 79] or experimental[4, 23]. However, since swimming speed is the result of the balance between tail thrust and body resistance, it may be interesting to study oscillatory swimming by recovering the self-propelled approach usually adopted for undulatory swimming. The mathematical model presented in the previous section is here modified to allow for the investigation of the axial self-propulsion of a flapping foil pushing a fishlike body which is approximated by defining only its mass and its resistance coefficient, i.e. a virtual body as proposed by Akoz et al.[3]. These assumptions, due to the known resistance and to the axial motion of the virtual body, allow for the evaluation of both the cost of transport and the Froude efficiency providing an easy comparison between the optimal conditions for the two performance measures.

1.3.1 The virtual body model

The application of the virtual body concept introduced by Akoz et al.[2] requires some adjustments to the mathematical model and to the locomotion procedure presented in the previous paragraphs. In this case we intend to study the axial motion of a swimming body $\mathcal{B}$ which is moving with a velocity $\mathbf{u}_b$ within an unbounded fluid domain $\mathcal{V}_\infty$ by maintaining the assumptions of an unbounded $2D$ incompressible flow field with constant density ρ, whose velocity vanishes at the far field boundary.

From the combination of eq.(1.1) and eq.(1.3), without eliminating the time derivatives, we obtain:

$$\frac{d}{dt}\int_{\mathcal{B}}\rho_b\,\mathbf{u}_b\,dV + \frac{d\mathbf{p}}{dt} = 0 \tag{1.25}$$

The whole body is divided into an active part $\mathcal{B}_T$ given by the tail and a completely passive one, named virtual body $\mathcal{B}_V$, whose presence is attested only by its mass and its viscous drag in the axial direction. Since we are only interested in the motion along the axial direction, in this case the inertial frame axes and the body frame axes are always parallel and the unknown locomotion speed is expressed as $\mathbf{u}_0 = U\,\mathbf{e}_1$. The total motion of the entire body may be split into

$$\mathbf{u}_b = \begin{cases} \mathbf{u}_0 & \text{if } x \in \mathcal{B}_V \\ \mathbf{u}_0 + \mathbf{u}_T & \text{if } x \in \mathcal{B}_T \end{cases} \tag{1.26}$$

where $\mathbf{u}_T$ is given by the prescribed heave and pitch motion of the tail

$$\mathbf{u}_T = V\,\mathbf{e}_2 + (\mathbf{x} - \mathbf{x}_0) \times \Omega\,\mathbf{e}_3 \qquad \mathbf{x} \in \mathcal{B}_T \tag{1.27}$$

and $\mathbf{x}_0$ is the position of the pivot point and V and Ω are the lateral and angular heave and pitch velocity, respectively. By combining (1.25) and (1.26) we obtain

$$\frac{d}{dt}(m\,\mathbf{u}_0) + \frac{d\mathbf{p}}{dt} = 0 \tag{1.28}$$

where m is the total mass given by the sum between the mass of the virtual body m_b and the mass of the caudal fin m_t. By taking the component of (1.28) along $\mathbf{e}_1$ to solve for the locomotion along
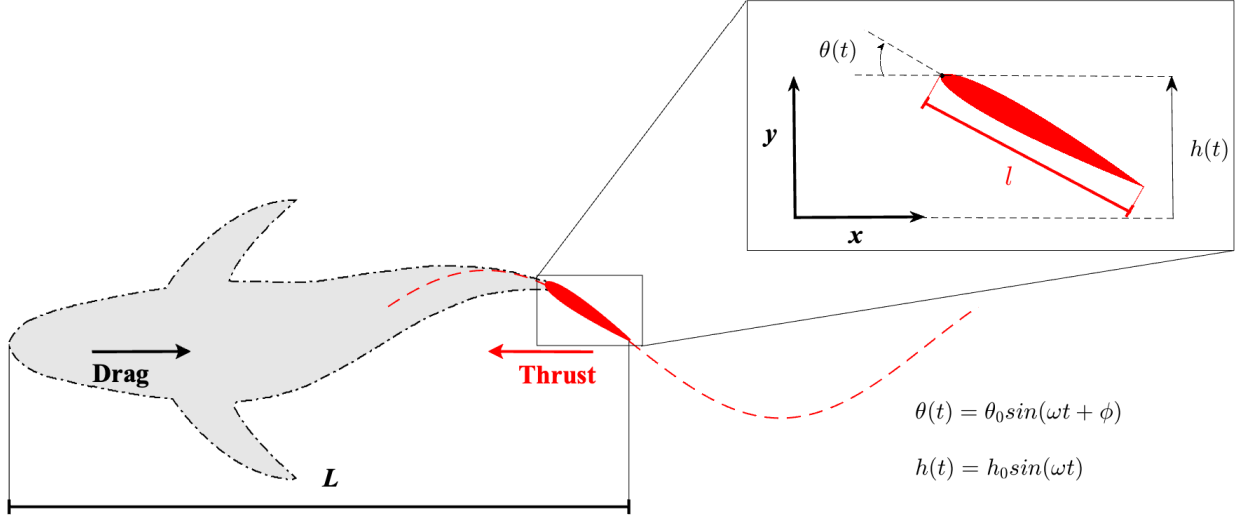
Figure 1.6: A cartoon for the virtual body (gray) and the tail propulsor (red) with a sketch of the exchanged forces. Details of the tail flapping motion are reported in the inset. An animation of the swimming fishlike model and of the related vortex wake is accessible online at https://doi.org/10.1038/s41598-021-01730-4.

the axial direction and by assuming that the surface integrals on the virtual body appearing within the total impulse $\mathbf{p}$ may be represented by its overall resistance D, it follows

$$\frac{d}{dt}(m\,U) + \frac{dp}{dt} + D = 0 \tag{1.29}$$

where the axial component p of the impulse contains only the contribution from the tail. By assuming zero initial conditions, (1.29) gives:

$$m\,U + p = -\int_0^t D\,dt \tag{1.30}$$

Finally, by considering the added mass coefficient in the axial direction m_{1j} evaluated only on the tail surface $\partial\mathcal{B}_\mathcal{T}$, we have

$$U\,(m_{11} - m) = -V\,m_{12} - \Omega\,m_{13} + p_v + \int_0^t D\,dt \tag{1.31}$$

where p_v is the vortical impulse due to the vortex shedding and to the circulation about the tail. The drag term appearing in the r.h.s. of (1.31) is expressed as $D = \frac{1}{2}\rho U^2 L C_D$, where L is the body length and C_D is the prescribed drag coefficient.

A cartoon for the virtual body and its tail propulsor with a sketch representing the exchanged forces and the flapping motion of the tail is reported in fig.1.6. An animation of the swimming fishlike

model and of the related vortex wake can be found in the supplementary material of paper 3[56] which is accessible online at https://doi.org/10.1038/s41598-021-01730-4.

1.3.2 Froude efficiency and cost of transport

The virtual body model described above allows for the evaluation of the self-propulsion velocity and the related cost of transport COT, but not only. In fact, the assigned resistance is now known even though it is perfectly balanced by the thrust given by the flapping tail, hence also the more standard Froude efficiency η may be evaluated and compared with the cost of transport to give very interesting insights almost impossible to achieve with more elaborated tools[2, 41]. To this purpose, to obtain
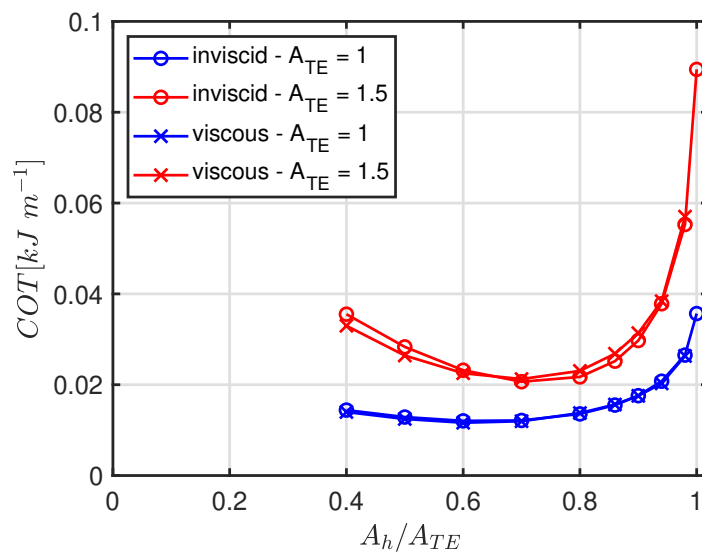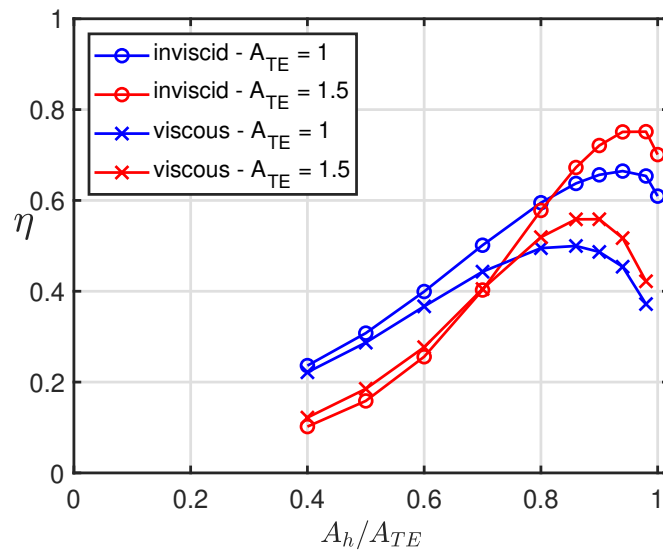
Figure 1.7: 1.7a Cost of transport of the whole body and 1.7b efficiency of the propulsor against A_h/A_{TE} for different peak-to-peak trailing edge oscillation amplitudes ($A_{TE} = 1$ and 1.5). Viscous and inviscid numerical solutions for a prescribed virtual body resistance.

the numerical results, parameters built on the assigned data like the ratio between the peak-to-peak trailing edge amplitude A_{te} and the pure heave non-dimensional peak-to-peak amplitude $A_h = 2h_0$ have been selected instead of the more common Strouhal number S_t and reduced frequency k_r, since the latter are defined by means of the unknown swimming speed. For instance, fig.1.7a shows the whole body performance in terms of cost of transport for the present inviscid model in comparison with a standard viscous solver to show a very satisfactory agreement between viscous and inviscid results. The considered values of the peak-to-peak trailing edge amplitude $A_{te} = 1$ and 1.5, normalized by the tail length l, correspond nearly to $0.15 - 0.2$ in terms of the ratio between the tail-beat amplitude and the total body length L, as frequently observed in nature[5]. The figure show a clear evidence of the classical U-shaped form for the COT curves[62, 81] with the minimum value appearing in a quite small range about the ratio $A_h/A_{TE} = 0.7$. Interestingly, the range where the maximum efficiency of the propulsor η is found, reported in fig.1.7b, is clearly different from the one where the minimum COT for the whole body occurs and corresponds to larger values of A_h/A_{TE}. The presence of the two optimal conditions, easily observable by the self-propulsion approach here adopted, indicates that there are different optimal gaits for different tasks. Specifically, the swimming gait associated to the minimum cost of transport, characterized by low swimming speed and low energy consumption, should be the target swimming condition for cruising tasks. On the other hand, a maximum in the propulsive efficiency is associated to a slightly larger expended energy accompanied by a very larger swimming speed, as request for fast traveling and escape gaits. In paper 3[56] the values of cost of transport and efficiency also illustrated in terms of the output value of the Strouhal number together with other relevant parameters such as the the proportional-feathering and the maximum effective angle of attack introduced by Lighthill[43] and Anderson[4], respectively, to identify optimal swimming performance.

1.3.3   Oscillatory vs Undulatory swimming mode

The results reported in the previous section have been obtained by considering the self-propelled axial motion of a virtual body having a certain resistance propelled by a flapping tail represented by a foil. A further step ahead may be obtained by comparing the flapping motion under consideration with an undulatory motion to look for possible similarities concerning both the existence of a phase velocity and the role of recoil motions.

The caudal fin kinematics is fully prescribed and its flapping motion is given by the combination of a heaving motion of the peduncle $h(t)$ and a pitching motion about the peduncle itself given by $\theta(t)$ defined as

$$h(t) = h_0 \sin(\omega t) \theta(t) = \theta_0 \sin(\omega t + \phi) \tag{1.32}$$

where h_0 is the maximum heave amplitude, θ_0 is the maximum pitch angle and f is the oscillation frequency. The pitch motion $\theta(t)$ has a phase angle $\phi = \pi/2$ hence, by considering sufficiently small values of the maximum pitch angle θ_0, the flapping motion of the tail may be approximated as

$$y(x,t) \approx h_0 \sin(2\pi f t) - \theta_0 x \cos(2\pi f t) \qquad 0 \leq x \leq l \tag{1.33}$$

where the chord of the foil has been confused with the abscissa x and l is the length of the tail. This approximated expression may be assimilated to the one for an undulatory motion of amplitude h_0

with a wavelength $\lambda \gg l$

$$y(x,t) = h_0 \sin(2\pi ft - \frac{2\pi}{\lambda}x) \approx h_0 \sin(2\pi ft) - \frac{2\pi}{\lambda}h_0 x \cos(2\pi ft) \qquad 0 \le x \le l_t \qquad (1.34)$$

and, by equating the coefficients of (1.33) and (1.34), we may evaluate the phase velocity of the flapping motion as

$$c = f\lambda \approx 2\pi f \frac{h_0}{\theta_0} \tag{1.35}$$

In other words, if $\lambda \gg l$, the flapping tail itself may be seen as a small portion of the longer wave whose undulating motion is perceived, instantaneously, as a local oscillation given by the heave and pitch motions. As an evidence for the presence of a well-defined phase velocity for oscillatory
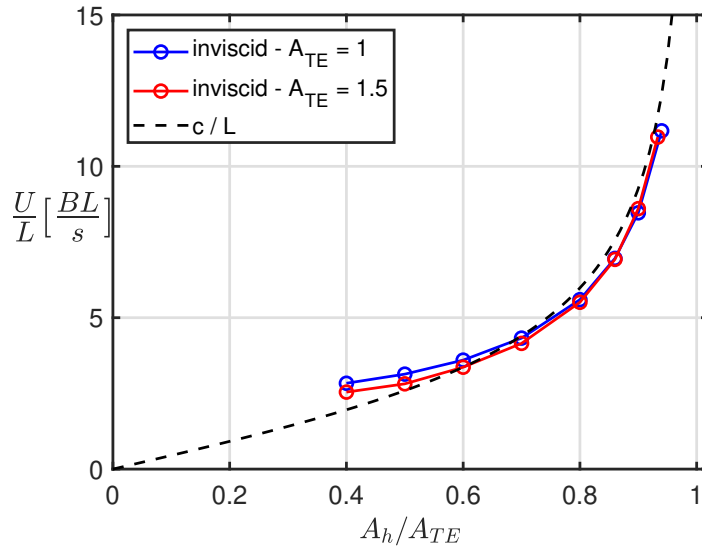
Figure 1.8: Mean steady state swimming velocity U/L and phase velocity c/L (dashed line) against A_h/A_{TE} for different peak-to-peak trailing edge oscillation amplitudes ($A_{TE} = 1$ and 1.5). Inviscid numerical results for zero resistance of the virtual body in axial motion.

motion, fig.1.8 shows the mean forward velocity at steady state in the ideal case of a virtual body with zero resistance for both $A_{te} = 1$ and 1.5. The results show that the asymptotic velocity nearly coincide with the phase velocity c obtained by eq.(1.35) which is independent from the amplitude A_{TE} as obtained for undulatory swimming in the specific case of inviscid flows (see paper 1[53]).

Since the oscillatory motion of the tail can be perceived as a limiting case of undulatory motion, it seems very likely that the several specific approximations commonly used to study this style of swimming are not so essential[16]. For instance, oscillatory swimming, classically investigated in axial motion by considering almost exclusively an isolated flapping caudal fin, should be analyzed by accounting for the free motion of the whole body, as commonly done for undulatory swimming. Actually, the recoil motions may play a crucial role also in the oscillatory case in spite of the common belief that the flapping motion essentially limited to the rear end of the body is associated to rather small recoil reactions with a low impact on the overall performance[44]. By recovering the complete theoretical and numerical models not accounting for the virtual body concept and by considering a limited deformation of the anterior body, though sufficient to allow for a prescribed flapping motion of the tail (see paper 4[57] for more details about the body geometry and deformation), it is possible

to analyze separately the different components of the recoil motions and their influence on the fish dynamics. Specifically, the potential and vortical contributions given by the interaction with the surrounding fluid and the geometrical recoil correction which instead is an a priori request to satisfy the equilibrium of the fishlike body for any given deformation.

To clarify the subtle concept of geometrical recoil it is useful to recall eq.(1.12) which expresses the requirement for the prescribed deformation to have the net linear and angular momenta equal to zero in the absence of the surrounding fluid. Any deformation which does not satisfy eq.(1.12) is not possible if no external forces are considered and should be corrected by the mentioned geometrical recoil correction.

Figure 1.9 reports an extremely simplified sketch of a flapping fishlike body to attack such a subtle
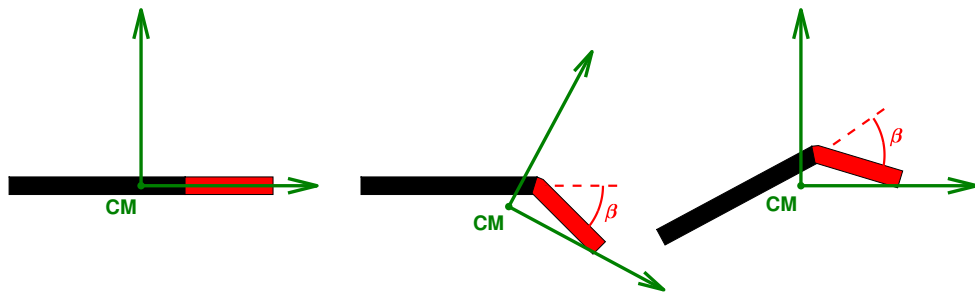

Figure 1.9: Sketch of a flapping fishlike body illustrating the geometrical recoil correction.

issue. The first frame on the left illustrates the sample of a body in its straight and undeformed configuration, while the second one illustrates a deformed one where the body rear-end is flexed by a clockwise angle β, to recall the tail of a fish. If anterior body is fixed, the rotation of the tail is going to induce a downward motion of the body center of mass CM and a clockwise rotation of the inertia principal axes, motions that should not be allowed since no external actions are applied. Finally, the last frame on the right shows the feasible configuration where the tail is still rotated by the angle β with respect to the anterior body, but where the center of mass and the principal axes perfectly match the ones for the undeformed configuration. The motion required to go from the second to the third sketch is the geometrical recoil correction. The identification of the geometrical recoil correction typical of the present model, as indicated by eq.(1.12), lead to a neat isolation of the fluid-induced component of the recoil and of its potential and vortical contributions to allow for an analysis of their effect of the kinematics of the body. Specifically, as illustrated in fig.1.10a, the acyclic potential field $\boldsymbol{u}_\phi$ generated by the caudal fin downstroke leads to a counterclockwise angular velocity Ω_ϕ in the opposite direction with respect to tail motion. It follows that the potential recoil contribution associated to added mass tends to counterbalance and to attenuate the tail oscillation. On the other hand, the vortical field reported in fig.1.10b shows an opposite behaviour since the fluid vortical velocity $\boldsymbol{u}_v$ induced by the vortex cluster just released into the wake is going to enhance the tail motion via the angular recoil velocity Ω_v.

Much more details on how the single recoil contributions are going to influence the tail flapping parameters and the locomotion performance are illustrated in paper 4[57], where a quantitative
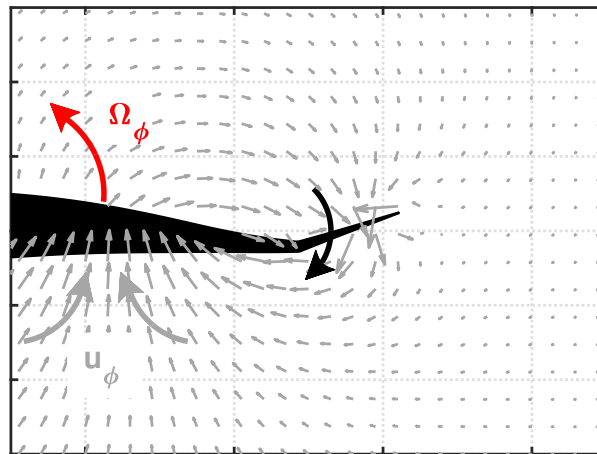
(a)
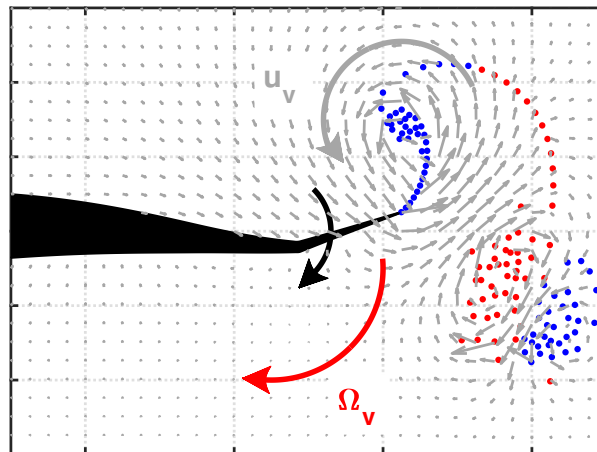
(b)

Figure 1.10: Flow field sketches for (a) the potential fluid recoil and (b) the vortical fluid recoil.

analysis is presented to give helpful suggestions to figure out the free motion of a biomimetic body in water.

1.4   Fast escape maneuvers

Fast maneuvers in fish swimming occur occasionally along with pray-predator encounters. These motions are characterized by very large accelerations and extreme turning capabilities to let fish succeed in escaping or in foraging needs during the everyday battle for survival. Such impressive performance has attracted biologists, physicists and engineers but is far from being completely understood and reproduced even by the more advanced technologies. Starting from the survey paper from Domenici and Blake[17] which provides a large set of experimental data on some of the

most common fast maneuvers kinematics, several subsequent studies[1, 10, 21, 27, 47, 70] pointed out the prominent role of the position and strength of the shed vortices at the end of the maneuver to evaluate the final velocity achieved by the fish. However, a quantitative analysis of the vorticity released into the wake and of the related momentum does not allow for a satisfactory description of the phenomena (see [20, 24, 64, 69]) since the vortex pattern is like the footprint of a terrestrial animal and cannot tell the whole story about the body dynamics[80]. Within this framework, the present impulse model is able to provide a significant improvement in the comprehension of the physics underlying fish fast start, due to the peculiar capability to isolate the potential and the vortical impulses.

One of the most common maneuver, the so called C-start, has been studied by accounting for all recoil motions as a mandatory request for the treatment of such complicated kinematics. For the sake of clarity, a typical example is represented in fig.1.11 where a few snapshots are reported to give a first glance idea of the different phases of the maneuver (complete animations are given in paper 5[55] and are available online at https://doi.org/10.1038/s41598-022-08923-5). The obtained numerical
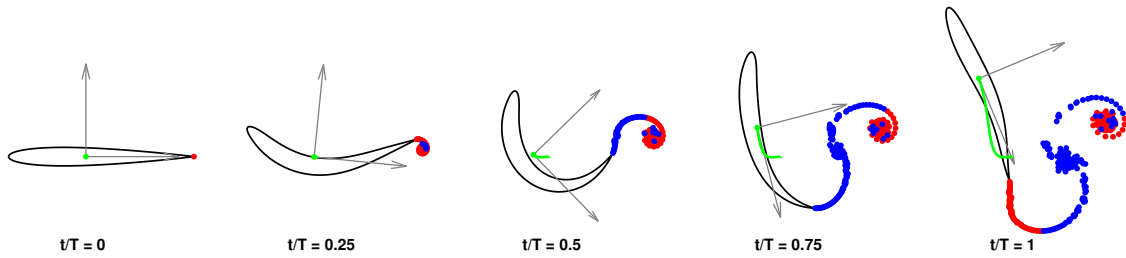

Figure 1.11: Snapshots of the C-start maneuver of a neutrally buoyant fish from the numerical simulation. Complete animations are given in paper 5[55] and are available online at https://doi.org/10.1038/s41598-022-08923-5.

results confirm that the vortical impulse is eventually dominant at the end of the maneuver, but it is not able to explain all the intermediate steps. In fact, the added mass and the related potential impulse have the larger impact on the extreme turning capabilities and accelerations of fish, which are strictly related to aquatic environment. Specifically, the time variation of the added mass coefficients m_{11} and m_{33} are recognized to be extremely important for the maneuver performance as already suggested by some authors in different context[66, 67, 72], but also the prevailing action of the mutual momentum transfer between the angular and forward directions is assessed as the main source of forward momentum. To give a quick anticipation of the results given in paper 5[55], the momentum conservation along the forward direction, i.e. the first equation of the complete system (1.22), is reported below

$$V_1(m_{11} - m_b) + V_2 m_{12} + \Omega m_{13} = P_{sh_1} + Pv_1 \tag{1.36}$$

where, for the sake of clarity, V_1 and V_2 are the linear velocity in the forward and lateral direction respectively, Ω is the angular velocity, P_{sh_1} is the pure potential momentum associated to the
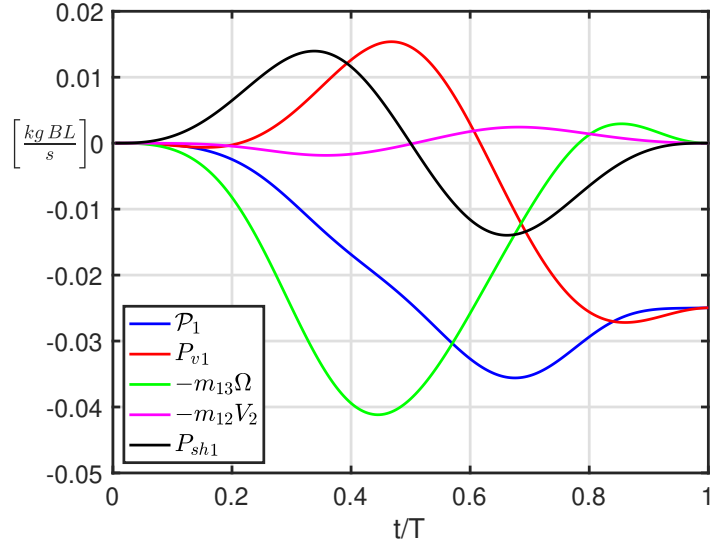
Figure 1.12: Fluid impulses for C-start maneuver: total forward impulse $\mathcal{P}_1$ and its contributions.

prescribed deformation and Pv_1 is the vortical momentum associated to the released vortices. By moving to the right-hand side all the terms which are not directly dependent from the forward velocity V_1, it follows

$$V_1(m_{11} - m_b) = P_{sh_1} + Pv_1 - V_2 m_{12} - \Omega m_{13} \equiv \mathcal{P}_1 \qquad (1.37)$$

where $\mathcal{P}_1$ collects all the terms on the right-hand side. Finally, fig.1.12 reports the time history of each forward momentum contribution for the C-start to show how, even if the total and vortical impulses $\mathcal{P}_1$ and Pv_1 perfectly coincide at the end of the maneuver, their substantial difference along the maneuver is obviously due to the potential terms with an overwhelming predominance of the coupling term $-m_{13}\Omega$ providing the momentum transfer from the angular to the forward direction.

Bibliography

[1] O. Akanyeti, J. Putney, Y. R. Yanagitsuru, G. V. Lauder, W. J. Stewart, and J. C. Liao. Accelerating fishes increase propulsive efficiency by modulating vortex ring geometry. *Proceedings of the National Academy of Sciences*, 114(52):13828–13833, 2017.

[2] E. Akoz, P. Han, G. Liu, H. Dong, and K. W. Moored. Large-amplitude intermittent swimming in viscous and inviscid flows. *AIAA Journal*, 57:1–8, 06 2019.

[3] E. Akoz and K. W. Moored. Unsteady propulsion by an intermittent swimming gait. *J. Fluid Mechanics*, 834:149–172, 2018.

[4] J. Anderson, K. Streitlien, D. Barrett, and M. Triantafyllou. Oscillating foils of high propulsive efficiency. *J. Fluid Mechanics*, 360:41–72, 1998.

[5] R. Bainbridge. The speed of swimming of fish as related to size and to the frequency and amplitude of the tail beat. *J. Experimental Biology*, 35:109–133, 1958.

[6] R. Bale, M. Hao, A. P. S. Bhalla, and N. A. Patankar. Energy efficiency and allometry of movement of swimming and flying animals. *PNAS*, 111, (21):7517–7521, 2014.

[7] R. Bale, M. Hao, A. P. S. Bhalla, N. Patel, and N. A.Patankar. Gray's paradox a fluid mechanical perspective. *Scientific Reports*, 4(1):5904, 2014.

[8] B. C. Basu and G. J. Hancock. The unsteady motion of a two-dimensional aerofoil in incompressible inviscid flow. *J. Fluid Mech.*, 87:159–178, 1978.

[9] G. K. Batchelor. *An Introduction to Fluid Dynamics*. Cambridge Univ. Press, New York, 1991.

[10] I. Borazjani. The functional role of caudal and anal/dorsal fins during the c-start of a bluegill sunfish. *J. Experimental Biology*, 216:1658–1669, 2013.

[11] I. Borazjani and F. Sotiropoulos. On the role of form and kinematics on the hydrodynamics of self-propelled body-caudal fin swimming. *J. Experimental Biology*, 213:89–107, 2010.

[12] G. Borrelli. De motu animalium. *Romae*, 1680.

[13] C. Breder. The locomotion of fishes. *Zoologica*, 4(5):159–295, 1926.

[14] J. Carling, T. L. Williams, and G. Bowtell. Self-propelled anguilliform swimming simultaneous solution of the two-dimensional navier-stokes equations and newtons laws of motion. *Journal of Experimental Biology*, 201(23):3143–3166, 1998.

[15] S. Childress. *An Introduction to Theoretical Fluid Dynamics*. Courant Lecture Notes, vol. 19, AMS, 2009.

[16] V. Di Santo, E. Goerig, D. Wainwright, O. Akanyeti, J. Liao, T. Castro-Santos, and G. Lauder. Convergence of undulatory swimming kinematics across a diversity of fishes. *Proceedings of the National Academy of Sciences*, 118:e2113206118, 12 2021.

[17] P. Domenici and R. W. Blake. The kinematics and performance of fish fast-start swimming. *The Journal of Experimental Biology*, 200:1165–1178, 1997.

[18] P. Domenici, A. D. M. Wilson, R. H. J. M. Kurvers, S. Marras, J. E. Herbert-Read, J. F. Steffensen, S. Krause, P. E. Viblanc, and P. C. J. Krause. How sailfish use their bills to capture schooling prey. *Proc. R. Soc. B.*, 281, 2014.

[19] J. D. Eldredge. A reconciliation of viscous and inviscid approaches to computing locomotion of deforming bodies. *Experimental Mechanics*, 50, 2010.

[20] C. Eloy. Optimal Strouhal number for swimming animals. *Journal of Fluids and Structures*, 30, 2012.

[21] B. P. Epps and A. H. Techet. Impulse generated during unsteady maneuvering of swimming fish. *Exp Fluids*, 43:691–700, 2007.

[22] R. Fernandez-Feria. Note on optimum propulsion of heaving and pitching airfoils from linear potential theory. *J. Fluid Mechanics*, 826:781–796, 2017.

[23] D. Floryan, T. V. Buren, C. W. Rowley, and A. J. Smits. Scaling the propulsive performance of heaving and pitching foils. *J. Fluid Mechanics*, 822:386–397, 2017.

[24] D. Floryan, T. Van Buren, and A. J. Smits. Swimmers wake structures are not reliable indicators of swimming performance. *Bioinspiration Biomimetics*, 15(2):024002, 2020.

[25] G. Gabrielli and T. von Kármán. What price speed? specific power required for propulsion. *Journal of the American Society for Naval Engineers*, 63(1):188–200, 1951.

[26] I. Garrick. *Propulsion of a Flapping and Oscillating Airfoil*, volume 567 of *National Advisory Committee for Aeronautics: Report*. NACA, 1936.

[27] M. Gazzola, W. M. van Rees, and P. Koumoutsakos. C-start: optimal start of larval fish. *J. Fluid Mech.*, 698:5–18, 2012.

[28] J. Gray. Studies in animal locomotion i. *J. Experimental Biology*, 10:88–104, 1933.

[29] J. Gray. Studies in animal locomotion ii. *J. Experimental Biology*, 10:386–390, 1933.

[30] J. Gray. Studies in animal locomotion iii. *J. Experimental Biology*, 10:391–400, 1933.

[31] J. Gray. Studies in animal locomotion VI. The propulsive power of the dolphin. *J. Experimental Biology*, 13, 1936.

[32] G. Graziani and P. Bassanini. Unsteady viscous flows about bodies: Vorticity release and forces. *Meccanica*, 37:283–303, 2002.

[33] J. L. Hess and A. M. O. Smith. Calculation of potential flow about arbitrary bodies. *Progress in Aerospace Sciences*, 8:1–138, 1967.

[34] K. Jones and M. Platzer. Numerical computation of flapping-wing propulsion and power extraction. *AIAA Paper*, 97:0826, 1997.

[35] E. Kanso. Swimming due to transverse shape deformations. *J. Fluid Mech.*, 631, 2009.

[36] S. Kern and P. Koumoutsakos. Simulations of optimized anguilliform swimming. *J. Experimental Biology*, 209(24):4841–4857, 2006.

[37] H. Lamb. *Hydrodynamics*. Cambridge Univ. Press, 6 edition, 1975.

[38] L. D. Landau and E. M. Lifschitz. *Fluid Mechanics*, volume 6. Pergamon Press, 2 edition, 1986.

[39] G. V. Lauder. Fish locomotion: Recent advances and new directions. *Annual Review of Marine Science*, 7, 2015.

[40] G. Li, U. Muller, J. van Leeuwen, and H. Liu. Body dynamics and hydrodynamics of swimming fish larvae: a computational study. *Journal of Experimental Biology*, 215:4015–4033, 2012.

[41] N. Li, X. Liu, and Y. Su. Numerical study on the hydrodynamics of thunniform bio-inspired swimming under self-propulsion. *PLOS One*, 12(3), 2017.

[42] J. Lighthill. Note on the swimming of slender fish. *J. Fluid Mechanics*, 9(2):305–317, 1960.

[43] J. Lighthill. Aquatic animal propulsion of high hydromechanical efficiency. *J. Fluid Mechanics*, 44:265–301, 1970.

[44] J. Lighthill. Large-amplitude elongated body theory of fish locomotion. *Proc. R. Soc. Lond. B*, 179:126–138, 1971.

[45] J. Lighthill. *An informal Introduction to Theoretical Fluid Dynamics*. Oxford Univ. Press, Oxford, 1986.

[46] E. Limacher, C. Morton, and D. Wood. Generalized derivation of the added-mass and circulatory forces for viscous flows. *Physical Review Fluids*, 2, 2018.

[47] G. Liu, Y. L. Yu, and B. G. Tong. Flow control by means of a traveling curvature wave in fishlike escape responses. *Physical Review E*, 84:056312, 2011.

[48] K. Lucas, G. Lauder, and E. Tytell. Airfoil-like mechanics generate thrust on the anterior body of swimming fishes. *PNAS*, 117(19):10585–10592, 2020.

[49] A. P. Maertens, A. Gao, and M. S. Triantafyllou. Optimal undulatory swimming for single fish-like body and for pair of interacting swimmers. *J. Fluid Mech.*, 813, 2017.

[50] J. N. Newman. *Marine Hydrodynamics*. MIT Press, 2017.

[51] F. Noca. *On the evaluation of time-dependent fluid dynamic forces on bluff bodies*. PhD thesis, California Institute of Technology, 1997.

[52] F. Noca, D. Shiels, and D. Jeon. A comparison of methods for evaluating time-dependent fluid dynamic forces on bodies, using only velocity fields and their derivatives. *J. Fluids and Structures*, 13, 1999.

[53] D. Paniccia, G. Graziani, C. Lugni, and R. Piva. On the role of added mass and vorticity release for self propelled aquatic locomotion. *J. Fluid Mechanics*, 918:A45, 2021.

[54] D. Paniccia, G. Graziani, C. Lugni, and R. Piva. The relevance of recoil and free swimming in aquatic locomotion. *Journal of Fluids and Structures*, 103:103290, 2021.

[55] D. Paniccia, G. Graziani, C. Lugni, and R. Piva. The fish ability to accelerate and suddenly turn in fast maneuvers. *Scientific Reports*, 12:4946, 2022.

[56] D. Paniccia, L. Padovani, G. Graziani, and R. Piva. The performance of a flapping foil for a self-propelled fishlike body. *Scientific Reports*, 11:22297, 2021.

[57] D. Paniccia, L. Padovani, G. Graziani, and R. Piva. Locomotion performance for oscillatory swimming in free mode. *Bioinspiration & Biomimetics*, 2022.

[58] J. B. Pettygrew. *Animal Locomotion.* H. S. King & Company, 1873.

[59] D. A. P. Reid, H. Hildenbrandt, J. T. Padding, and C. K. Hemelrijk. Fluid dynamics of moving fish in a two-dimensional multiparticle collision dynamics model. *Physical Review E*, 85, 2012.

[60] P. G. Saffman. The self-propulsion of a deformable body in a perfect fluid. *J. Fluid Mech.*, 28(2), 1967.

[61] P. G. Saffman. *Vortex dynamics.* Cambridge Univ. Press, Cambridge, 1992.

[62] V. D. Santo, C. P. Kenaley, and G. V. Lauder. High postural costs and anaerobic metabolism during swimming support the hypothesis of a u-shaped metabolism-speed curve in fishes. *PNAS*, 114(49):13048–13053, 2017.

[63] W. W. Schultz and P. W. Webb. Power requirements of swimming: Do new methods resolve old questions? *Integrative Comparative Biology*, 42(5):1018–25, 2002.

[64] A. Smits. Undulatory and oscillatory swimming. *J. Fluid Mechanics*, 874:1–70, 2019.

[65] S. Sohn. A computational model of the swimming dynamics of a fish-like body in two dimensions. *Physics of Fluids*, 33:121902, 12 2021.

[66] S. C. Steele, J. M. Dahl, G. D. Weymouth, and M. S. Triantafyllou. Shape of retracting foils that model morphing bodies controls shed energy and wake structure. *J. Fluid Mechanics*, 805:355–383, 2016.

[67] S. C. Steele, G. D. Weymouth, and M. S. Triantafyllou. Added mass energy recovery of octopus-inspired shape change. *J. Fluid Mechanics*, 810:155–174, 2017.

[68] G. I. Taylor. Analysis of the swimming of long and narrow animals. *Proc. Roy. Soc. A*, 214, 1952.

[69] G. K. Taylor. Simple scaling law predicts peak efficiency in oscillatory propulsion. *Proceedings of the National Academy of Sciences*, 115(32):8063–8065, 2018.

[70] M. S. Triantafyllou, G. D. Weymouth, and J. M. Miao. Biomimetic survival hydrodynamics and flow sensing. *Annu. Rev. Fluid Mech.*, 48, 2016.

[71] T. von Kármán and J. M. Burgers. *E. General Aerodynamic Theory. Perfect Fluids*, volume 2 of *Aerodynamic Theory, Durand W.F. (Ed.)*, page 308. Springer Verlag, 1935.

[72] G. D. Weymouth, V. Subramaniam, and M. S. Triantafyllou. Ultra-fast escape maneuver of an octopus-inspired robot. *Bioinspir. Biomim.*, 10:016016, 2015.

[73] M. J. Wolfgang, J. M. Anderson, M. A. Grosenbaugh, D. K. P. Yue, and M. S. Triantafyllou. Near-body flow dynamics in swimming fish. *J. Experimental Biology*, 202, 1999.

[74] J. C. Wu. Theory for aerodynamic force and moment in viscous flows. *AIAA J.*, 19(4):432–441, 1981.

[75] J. Z. Wu, H. Y. Ma, and M. D. Zhou. *Vortical Flows.* Springer, 2015.

[76] T. Wu. Fish swimming and bird/insect flight. *Annu. Rev. Fluid Mechanics*, 43:25–58, 2011.

[77] T. Y. Wu. Swimming of a waving plate. *J. Fluid Mech.*, 10(3):321 – 344, 1961.

[78] Y. Yang, G. Wu, Yu, and B. Tong. Two-dimensional self-propelled fish motion in medium an integrated method for deforming body dynamics and unsteady fluid dynamics. *Chinese Physics Letters*, 25(2):597–600, 2008.

[79] J. Young and J. C. S. Lai. Mechanisms influencing the efficiency of oscillating airfoil propulsion. *AIAA Journal*, 45(7):1695–1702, 2007.

[80] J. Zhang. Footprints of a flapping wing. *J. Fluid Mechanics*, 810, 2017.

[81] J. Zhu, C. White, D. K. Wainwright, V. D. Santo, G. V. Lauder, and H. Bart-Smith. Tuna robotics: A high-frequency experimental platform exploring the performance space of swimming fishes. *Science Robotics*, 4:eaax4615, 2019.

Papers

The present chapter contains the five papers as the crowning achievement of this research work. The papers are given in the order in which they are cited in the outline of the research:

1. ***On the role of added mass and vorticity release for self-propelled aquatic locomotion*** published on the Journal of Fluid Mechanics on May 2021;

2. ***The relevance of recoil and free swimming in aquatic locomotion*** published on the Journal of Fluids and Structures on May 2021;

3. ***The performance of a flapping foil for a self-propelled fishlike body*** published on Scientific Reports on November 2021;

4. ***Locomotion performance for oscillatory swimming in free mode*** published on Bioinspiration & Biomimetics on November 2022;

5. ***The fish ability to accelerate and suddenly turn in fast maneuvers*** published on Scientific Reports on March 2022.

JFM PAPERS
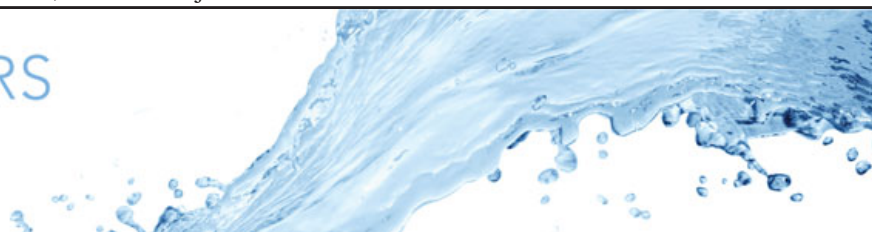
On the role of added mass and vorticity release for self-propelled aquatic locomotion

D. Paniccia[1], G. Graziani[1],†, C. Lugni[2,3] and R. Piva[1]

[1]Dept. of Mechanical and Aerospace Engineering, Univ. of Rome "La Sapienza", 00184 Rome, Italy

[2]CNR-INM, Marine Technology Research Institute, 00128 Rome, Italy

[3]Department of Marine Technology, Centre for Autonomous Marine Operations and Systems (AMOS), NTNU, 7491, Trondheim, Norway

Aquatic locomotion of a deformable body from rest up to its asymptotic speed is given by the unsteady motion which is produced by a series of periodic reactions dictated by the body configuration and by the style of swimming. The added mass plays a crucial role, not only for the initial burst, but also along each manoeuvre, to accelerate the surrounding fluid for generating the kinetic energy and to enable vortex shedding in the wake. The estimate of these physical aspects has been largely considered in most theoretical models, but not sufficiently deepened in many experimental and numerical investigations. As a motivation, while the vortical structures are easily detectable from the flow field, the added mass, on the contrary, is usually embedded in the overall forcing terms. By the present impulse formulation, we are able to separate and to emphasize the role of the added mass and vorticity release to evaluate in a neat way their specific contributions. The precise identification of the added mass is also instrumental for a well-posed numerical problem and for easily readable results. As a further point, the asymptotic speed is found to be guided either by the phase velocity of the prescribed undulation and by the unavoidable recoil motion induced by the self-propelled swimming. The numerical results reported in the present paper concern simplified cases of non-diffusing vorticity and two-dimensional flow.

Key words: flow–structure interactions, propulsion, swimming/flying

† Email address for correspondence: g.graziani@uniroma1.it

D. Paniccia, G. Graziani, C. Lugni and R. Piva

1. Introduction

Understanding animal locomotion in water, namely fish or cetacean swimming, has always attracted the attention of scientists, since the deep observations that Leonardo da Vinci described in his notes (e.g. *Atlanticus Codex folio 571 A recto*) more than five centuries ago. Almost two hundred years later, Borrelli, another Italian scientist, in the second half of the 17th century analysed in his book '*De motu animalium*' the fish's motion in a very detailed manner by enhancing the essential role of the tail, as illustrated very clearly in some of his drawings.

Starting from the end of the 19th century, more systematic research has been undertaken by several zoologists, especially in England, to classify fishes in terms of tail, appendages and body movements instrumental for their propulsion. A great advance was given, in the first half of the last century, by the experimental work of Gray (1933), who explained for the first time the kinematics of swimming by showing the essential role of a travelling wave moving backwards along the fish's body. Starting from the above findings, Taylor (1952) formulated a very successful model, now named the resistive model, well suited for swimming modes dominated by viscous forces.

On the contrary, at the start of the 1960s, Lighthill (1960) and Wu (1961) separately proposed a theoretical approach to study swimming modes dominated by inertial effects, i.e. for essentially inviscid flows, henceforth named the reactive model. For this purpose they considered an elongated body with a prescribed wave deformation moving from head to tail with velocity V, while immersed and swimming against a stream with a constant velocity U slightly lower than V. In a very elegant way, they predicted the power injected by the body into the surrounding fluid, the power transferred to the wake and, from the overall balance, the propulsive power required to overcome the unavoidable resistance. Essentially, the intention was to find the thrust of a deformable body by an ingenious and properly simplified formulation to allow for the evaluation of the Froude efficiency of a swimmer. Their model, described in several papers, stresses the role of the added mass as a basic mechanism for the transfer of energy to the fluid, as required for the production of the thrust and of the accompanying vortex wake.

Following their seminal work, a large number of papers appeared later on proposing many experimental techniques and numerical methods which consider a deformable body, fixed in its position in a uniform stream or tethered with the opposite velocity in a quiescent fluid. Among the experimental contributions let us mention Lauder & Tytell (2005), who provided a description of the major experimental set-ups, Tytell (2004), who compared data obtained by particle image velocimetry with the estimates given by Lighthill and Wolfgang *et al.* (1999), for the combined use of experimental and numerical results. Among the numerical contributions we recall Dong & Lu (2007), who reproduced for a viscous flow the conditions proposed by Lighthill and Wu, and Borazjani & Sotiropoulos (2009), who suggested finding, for a given velocity, the equilibrium condition for self-propelled swimming. In some contributions the recoil reactions, introduced by Lighthill to satisfy the equilibrium equations for a body under a prescribed deformation, were recognized as a point of crucial importance for a correct evaluation of the swimming efficiency, see e.g. Reid *et al.* (2012) and Maertens, Gao & Triantafyllou (2017). Due to the recoil effect, the shape deformation generated by the fish for the actual locomotion gives rise to specific reactions, which modify significantly the exchanged forces and moments, hence the overall performance and the swimming trajectory. However, the procedure to obtain the full dynamics of the body under a prescribed inflow velocity is quite elaborate, hence, different routes seem more appropriate for a self-propelled locomotion.

An alternative approach in terms of centre-of-mass velocity components as unknowns of the problem was originally introduced by Saffman (1967) and subsequently adopted in a seminal paper by Carling, Williams & Bowtell (1998). On the same line of reasoning, Kern & Koumoutsakos (2006) extended the procedure to find optimal solutions for three-dimensional (3-D) flows and Kanso (2009) obtained the locomotion variables of the swimmer's centre of mass by enforcing directly the conservation of the total momentum. Actually, to study a body in self-propulsion immersed in an otherwise quiescent fluid a coupled body–fluid system has to be taken into consideration with a particular attention paid to the exchange of internal forces (see Eldredge 2010). Since thrust and drag counterbalance, instead of trying to calculate a propulsion power that is not easily identified (Bale *et al.* 2014), the Froude efficiency has to be replaced by some other measure. The cost of transport (COT), i.e. the inverse of the well-known miles per gallon adopted for cars and other vehicles (von Kármán & Gabrielli 1950), is given by the ratio between the expended energy and the travelled distance and becomes the proper measure in this case.

Afterwards, a very large scientific production flourished in the last decade with a focus essentially on the free-swimming COT of different species with different shape deformations and styles of swimming (see e.g. Maertens, Triantafyllou & Yue 2015; Borazjani & Sotiropoulos 2010). Particular attention was also paid to the efficiency parameters and to the different energy contributions spent during self-propelled swimming (Wang, Yu & Tong 2018). A large number of papers are based on the combined solution of the deformable body dynamics and of the Navier–Stokes equations for incompressible viscous flows by different computational methods (see e.g. Yang *et al.* 2008; Gazzola *et al.* 2011; Bhalla *et al.* 2013) together with under-relaxation or penalization techniques to gain the overall stability of the integration procedure. A historical survey and a comprehensive review of the most common approaches is given in several books, e.g. Webb (1975) and Videler (1993) and many review articles (e.g. Lighthill 1969; Wu 2011; Lauder 2015; Smits 2019) also appeared in specific journals covering either fluid dynamics and biological aspects.

An accurate observation of the previous scientific findings, with a focus on the role of added mass and of the vorticity release, makes it easier to summarize now the main points that we like to account for when analysing self-propelled bodies:

   (i) the motion of a deformable body in an infinite fluid domain is characterized by the absence of external forces and the average total momentum is conserved;

  (ii) the internal forces exchanged by the swimming body with the surrounding fluid, i.e. thrust and drag, are mutually entangled, hence they are not clearly identified;

 (iii) the real trajectory must account for all the recoil reactions, introduced by the prescribed deformation of the main body;

 (iv) the solution of the fluid–body interaction should be solved by considering the full system of equations with the kinematic variables as output of the problem;

  (v) the identification of the added mass terms leads to a naturally well-posed problem and, at the same time, provides a proper physical interpretation of the numerical results;

 (vi) the standard efficiency measures are not easy to define, since the thrust is not available for steady free swimming and the COT has to be used; and

(vii) the enforced undulation is characterized by a phase velocity that is going to influence the steady state asymptotic value of the locomotion velocity and the location of the released vortices along the wake.

D. Paniccia, G. Graziani, C. Lugni and R. Piva

The purpose of the present work is to adopt a classical impulse formulation, which may be expressed in terms of potential flow and concentrated vorticity, to consider a 2-D fully immersed deformable body in the case of vanishing viscosity. The intention is to use this highly simplified impulse model with the ambitious objective to clarify the role of added mass and of vorticity release in free swimming either for the acceleration during the initial transient phase or for the asymptotic velocity to be reached at steady state.

2. Mathematical model

The self-propelled motion of an undulating body in an infinite N-dimensional volume of fluid V_∞ is analysed by considering a fluid–body domain with no external forces applied. Hence, the exchanged forces and moments between fluid and body appear as internal actions. The body motion is computed by solving the dynamics equations of the body centre of mass in an otherwise quiescent unbounded fluid.

With this aim, among several possible expressions for the linear and the angular momentum we adopt the classical formulation in terms of potential and vortical impulses that has been widely discussed in the literature (see e.g. Noca 1997; Wu, Ma & Zhou 2015). In this framework we can easily highlight the acyclic potential contribution as well as the effects of the bound and free vorticities.

2.1. *Force and moment acting on the body*

The fluid momentum is expressed, via a renown vector identity (A1), by two terms representing the field vorticity and the vortex sheet over the body surface which, properly combined, readily lead to the vortical and the potential impulse. An analogous vector identity (A3) holds for the angular momentum. As has been repeatedly proven, the sum of these two impulses has the most significant property of the momentum, i.e. the forces exchanged between the body and the surrounding flow field are obtained by the time derivative of the impulses and an analogous relationship holds for the moment of the forces. At the same time, the total impulse does not suffer the poor convergence of the momentum over an unbounded domain. Actually, the momentum does not show absolute convergence, but only a conditional one. However, its finite value can be found without any ambiguity through the evaluation of the kinetic energy (see, among others, Landau & Lifschitz 1986; Childress 2009). As a further point, the impulse formulation enjoys the important property of being linear with respect to the unknown kinematic variables, so as to permit the isolation of the potential contribution, related to the added mass characterizing fast manoeuvres, and of the vortical contribution, usually dominant when the steady state conditions are reached. We will see that this property has a paramount positive effect for the numerical solution of the equations, providing quite naturally a well-posed problem. As a final advantage, the conservation of the total impulse, peculiar to the self-propelled body, does not need the time derivation, as usually required to obtain the forces, and the successive time integration to find the kinematics of the body, providing a better accuracy together with a significant reduction of the computational effort.

We consider an impermeable, flexible body whose bounding surface S_b is moving with velocity u_b given by the prescribed deformation. We assume an incompressible fluid with density ρ. The outer boundary is stationary in an absolute reference frame and the fluid velocity is assumed to vanish at the far field boundary. As previously anticipated, the force

acting on the body, F_b, is expressed through the time derivative of the total impulse p

$$F_b = -\frac{\mathrm{d}p}{\mathrm{d}t}, \tag{2.1}$$

where p is defined, by using the well-known vector identity (A1) for the unbounded fluid volume, as

$$p = \frac{1}{N-1}\left[\int_{V_\infty} \rho\, x \times \omega\, \mathrm{d}V + \int_{S_b} \rho\, x \times (n \times u^+)\, \mathrm{d}S\right], \tag{2.2}$$

where $N = 2, 3$ is the flow dimension and the integral over the external boundary receding to infinity has been proven to vanish (Noca 1997), ω is the vorticity and u^+ indicates the limiting value of the fluid velocity on S_b. The normal to S_b, n, points into the flow domain and all of the vorticity is enclosed within the fluid volume V_∞ which extends to infinity. As shown elsewhere (Graziani & Bassanini 2002), the right-hand side of (2.2) is independent of the choice of the reference frame origin.

For a better comprehension, to account for the boundary condition on the body, which is anyhow satisfied, we may recast (2.1) by adding and subtracting a boundary integral involving u_b,

$$F_b = -\frac{\mathrm{d}}{\mathrm{d}t}\left\{\frac{1}{N-1}\int_{V_\infty}\rho\, x \times \omega\, \mathrm{d}V + \frac{1}{N-1}\int_{S_b}\rho\, x \times [n \times (u^+ - u_b)]\, \mathrm{d}S \right.$$
$$\left. +\frac{1}{N-1}\int_{S_b}\rho\, x \times (n \times u_b)\, \mathrm{d}S\right\}, \tag{2.3}$$

where the jump in tangential velocity appears as a vortex sheet concentrated on the body surface to give the volume integral $\int_{V_\infty}\rho\, x \times \gamma\, \mathrm{d}V$, where $\gamma = [n \times (u^+ - u_b)]\delta(x - x_b)$.

The formulation (2.3) highlights the vortex sheet term, leading to the identification of the added mass, separately from the field vorticity contribution. If, on the contrary, the total vorticity

$$\hat{\omega} = \omega + \gamma = \omega + [n \times (u^+ - u_b)]\delta(x - x_b), \tag{2.4}$$

is considered, the added mass would be embedded and fully hidden within the field vorticity, as discussed by Limacher, Morton & Wood (2018).

Similarly to what is described above for the force, an expression for the angular moment (positive anticlockwise) on the body can be obtained. Here, we consider the moment with respect to a given pole (to be specified later either as the origin of the ground reference frame or as the body centre of mass), so x is the generic distance of the field point from the pole.

By defining the angular impulse π as:

$$\pi = -\frac{1}{2}\left[\int_V \rho\, |x|^2\omega\, \mathrm{d}V + \int_{S_b}\rho\, |x|^2(n \times u^+)\, \mathrm{d}S\right], \tag{2.5}$$

the expression for the angular moment is written as

$$M_b = -\frac{\mathrm{d}\pi}{\mathrm{d}t}. \tag{2.6}$$

2.2. *Potential and vortical impulse*

A Helmholtz decomposition is applied to express the velocity field as the sum of the acyclic and vorticity related components

$$\boldsymbol{u}^+ = \nabla\phi + \nabla \times \boldsymbol{\Psi} = \nabla\phi + \boldsymbol{u}_w, \tag{2.7}$$

where ϕ and $\boldsymbol{\Psi}$ are referred to as the scalar and the (solenoidal) vector potentials, and are given by the solution of the Laplace/Poisson equation, subject to the impermeable boundary condition on S_b, i.e. $\nabla\phi \cdot \boldsymbol{n} = \boldsymbol{u}_b \cdot \boldsymbol{n}$ and $(\nabla \times \boldsymbol{\Psi}) \cdot \boldsymbol{n} = 0$ respectively, and to the vanishing velocity at infinity. To enlighten the contribution of the above potentials to the force, let us now express the impulse $\boldsymbol{p}$ appearing in (2.1) in terms of both potential and vortical impulses, $\boldsymbol{p}_\phi$ and $\boldsymbol{p}_v$, as

$$\boldsymbol{p} = \boldsymbol{p}_\phi + \boldsymbol{p}_v. \tag{2.8}$$

The vortical impulse on the right hand-side of (2.8) is

$$\boldsymbol{p}_v = \frac{1}{N-1}\left[\int_{V_\infty} \rho\, \boldsymbol{x} \times \boldsymbol{\omega}\, \mathrm{d}V + \int_{S_b} \rho\, \boldsymbol{x} \times (\boldsymbol{n} \times \boldsymbol{u}_w)\, \mathrm{d}S\right] = \frac{1}{N-1}\int_{V_\infty} \rho\, \boldsymbol{x}\, \times\, \boldsymbol{\omega}_a\, \mathrm{d}V, \tag{2.9}$$

where part of the bound vorticity on S_b has been added to the released vorticity to obtain the additional vorticity as introduced by Lighthill

$$\boldsymbol{\omega}_a = \boldsymbol{\omega} + (\boldsymbol{n} \times \boldsymbol{u}_w)\, \delta(\boldsymbol{x} - \boldsymbol{x}_b) \tag{2.10}$$

that may be expressed, once combined with (2.4), to reproduce the original definition

$$\boldsymbol{\omega}_a = \hat{\boldsymbol{\omega}} - [\boldsymbol{n} \times (\nabla\phi - \boldsymbol{u}_b)]\, \delta(\boldsymbol{x} - \boldsymbol{x}_b). \tag{2.11}$$

The potential impulse $\boldsymbol{p}_\phi$ on the right hand-side in (2.8) is given by

$$\boldsymbol{p}_\phi = -\rho \int_{S_b} \phi\, \boldsymbol{n}\, \mathrm{d}S, \tag{2.12}$$

where the vector identity (A2) has been used. Let us notice that this term has been named also the virtual momentum by Saffman (1992) or impulse of the fluid by Lamb (1975) and its time derivative defines, in a general sense, the added mass force that, for rigid motions, may be expressed in the classical form given by the Kirchhoff base potentials.

The expression for the angular momentum can be similarly obtained by separating the vortical and the potential contributions by using the vector identity (A3) and the generalized Stokes theorem (A4). We split the angular impulse (2.5) as $\boldsymbol{\pi} = \boldsymbol{\pi}_\phi + \boldsymbol{\pi}_v$, where the angular potential impulse is defined as

$$\boldsymbol{\pi}_\phi = -\tfrac{1}{2}\int_{S_b} \rho\, |x|^2 (\boldsymbol{n} \times \nabla\phi)\, \mathrm{d}S = -\rho \int_{S_b} \boldsymbol{x} \times \phi\boldsymbol{n}\, \mathrm{d}S, \tag{2.13}$$

and the angular vortical impulse is

$$\boldsymbol{\pi}_v = -\tfrac{1}{2}\int_V \rho\, |x|^2 \boldsymbol{\omega}\, \mathrm{d}V - \tfrac{1}{2}\int_{S_b} \rho\, |x|^2 (\boldsymbol{n} \times \boldsymbol{u}_w)\, \mathrm{d}S. \tag{2.14}$$

As a comment to this section, a unified theoretical treatment of the impulse formulation has been presented by taking into account the main different contributions on the subject (see e.g. Saffman 1967; Kanso 2009; Eldredge 2010). Concerning the vorticity field, particular attention is paid to the bound vorticity and to its relationship with the added mass force (see e.g. Lighthill 1960; Limacher 2019).

3. Locomotion

We study now the planar motion of a deformable body $\mathcal{B}$ within an infinite fluid domain $\mathcal{V}$. We use a Cartesian inertial frame (e_1, e_2, e_3). The body motion occurs in the plane (e_1, e_2) and its translation with respect to a given reference point in $\mathcal{B}$ is $x_o = x_o\,e_1 + y_o\,e_2$. Moreover, the body may undergo a rotation β about the axis e_3.

The locomotion of the deformable body is obtained by coupling the body dynamics and the fluid dynamics actions. If we consider the body–fluid system $(\mathcal{V}_b + \mathcal{V}_f)$, no external forces or moments are present and therefore the linear and angular momenta are conserved

$$\frac{\mathrm{d}}{\mathrm{d}t}\left[\int_{\mathcal{V}_b} \rho_b\,u_b\,\mathrm{d}V + \int_{\mathcal{V}_f} \rho\,u\,\mathrm{d}V\right] = 0, \tag{3.1}$$

$$\frac{\mathrm{d}}{\mathrm{d}t}\left[\int_{\mathcal{V}_b} \rho_b\,x \times u_b\,\mathrm{d}V + \int_{\mathcal{V}_f} \rho\,x \times u\,\mathrm{d}V\right] = 0. \tag{3.2}$$

The motion of the body can be expressed as the sum of the prescribed deformation (shape variations with velocity u_{sh}) plus the motion of the frame with origin in the centre of mass (translational, u_{cm}, and rotational, Ω, velocity).

In the ground inertial frame the angular velocity is $\Omega = \dot{\beta}\,e_3 \equiv \Omega\,e_3$. The linear velocity is $u_{cm} = \dot{x}_o e_1 + \dot{y}_o e_2$. Thus we can express the body motion as

$$u_b = u_{sh} + u_{cm} + \Omega \times x', \tag{3.3}$$

where x' is the position vector in the body frame, i.e. $x = x_{cm} + x'$. Following (3.3), the prescribed deformation of the body has to conserve linear and angular momenta

$$\int_{\mathcal{V}_b} \rho_b u_{sh}\,\mathrm{d}V = 0, \tag{3.4}$$

$$\int_{\mathcal{V}_b} \rho_b x' \times u_{sh}\,\mathrm{d}V = 0. \tag{3.5}$$

By considering that the second term in (3.1) is the force acting on the fluid, which is opposite to the force on the body and by using the body mass m_b, combining with (2.1) we obtain

$$\frac{\mathrm{d}}{\mathrm{d}t}(m_b\,u_{cm}) + \frac{\mathrm{d}p}{\mathrm{d}t} = 0, \tag{3.6}$$

where u_{cm} is clearly identified as the locomotion velocity of the body and p is now expressed in terms of x', since the independence on the origin of the reference system. In this way, the interaction with the fluid gives directly the full motion of the undulating body. Otherwise, if ((3.4)–(3.5)) were not satisfied by the prescribed deformation, additional rigid motions would appear and (3.3) should be consistently modified (see Bhalla *et al.* 2013). By assuming zero initial conditions (3.6) gives

$$m_b\,u_{cm} + p = 0. \tag{3.7}$$

Similarly, the angular impulse in two dimensions is recast from (2.5) in terms of the distance x' as $\pi' = (\pi - x_o \times p) \cdot e_3$ and the angular momentum balance can be expressed

as

$$\frac{\mathrm{d}}{\mathrm{d}t}(I_{zz}\,\Omega) + \frac{\mathrm{d}\boldsymbol{\pi}'}{\mathrm{d}t} = 0, \tag{3.8}$$

or, by using the body frame and removing the time derivative

$$I_{zz}\,\Omega + \pi' = 0. \tag{3.9}$$

In the case of a massless body ($m_b = 0$ and $I_{zz} = 0$) we recover the equations reported by Kanso (2009). Let us notice that, according to what was originally proposed by Saffman (1967), the system of (3.7) and (3.9) provides the evaluation of the body velocities without considering time derivatives, as required when using the standard equations (3.6) and (3.8).

The scalar potential introduced by the Helmholtz decomposition is further divided as $\phi = \phi_{sh} + \phi_{loc}$, as suggested by Saffman (1967), where ϕ_{sh} is given by the imposed deformation velocity $\boldsymbol{u}_{sh}$ and ϕ_{loc} is given by the combination of the locomotion linear and angular velocities, according to the related boundary conditions on S_b

$$\frac{\partial\phi_{sh}}{\partial n} = \boldsymbol{u}_{sh} \cdot \boldsymbol{n}, \quad \frac{\partial\phi_{loc}}{\partial n} = (\boldsymbol{u}_{\mathrm{cm}} + \boldsymbol{\Omega} \times \boldsymbol{x}') \cdot \boldsymbol{n}. \tag{3.10a,b}$$

Analogously, the linear and angular impulses are given by

$$\boldsymbol{p}_\phi = \boldsymbol{p}_{sh} + \boldsymbol{p}_{loc}, \quad \pi'_\phi = \pi'_{sh} + \pi'_{loc}. \tag{3.11a,b}$$

Finally, the locomotion impulses, $\boldsymbol{p}_{loc}$ and π'_{loc}, may be expressed in terms of the added mass coefficients reported in the classical treatises (see e.g. Lamb 1975) that, for completeness, are briefly recalled below. For a body motion with linear velocity $\boldsymbol{u}_{\mathrm{cm}}$ and angular velocity Ω, we consider the Kirchhoff base potentials Φ_j defined through the boundary conditions

$$\frac{\partial\Phi_1}{\partial n} = \boldsymbol{n} \cdot \boldsymbol{e}_1, \quad \frac{\partial\Phi_2}{\partial n} = \boldsymbol{n} \cdot \boldsymbol{e}_2, \quad \frac{\partial\Phi_3}{\partial n} = \boldsymbol{x}' \times \boldsymbol{n} \cdot \boldsymbol{e}_3 \tag{3.12a–c}$$

to have $\phi_{loc} = \dot{x}_0\Phi_1 + \dot{y}_0\Phi_2 + \Omega\Phi_3$. It follows for the added mass coefficient m_{ij} that

$$m_{ij} = \rho \int_{S_b} \Phi_i \frac{\partial\Phi_j}{\partial n} \, \mathrm{d}S. \tag{3.13}$$

To compute the numerical solution we express the locomotion equations in a coordinate frame attached to the body. For this purpose we consider the ground fixed frame $\{\boldsymbol{e}_1, \boldsymbol{e}_2, \boldsymbol{e}_3\}$ and the body frame $\{\boldsymbol{b}_1, \boldsymbol{b}_2, \boldsymbol{b}_3\}$ as sketched in figure 1. The origin of the body frame is in cm, i.e. $\boldsymbol{x}_o \equiv \boldsymbol{x}_{\mathrm{cm}}$ and $\boldsymbol{b}_3$ is parallel to $\boldsymbol{e}_3$. Accordingly, the linear velocity $\boldsymbol{V}_{\mathrm{cm}} = V_1\boldsymbol{b}_1 + V_2\boldsymbol{b}_2$ and the momenta $\boldsymbol{P}$, Π are related to the corresponding variables in the fixed frame by

$$\boldsymbol{u}_{\mathrm{cm}} = \boldsymbol{R}\,\boldsymbol{V}_{\mathrm{cm}}, \quad \boldsymbol{p} = \boldsymbol{R}\boldsymbol{P}, \quad \pi' = \Pi, \tag{3.14a–c}$$

where $\boldsymbol{R}$ is the rotation matrix relating the inertial to the body frame. Analogously, the coordinates in the body frame are $\boldsymbol{X} = \boldsymbol{R}^T\,\boldsymbol{x}'$.

Accounting for (3.14a–c), the impulses related to the body deformation, $\boldsymbol{P}_{sh}$ and Π_{sh}, are expressed according to (2.12) and (2.13), respectively, while the vorticity related quantities, $\boldsymbol{P}_v$ and Π_v, are defined through (2.9) and (2.14). The locomotion velocities, which are
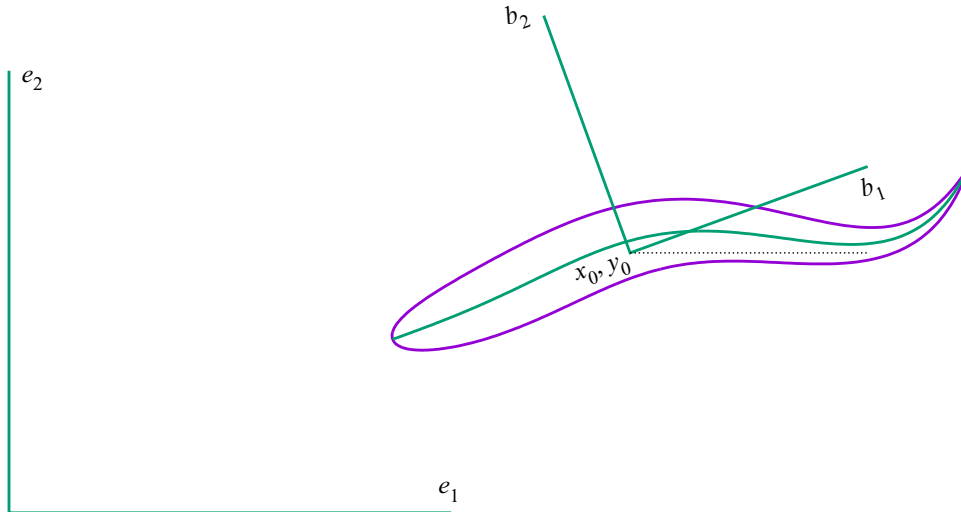
Added mass and vorticity release for self-propelled locomotion

Figure 1. Ground and body reference frames.

multiplied by the added mass coefficients (3.13) within $\boldsymbol{P}_{loc}$ and Π_{loc}, can be shifted to the left hand-side to yield the system of equations for the body motion

$$
\left.
\begin{aligned}
V_1 \, (m_{11} - m_b) + V_2 \, m_{12} + \Omega \, m_{13} &= P_{sh1} + P_{v1}, \\
V_1 \, m_{21} + V_2 \, (m_{22} - m_b) + \Omega \, m_{23} &= P_{sh2} + P_{v2}, \\
V_1 \, m_{31} + V_2 \, m_{32} + \Omega \, (m_{33} - I_{zz}) &= \Pi_{sh} + \Pi_v.
\end{aligned}
\right\}
\tag{3.15}
$$

The added mass terms, appearing on the left hand-side of (3.15), together with the body inertial properties, give the coefficient matrix for the unknown variables V_1, V_2 and Ω. The known terms appearing on the right hand-side are the impulse contributions due to shape deformation and vorticity. This equation system recalls and generalizes the model ingeniously proposed by Saffman (1967) and Lighthill (1970). The body mass m_b is assumed to be constant while I_{zz} and m_{ij} change in time according to the shape deformation. Let us stress again that the part of the added mass terms related to ϕ_{loc} now appears on the left-hand side, leading to a well-posed problem, as briefly described in the following section together with the main details of the numerical model. The separation of ϕ_{sh} and ϕ_{loc} is also instrumental to identifying the exchange of added mass energy among shape deformation and locomotion (see Spagnolie & Shelley 2009; Steele 2016). We would like to underline that the part of the potential impulses related to ϕ_{sh} in (3.15), as suggested by Kanso (2009), has to stay on the right hand-side together with the vortical impulses, since they both involve known quantities. As a further comment, a detailed account of the single contributions is the essential tool for arguing about the aim of the paper, i.e. a proper evaluation of the role of added mass and vorticity release when discussing the numerical results.

4. About the numerical model

The mathematical model described so far is valid in general although, from now on, restricted to the locomotion of 2-D bodies to facilitate the analysis of the results while maintaining the most important aspects of the problem. As a further step in the same direction, we consider here an accurate but simplified numerical model which does not involve vorticity diffusion, in the way suggested by Schultz & Webb (2002), to find sufficiently accurate results for this complicated problem. The evaluation of both potential

and vortical impulses can be obtained by the discretization of the body surface and by a suitable model for the release of the concentrated vortex sheet via a Kutta condition to mimic the presence of a vanishing viscosity. Some of the techniques adopted in the numerical method for the evaluation of the two impulses are briefly described below, but we would like to illustrate first the capability of the present model to provide a well-posed linear system.

Actually, the time derivatives, usually needed with the classical pressure formulation, may lead to a poor stability of the equation system, since the forces and moments are directly dependent on the unknown velocity components. Some authors, e.g. Carling *et al.* (1998), Kern & Koumoutsakos (2006) and Borazjani & Sotiropoulos (2010), tried to overcome these difficulties by using under-relaxation expressions which had to be accurately chosen to obtain stability and to minimize their influence on the numerical accuracy of the procedure. A more physical approach was adopted in Maertens *et al.* (2017) by introducing a prescribed added mass matrix M_a, whose coefficients are estimated and properly tuned from the stretched straight configuration. By adding to both sides of the equation the same term representing this approximated value, the idea is to counterbalance the real added mass embedded within the forcing term. The impulse formulation adopted here allows for the removal of the time derivatives present in (3.6) and (3.8), hence no stability issues should be considered. At the same time, the linearity of the vorticity terms allows us to isolate and separate the contribution of the added mass, which is correctly evaluated at each time step and properly moved to the left hand-side, giving a well-posed system of equations able to hold even when treating massless bodies (see Eldredge 2010).

To achieve neat and simple results, as anticipated above, we consider the case of potential flow with a concentrated vorticity on the body surface and its subsequent shedding at the trailing edge into the vortex wake. The flow solutions are obtained by using an unsteady potential code based on the approach of Hess & Smith (1967) while the wake release is taken into account by following the procedure described in Basu & Hancock (1978). The body boundary is approximated by a finite number of panels, each with a local, uniform source strength, and all with a constant circulation density. The impermeability condition on each panel together with a suitable unsteady Kutta condition are needed to evaluate the source strengths and the uniform circulation density γ. According to Kelvin's theorem, any change in circulation about the airfoil results in the release of vorticity by a wake panel attached to the trailing edge which, at each time step, is lumped into a point vortex and shed into the wake.

As described in the previous section, even if the equations are written in the ground frame of reference, the solution is achieved in a coordinate system attached to the body which moves according to V_1 and V_2 and rotates according to Ω. Actually, this is the proper frame to define the deformation which should not be dependent on the interaction with the fluid. At each time step, the body, deforming with V_{sh}, is invested with a water speed given by the combination of $-V_1$, $-V_2$ and $-\Omega$, which is required for the unsteady Kutta condition and it is essential for the evaluation of the length and inclination of the wake panel behind the body through several iterations.

Finally, it is important to notice that the linear velocity components V_1 and V_2, named, from now on, the forward and lateral velocities, respectively, change their directions at each time step, since the equations of motion are written in the body frame coordinates. After a transient acceleration phase, the body, even maintaining an oscillating pattern, reaches an asymptotic steady state with a constant mean value of the forward velocity while the mean lateral and angular velocities are equal to zero. As a consequence, in the following section, the numerical results are shown in terms of the forward velocity, whose mean

value represents the actual locomotion velocity. An animation showing the body motion, obtained by projecting the velocity components V_1 and V_2 along the x and y directions of the ground frame of reference (animation-link), is helpful to better illustrate the actual gait of the body. As a final comment, the above numerical model may be considered as part of the splitting procedure introduced by Chorin (1973) which, accounting for diffusive vorticity, leads directly to the classical vortex method for viscous flow (see e.g. Graziani, Ranucci & Piva 1995; Koumoutsakos & Leonard 1995; Eldredge, Colonius & Leonard 2002).

5. Numerical results and discussion

We would like to analyse in the present section the free swimming of a deformable body with a focus on the asymptotic steady state condition. The fish undulates with a prescribed periodic deformation characterized by a specific phase velocity and, after a transient, the fish reaches a steady state under the combination of potential and vortical velocity contributions. Let us note that the resulting value depends only on the phase velocity while the single contributions may vary with the deformation amplitude. As anticipated in the previous sections, the standard efficiency measures are not suitable, while the present results provide the data needed for the evaluation of the cost of transport. As a further point, the results allow for interesting considerations of the transient phases, which are also illustrated through the representation of the wake patterns.

5.1. *Body shape and kinematics*

The swimming fish at rest is represented by a shape corresponding to a NACA0012 airfoil with a chord length c equal to 1. Previous works employed a large number of different approaches to describe fish undulation. Some of the proposed analytical expressions for the lateral displacement of the mid-line were obtained by fitting data from direct fish observations (see e.g. Hess & Videler 1984; Lauder & Tytell 2005). These analytical expressions consist of a travelling wave usually multiplied by a polynomial amplitude modulation, thus allowing for direct control of geometrical parameters, such as the tail-beat amplitude. An additional mathematical condition is required to enforce the inextensibility given by

$$\left(\frac{\partial y_c}{\partial s}\right)^2 + \left(\frac{\partial x_c}{\partial s}\right)^2 = 1, \tag{5.1}$$

where x_c and y_c are the mid-line coordinates and s represents the curvilinear coordinate along the mid-line itself. To satisfy implicitly this condition, some authors proposed a deformation in terms of the mid-line curvature from which the lateral displacement follows (Kern & Koumoutsakos 2006; Wang *et al.* 2018).

Here, a different parameterization based on the instantaneous local slope of the mid-line is proposed as more affordable for bio-mimetic applications, hereafter referred to as synthetic deformation. The slope of the mid-line is defined by the following expression for a travelling wave of constant amplitude $d\beta$ and a wavenumber k related to a wavelength along s

$$\beta(s, t) = d\beta \sin(ks - \omega t), \tag{5.2}$$

where ω is the angular frequency. An amplitude modulation may eventually be added to reproduce the deformations given by other authors. The instantaneous coordinates of the
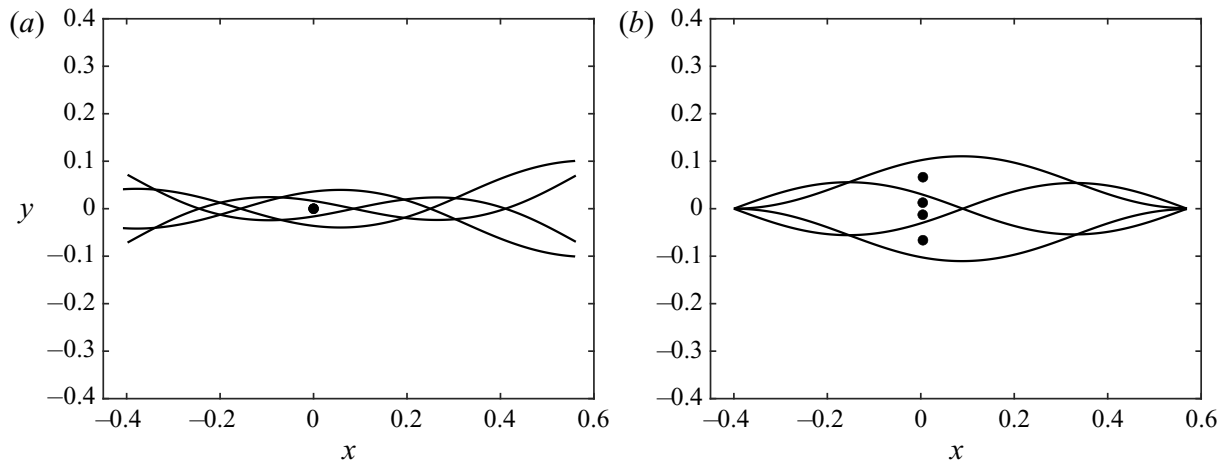
Figure 2. (*a*) Corrected mid-line envelop in order to satisfy (3.4) and (3.5). (*b*) Mid-line envelop obtained by the direct integration of (5.2). The dots represent the centre-of-mass positions.

airfoil mid-line are obtained by integrating (5.2)

$$x_c(s, t) = \int_0^s \cos(\beta(s, t)) \, ds, \tag{5.3}$$

$$y_c(s, t) = \int_0^s \sin(\beta(s, t)) \, ds, \tag{5.4}$$

and the inextensibility condition is automatically satisfied. The normal to each cross-section of the body is the same as that of the mid-line and the total area is preserved at convergence during the deformation.

In the absence of surrounding fluid, namely, with no external forces and moments, (3.4) and (3.5) hold to maintain the centre of mass position of the body, as well as its principal axes (figure 2*a*). If these equations are not satisfied, the centre of mass would move under spurious forces (figure 2*b*), hence, the deformation has to be properly corrected by removing the rigid displacements so to obtain the mid-line envelope in figure 2(*a*).

5.2. *Swimming velocity and expended energy*

The present section contains the results for a neutrally buoyant ($\rho = \rho_b/\rho_f = 1$) body undulating with a fixed angular frequency $\omega = 2\pi f = 10$ rad s^{-1}, unless otherwise indicated. For all the analysed cases, the wavenumber k is set to 2π m^{-1}, i.e. the wavelength λ is equal to the chord length c, hence corresponding to a phase speed which, according to (5.2), is given by

$$\frac{\omega}{k} = f\lambda = 1.59 \text{ m s}^{-1}. \tag{5.5}$$

The forward locomotion velocity component U is shown in figure 3 for different deformation amplitudes $\delta\beta$. By increasing $\delta\beta$, we notice larger transient acceleration and a steady state velocity that is slightly decreasing. However, due to the inextensibility condition, the wavelength L, associated with the instantaneous deformation and measured along the forward direction (see figure 4) may be quite different from the prescribed λ.
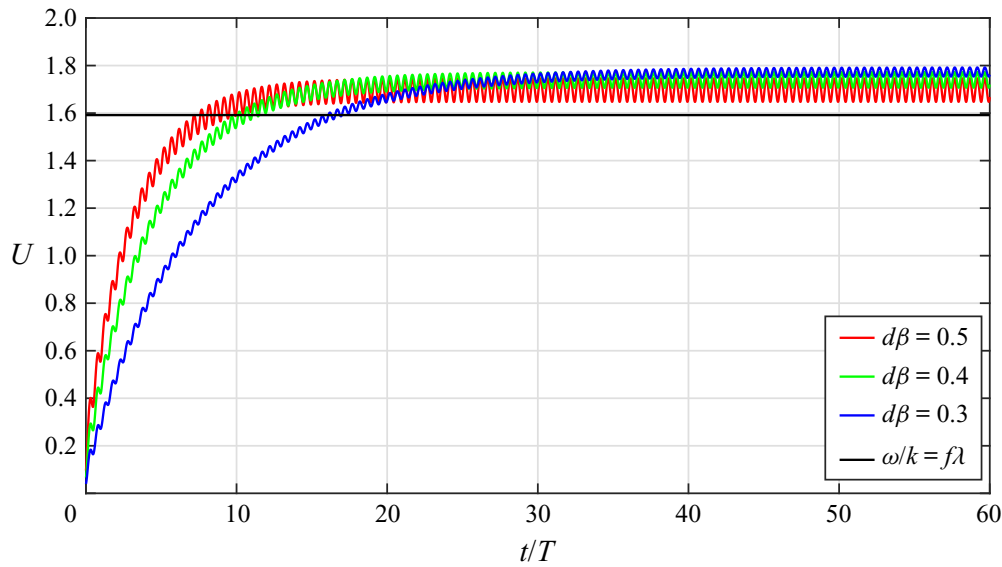
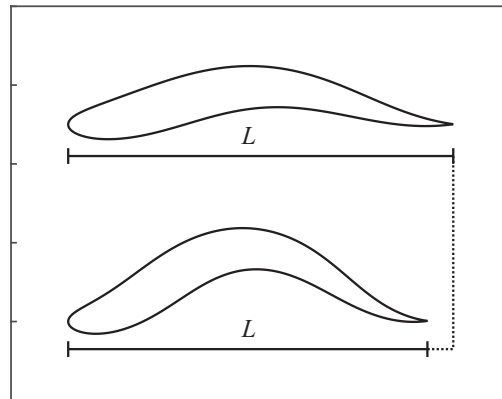Figure 3. Forward swimming velocity for different undulation amplitudes.

Figure 4. Equivalent wavelength λ_e.

From this observation, an equivalent wavelength λ_e is defined as

$$\lambda_e = \frac{1}{T} \int_t^{t+T} L(t) \, dt, \tag{5.6}$$

which leads to an equivalent phase velocity of the body deformation given by

$$\frac{\omega}{k_e} = f\lambda_e. \tag{5.7}$$

As a consequence, the asymptotic value of the slip velocity, defined as the ratio between the swimming speed and the equivalent phase velocity, does not change with $d\beta$, as shown in figure 5, namely, the body moves with a forward velocity which only depends on the backward travelling wave velocity, and not on its amplitude. Since the model does not consider any dissipative effect, the above result seems reasonable, while, under the action of viscous resistance, the slip velocity would definitely be lower and the deformation amplitude would start to play a significant role (Smits 2019). For comparison, we report in figure 6 the results for the velocity components for the present model and a carangiform deformation together with those for the viscous model by Yang *et al.* (2008). The figure confirms that the main effect of the viscous resistance is a consistent reduction of the
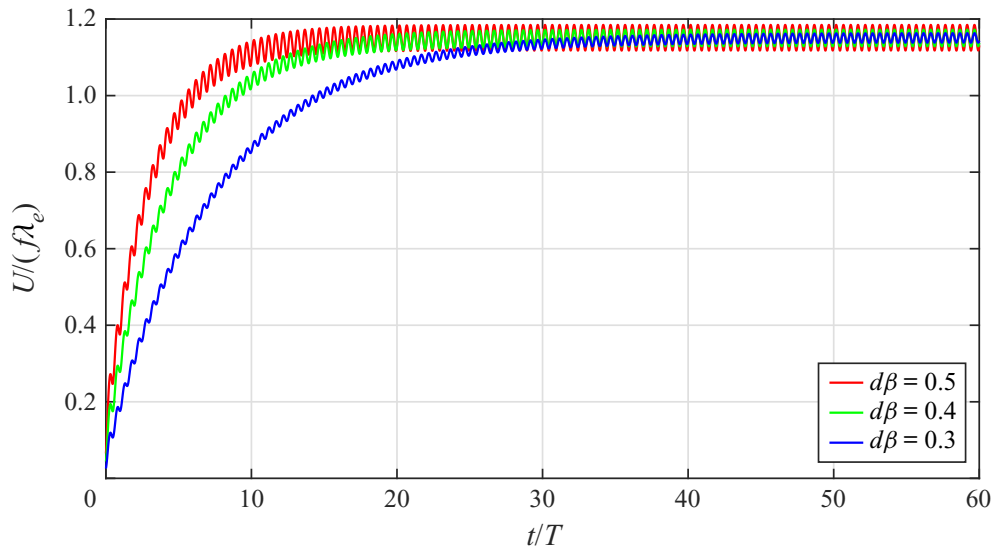
918 A45-13

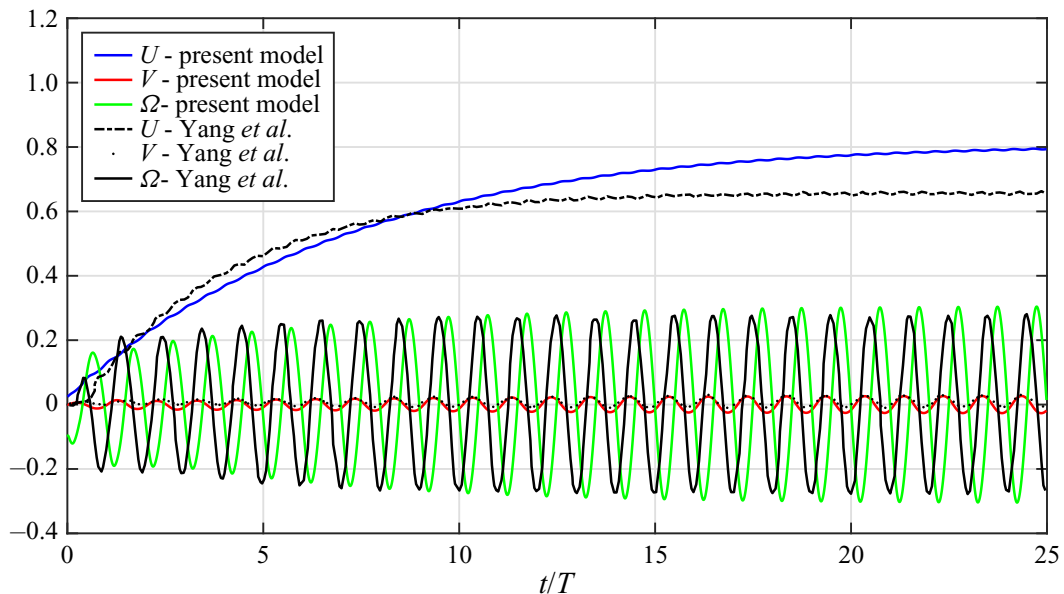Figure 5. Slip velocity for different undulation amplitudes.

Figure 6. Velocity components (U, V, Ω) for carangiform deformation: present vs viscous results (Yang *et al.* 2008).

steady state locomotion velocity which may otherwise be predicted by introducing a model approximation for the viscous drag (see e.g. Akoz & Moored 2018). In this case, numerical results not reported here reproduce an increasing trend of the asymptotic swimming velocity with the deformation amplitude, as shown by analogous findings in the literature (e.g. Zhang *et al.* 2018).

As discussed previously, the effects of added mass and vorticity release on the swimming speed may be easily highlighted. Actually, due to the linearity of the system of (3.15), the kinematic variables U, V and Ω are given by adding the potential and the vortical impulses. The corresponding forward velocity contributions, U_ϕ and U_w, are illustrated in figures 7(a) and 7(b) in the form of the slip velocity. For growing amplitude, $U_\phi/(f\lambda_e)$ increases and $U_w/(f\lambda_e)$ decreases and their sum remains constant, as anticipated in figure 5. Let us observe that U_ϕ, due to the added mass, reaches instantaneously a steady state value, and U_w, due to vortex shedding, grows in time with
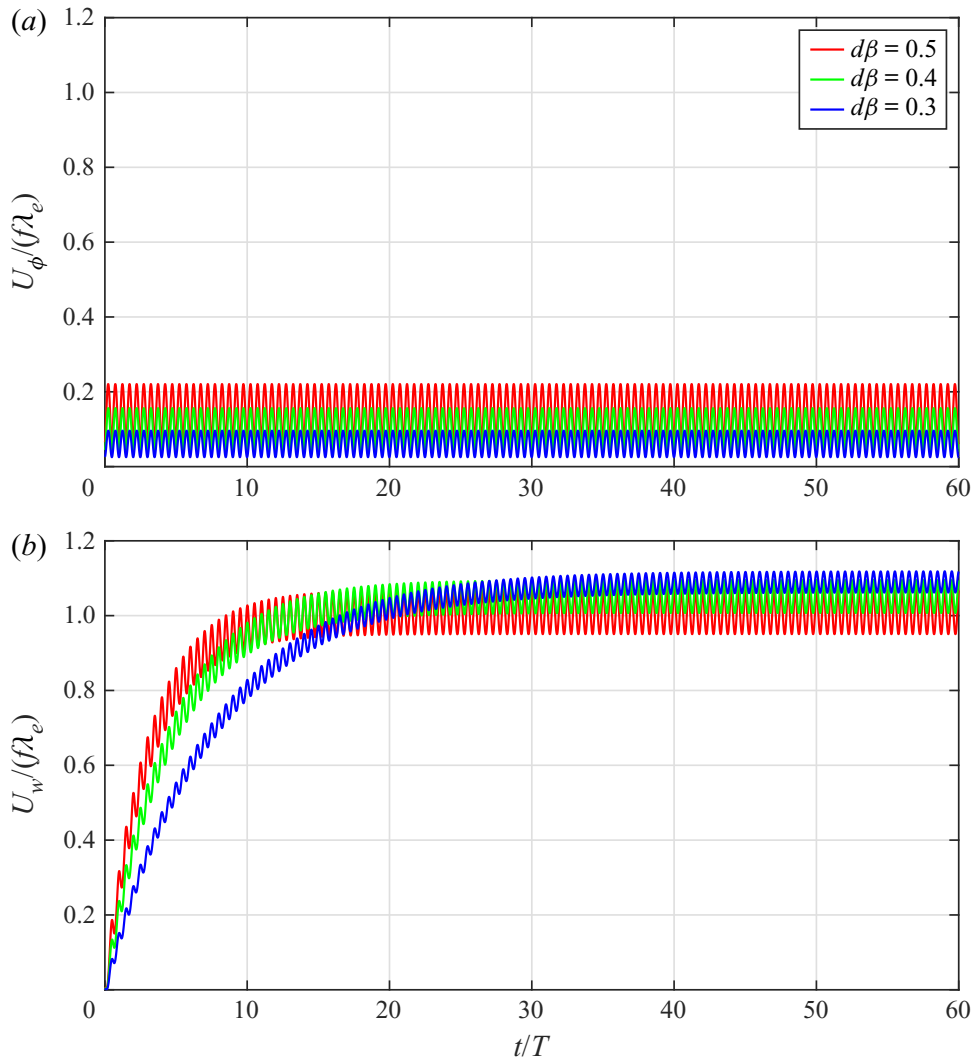
Added mass and vorticity release for self-propelled locomotion

Figure 7. Forward component of the slip velocity for $\rho = 1$ and different undulation amplitudes: (*a*) potential contributions; (*b*) vorticity contributions

a certain delay. At the same time, it is worth stressing that the rate of change of U_w in the transient is deeply related to the pure potential impulses since a larger added mass contribution induces a larger acceleration and a more intense vortex shedding, as shown in figure 8 and firmly stated by Limacher *et al.* (2018). From the above considerations, we can deduce that, for conditions usually adopted for efficient cruising at steady state, we should reduce U_ϕ, hence the contribution due to p_{sh} and π_{sh}, to have a lower intensity of the released vortices. In these conditions, the total velocity is essentially given by U_w, which may reach a large value although maintaining a weak vortex shedding. On the contrary, a large U_ϕ contribution is required in escape manoeuvres such as a C-start to give the initial instantaneous burst together with a larger acceleration accompanied by a larger energy consumption, as discussed below, which, however, is not a priority in this case. The following vortical contribution becomes eventually predominant at the end of the C-start manoeuvre, in a way analogous to, but more pronounced than, the steady swimming results.

At this point, looking at figure 5, we observe that the steady state velocity does not match the phase velocity and the following question arises: Why does the slip velocity differ from one? Actually, the wave phase velocity generated by the body and transferred to the fluid appears to depend on the whole motion of the body, i.e. prescribed undulation
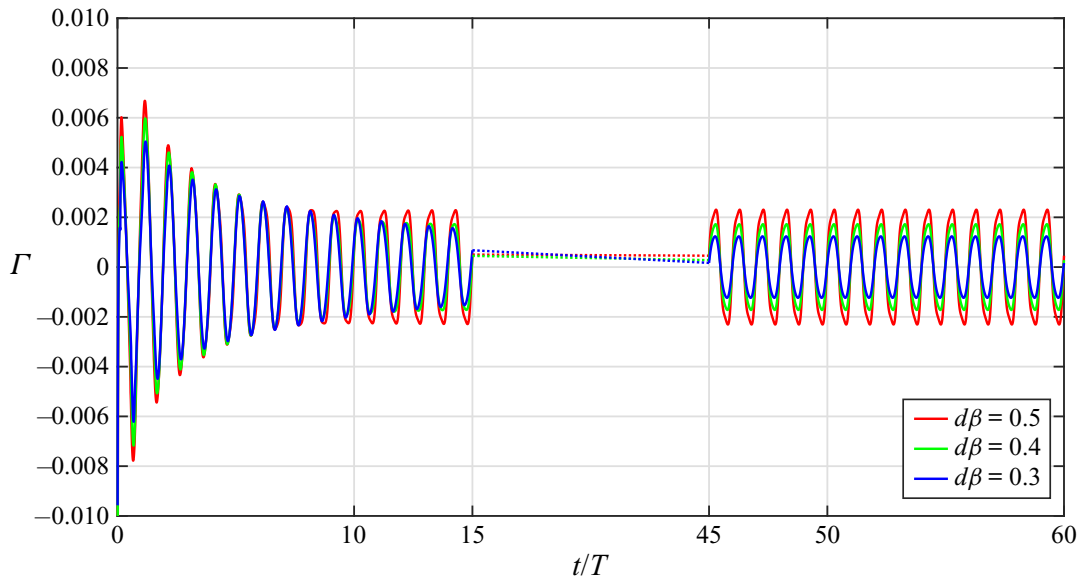
918 A45-15

Figure 8. Released circulation for different undulation amplitudes.

plus recoil. To verify the above observation, it is helpful to consider a well-established analytical model which may allow for a better understanding of the obtained results. More specifically, the elongated body theory (Lighthill 1960) provides an analytical expression to evaluate the time averaged thrust exerted on an undulating body by a fluid with an assigned uniform velocity U and a given lateral displacement $h(x, t)$

$$\bar{T} = \frac{1}{2}\rho_f A(L) \left[\overline{\left(\frac{\partial h}{\partial t}\right)^2} - U^2 \overline{\left(\frac{\partial h}{\partial x}\right)^2} \right]_{x=L}, \qquad (5.8)$$

where $A(L)$ is the added mass associated with the trailing edge of the body and the overline indicates a mean value over time. Afterwards, Lighthill introduced the concept of recoil associated with the displacement h, in terms of lateral and angular rigid motions that must be added to h in order to respect the corresponding equilibrium equations. For the sake of conciseness, only the equation for the lateral momentum balance is reported here

$$\rho_b \int_0^L S(x) \frac{\partial^2 h}{\partial t^2} \, dx = -\rho_f \int_0^L \left(\frac{\partial}{\partial t} + U\frac{\partial}{\partial x}\right) \left[A(x) \left(\frac{\partial h}{\partial t} + U\frac{\partial h}{\partial x}\right) \right] dx, \qquad (5.9)$$

where $S(x)$ is the cross-sectional area of the elongated body and $A(x)$ is the related added mass.

By introducing a travelling wave $\tilde{h}$ with phase velocity ω/k and amplitude a, i.e.

$$\tilde{h}(x, t) = a \sin(kx - \omega t), \qquad (5.10)$$

it is easy to show that zero thrust in (5.8) can be achieved if the velocity U is equal to the phase velocity. In fact, assuming $U = \omega/k$, the right-hand side of (5.9) is always equal to zero for the wave kinematic condition

$$\frac{\partial \tilde{h}}{\partial t} + \frac{\omega}{k} \frac{\partial \tilde{h}}{\partial x} = 0, \qquad (5.11)$$

while the left-hand side is different from zero, unless particular choice is made for $S(x)$,

918 A45-16

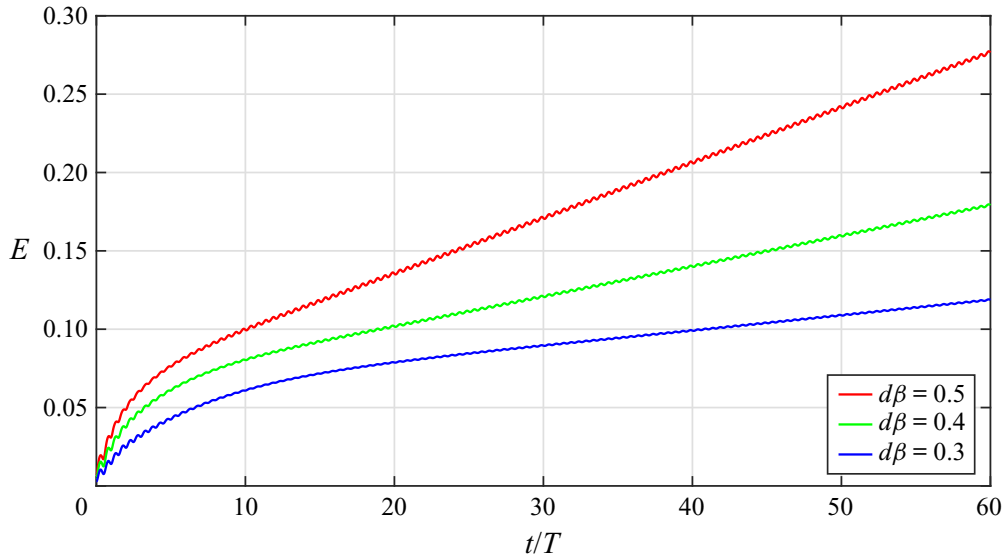*Added mass and vorticity release for self-propelled locomotion*

Figure 9. Time behaviour of the fluid kinetic energy for different deformation amplitudes.

i.e. the shape of the body. Hence, in principle, $\tilde{h}$ should be modified by taking into account the recoil motions $B(x, t)$ (see e.g. Singh & Pedley 2008)

$$h(x, t) = \tilde{h}(x, t) + B(x, t). \tag{5.12}$$

When the recoil is added to the original undulation, the total motion h no longer annihilates the thrust (5.8) for $U = \omega/k$, but either a rigid translation and/or a rotation motion modifies the asymptotic velocity as

$$U = \chi \frac{\omega}{k}, \tag{5.13}$$

where the factor χ, which can be evaluated by a very simple approximation, is larger than one for the present case. As a further assessment, let us notice that (5.9) is directly satisfied by $\tilde{h}$ when ρ_b, appearing on the left-hand side, is equal to zero, i.e. when a massless body is considered (see Kanso 2009). It follows that, in these conditions, no recoil motion occurs and the asymptotic velocity U is always equal to ω/k. In fact, a massless body is able to achieve the same forward speed as that of the fluid pushed backwards by the travelling wave since, in principle, the presence of the body is only attested by its virtual mass given by the surrounding fluid. If we extend the above reasoning, valid for the undulating body in a uniform stream, to the case of self-propelled locomotion, the same conclusion may be reached for the mean force in the forward direction, whose value tends to vanish at steady state conditions.

The just mentioned influence of the recoil on a prescribed deformation may be of great interest also for different phenomena related to swimming control means. For instance, by looking at (3.15) we may see how all the velocity components may substantially vary with the added mass coefficient m_{ij}, as perceived by certain types of fish able to change their configuration during a predator–prey interaction, as done by the sailfish by raising its dorsal fin (see Paniccia *et al.* 2021).

From an energy point of view, an intense vortex shedding results in a high consumption in terms of kinetic energy released into the flow field, as shown by figure 9. The fluid

918 A45-17

D. Paniccia, G. Graziani, C. Lugni and R. Piva

kinetic energy is obtained (see Graziani *et al.* 1995; Kanso 2009) as

$$E = \frac{1}{2} \int_S \phi \frac{\partial \phi}{\partial n} \, \mathrm{d}S + \frac{1}{2} \int_S (\boldsymbol{u}_w \times \boldsymbol{\psi}) \cdot \boldsymbol{n} \, \mathrm{d}S + \frac{1}{2} \int_V \boldsymbol{\psi} \cdot \boldsymbol{\omega} \, \mathrm{d}V. \qquad (5.14)$$

The first two integrals in (5.14) give a contribution which is negligible at steady state conditions, as a consequence of the oscillatory nature of the surface integrals. Actually, the time derivative of the injected energy can be estimated by the last integral, known as the excess energy, and its mean rate of change is a good approximation to the mean power transferred by the body to the fluid. Since the COT is defined as the ratio between the mean power required and the mean swimming velocity, we may see, by combining the results of figures 3 and 9, that high undulation amplitudes are more effective in terms of acceleration but less favourable in terms of COT. If different kinematics are considered, the mean forward velocity may be quite different and the comparison would be less immediate. For a further deepening it would be important to consider a dimensionless form of the COT, by the slip velocity and an appropriate reference power (Bale *et al.* 2014) to allow for a comparison among species characterized by very different masses and styles of swimming.

5.3. *Released vorticity and wake pattern*

From the above discussion, it is clear that a large contribution to the swimming velocity is associated with the release of vorticity, which plays an essential role in building up the final asymptotic steady state. As the vorticity is released, the body experiences a force along the direction of motion, whose nature may be understood by looking at the wake pattern, as first pointed out by von Kármán & Burgers (1935). The renown Kármán vortex street, which identifies a drag force on a blunt body, consists of vortex pairs of opposite sign arranged so that the clockwise eddies are positioned above the counterclockwise ones. In the case of an undulating fish-like body, a very similar phenomenon may occur due to the lateral displacement of the tail tip, leading to an inverse shedding sequence and to a wake pattern, known as the reverse Kármán street, in general associated with a propulsive capability of the swimmer. From a qualitative point of view, the wake pattern visualization may give a first glance evaluation of the force experienced by the body, without detailed calculations of local values along the surface. For instance, both types of Kármán street may be easily visualized with the present model by a numerical experiment able to obtain both an acceleration phase, representative of thrust, and a deceleration phase, representative of drag. The body initially undulates with an angular frequency $\omega_1 = 10 \, \mathrm{rad\,s}^{-1}$ and accelerates towards the corresponding asymptotic speed, then, if the frequency is abruptly halved, a deceleration occurs up to the new asymptotic speed as shown in figure 10. Correspondingly, figure 11 shows in a neat way the two different types of wake pattern, which reveal the different orientation of the so-called mushrooms, interestingly named footprints by Zhang (2017), which are related to the exchange of forces between fluid and body. However, this correspondence is not always well defined since, for steady locomotion, no average forces are exchanged and the wake configuration does not show a sharp distinction among the two patterns. In this case, it seems reasonable to say that a one-to-one correspondence between the swimming performance and the structure of the wake is not so easy to detect (Smits 2019).

6. Final remarks and comments

Self-propelled aquatic locomotion has to be studied by a proper procedure to allow for the undulating body to be completely free to swim, obeying the equilibrium of the internal
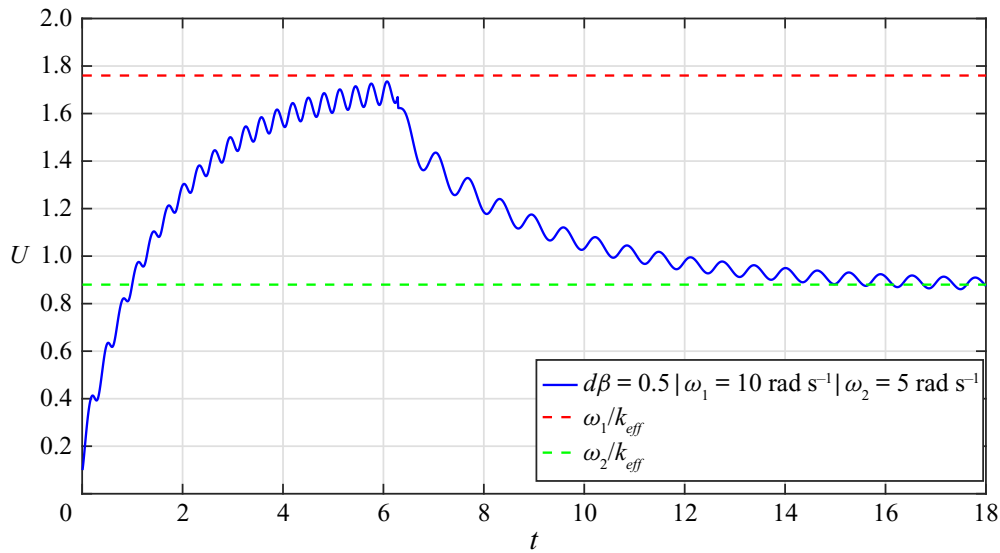
Figure 10. Time history of the forward swimming velocity in the presence of an abrupt frequency change: from $\omega_1 = 10$ rad s^{-1} to $\omega_2 = 5$ rad s^{-1}.
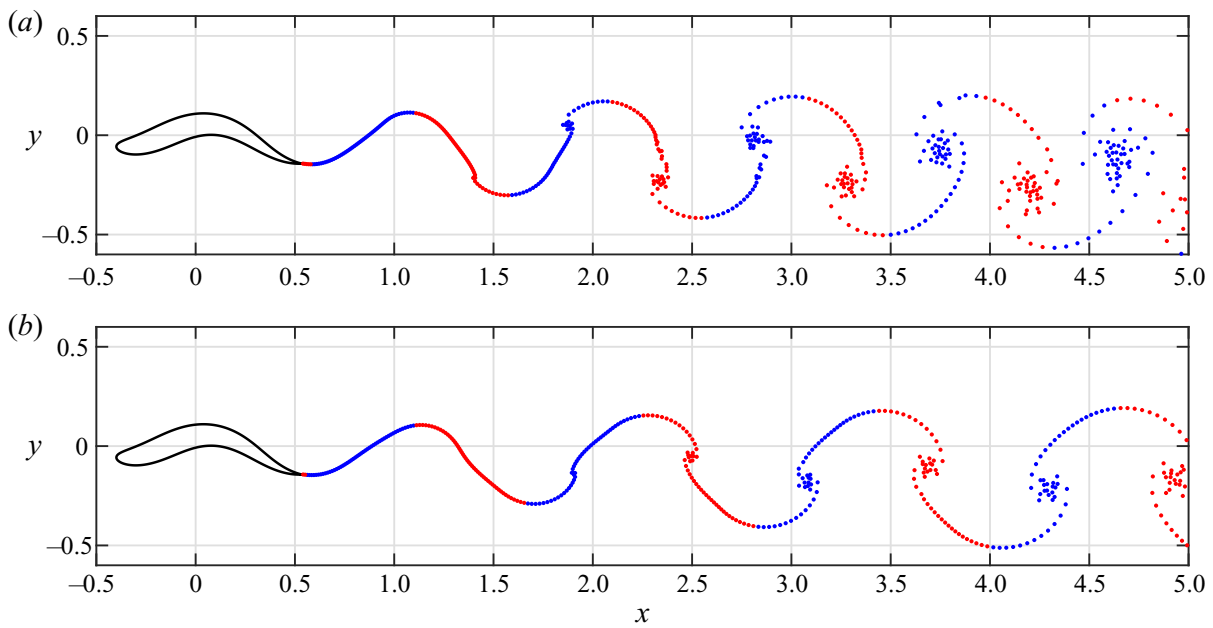

Figure 11. Acceleration phase reverse Kármán street wake pattern (*a*). Deceleration phase direct Kármán street wake pattern (*b*).

forces exchanged with the surrounding fluid. However, at steady state, many experimental and computational investigations, with notable exceptions in recent times, have been carried out by considering the body, with a prescribed deformation, in the presence of an incoming uniform stream or tethered with the opposite velocity. In these cases, the aim was to find the thrust and the injected power to evaluate the Froude efficiency. In fact, the most renowned physical models, built on those assumptions, were frequently taken as a guide and a theoretical framework to discuss the output of the investigations. At the same time, the desire to account for the recoil forces, as frequently recommended for the study of free swimming, led to quite involved procedures when a body under an incoming uniform stream was assumed.

918 A45-19

D. Paniccia, G. Graziani, C. Lugni and R. Piva

A completely different approach, proposed in the last decades, considered instead the locomotion velocity as the primary variable for free swimming of a deformable body, which has to be taken as part of a full system together with the surrounding fluid otherwise at rest. To better understand the intertwining effects of the added mass and the vorticity release, a 2-D model with concentrated vorticity was adopted to provide a flexible tool to cope with the complexity of the self-propelled motion accelerating from zero to a steady state asymptotic velocity. For this purpose, several simulations were reported to clarify the physical contributions due to added mass and to vorticity release in terms of motion and expended power.

On the one hand, the effect of the added mass, easily expressed in terms of the non-circulatory potential impulses, provides the instantaneous burst, which is essential to activate the release of vorticity shed into the wake. On the other hand, the effect of the released vortices, easily measured by the vortical impulse, leads to a gradual increase of the velocity up to steady state. The combined action of the above physical phenomena is clearly shown by the time history of the velocity whose asymptotic value is guided by the phase velocity of the travelling wave together with a proper account of the recoil motion. The starting acceleration, which is increasing for larger amplitudes of the deformation, provides a fast escape even though with a larger request of energy.

The kinematic variables, as the natural unknowns of the free-swimming problem, give the trajectory of the deformable body i.e. the motion generated by the internal forces exchanged with the surrounding fluid, including a complete account of the recoil reactions. Several results reported in Paniccia *et al.* (2021) show that, any attempt to constrain the trajectory by reducing the degrees of freedom in the numerical solution, would lead to different body motions less efficient than free swimming. The request to compare different gaits leads, in a straightforward way, to measurement of the efficiency by using the output of the present model, i.e. the velocity and the expended power, as clearly expressed by the COT, since the traditional Froude efficiency is not a proper measure in this case.

To have a preliminary account of the role of vorticity diffusion, missing in the present model, a simple approximation has been devised to evaluate how the influence of the deformation amplitude may be sensitive to the presence of an extra resistance. The results are encouraging and the decrease of the asymptotic velocity for lower amplitudes of the deformation confirmed previous results. A step forward, able to maintain the valid properties of the present model, should take into account the diffusion of vorticity, to recover a handy viscous vortex model (see e.g. Rossi, Colagrossi & Graziani 2015; Durante *et al.* 2017), for a more realistic representation of a larger number of physical cases. As an ultimate comment, we would like to mention that the above analysis, beyond its theoretical interest, may be of great help in defining, as briefly observed for certain types of fish, some suitable parameters for bio-mimetic design of engineering applications with a focus on simplified control means.

Author ORCIDs.
G. Graziani https://orcid.org/0000-0002-7522-6755;
C. Lugni https://orcid.org/0000-0003-3747-6048.

Appendix A

For the sake of convenience we report below a few vector identities used to obtain some of the expressions reported within the previous sections.

Given a vector field $\boldsymbol{u}$ defined over a volume V bounded inside by S_b and outside by S, the following vector identity holds ($N = 2,3$ is the dimension of the space and the normal $\boldsymbol{n}$ points in V on S_b and outwards on S)

$$\int_V \boldsymbol{u}\,\mathrm{d}V = \frac{1}{N-1}\int_V \boldsymbol{x}\times\boldsymbol{\omega}\,\mathrm{d}V + \frac{1}{N-1}\int_{S_b}\boldsymbol{x}\times(\boldsymbol{n}\times\boldsymbol{u})\,\mathrm{d}S$$
$$-\frac{1}{N-1}\int_S \boldsymbol{x}\times(\boldsymbol{n}\times\boldsymbol{u})\,\mathrm{d}S. \qquad (A1)$$

Given a single-valued scalar field ϕ and a closed surface S, from the generalized Stokes' theorem it holds (referred to by Noca as the pressure identity)

$$\frac{1}{N-1}\int_S \boldsymbol{x}\times(\boldsymbol{n}\times\nabla\phi)\,\mathrm{d}S = -\int_S \phi\boldsymbol{n}\,\mathrm{d}S. \qquad (A2)$$

For the same vector field in (A1) (Wu *et al.* 2015)

$$\int_V \boldsymbol{x}\times\boldsymbol{u}\,\mathrm{d}V = -\tfrac{1}{2}\int_V |x|^2\boldsymbol{\omega}\,\mathrm{d}V - \tfrac{1}{2}\int_{S_b}|x|^2\boldsymbol{n}\times\boldsymbol{u}\,\mathrm{d}S + \tfrac{1}{2}\int_S |x|^2\boldsymbol{n}\times\boldsymbol{u}\,\mathrm{d}S. \qquad (A3)$$

Given a scalar field ϕ and a closed surface S, it holds that

$$\tfrac{1}{2}\int_S |x|^2(\boldsymbol{n}\times\nabla\phi)\,\mathrm{d}S = \int_S \boldsymbol{x}\times\phi\boldsymbol{n}\,\mathrm{d}S. \qquad (A4)$$

REFERENCES

Akoz, E. & Moored, K.W. 2018 Unsteady propulsion by an intermittent swimming gait. *J. Fluid Mech.* **834**, 149–172.

Bale, R., Hao, M., Bhalla, A.P.S. & Patankar, N.A. 2014 Energy efficiency and allometry of movement of swimming and flying animals. *Proc. Natl Acad. Sci.* **111** (21), 7517–7521.

Basu, B.C. & Hancock, G.J. 1978 The unsteady motion of a two-dimensional aerofoil in incompressible inviscid flow. *J. Fluid Mech.* **87** (1), 159–178.

Bhalla, A.P.S., Bale, R., Griffith, B.E. & Patankar, N.A. 2013 A unified mathematical framework and an adaptive numerical method for fluid-structure interaction with rigid deforming and elastic bodies. *J. Comput. Phys.* **250**, 446–476.

Borazjani, I. & Sotiropoulos, F. 2009 Numerical investigation of the hydrodynamics of anguilliform swimming in the transitional and inertial flow regimes. *J. Expl Biol.* **212**, 576–592.

Borazjani, I. & Sotiropoulos, F. 2010 On the role of form and kinematics on the hydrodynamics of self-propelled body/caudal fin swimming. *J. Expl Biol.* **213**, 89–107.

Carling, J., Williams, T.L. & Bowtell, G. 1998 Self-propelled anguilliform swimming simultaneous solution of the two-dimensional Navier–Stokes equations and Newtons laws of motion. *J. Expl Biol.* **201**, 3143–3166.

Childress, S. 2009 *An Introduction to Theoretical Fluid Dynamics*. Courant Lecture Notes, vol. 19. AMS.

Chorin, A.J. 1973 Numerical study of slightly viscous flow. *J. Fluid Mech.* **57**, 785–796.

Dong, G. & Lu, X. 2007 Characteristics of flow over traveling wavy foils in a side-by-side arrangement. *Phys. Fluids* **19**, 057107.

Durante, D., Rossi, E., Colagrossi, A. & Graziani, G. 2017 Numerical simulations of the transition from laminar to chaotic behaviour of the planar vortex flow past a circular cylinder. *Commun. Nonlinear Sci. Numer. Simul.* **48**, 18–38.

Eldredge, J.D. 2010 A reconciliation of viscous and inviscid approaches to computing locomotion of deforming bodies. *Exp. Mech.* **50**, 1349–1353.

D. Paniccia, G. Graziani, C. Lugni and R. Piva

ELDREDGE, J.D., COLONIUS, T. & LEONARD, A. 2002 A vortex particle method for two-dimensional compressible flow. *J. Comput. Phys. Mech.* **179**, 371–399.

GAZZOLA, M., CHATELAIN, P., VAN REES, W.M. & KOUMOUTSAKOS, P. 2011 Simulations of single and multiple swimmers with non-divergence free deforming geometries. *J. Comput. Phys.* **230**, 7093–7114.

GRAY, J. 1933 Studies in animal locomotion. *J. Expl Biol.* **10**, 386–400.

GRAZIANI, G. & BASSANINI, P. 2002 Unsteady viscous flows about bodies: vorticity release and forces. *Meccanica* **37**, 283–303.

GRAZIANI, G., RANUCCI, M. & PIVA, R. 1995 From a boundary integral formulation to a vortex method for viscous flows. *Comput. Mech.* **15**, 30l–314.

HESS, F. & VIDELER, J.J. 1984 Fast continuous swimming of saithe (pollachius virens): a dynamical analysis of bending moments and muscle power. *J. Expl Biol.* **109**, 229–251.

HESS, J.L. & SMITH, A.M.O. 1967 Calculation of potential flow about arbitrary bodies. *Prog. Aerosp. Sci.* **8**, 1–138.

KANSO, E. 2009 Swimming due to transverse shape deformations. *J. Fluid Mech.* **631**, 127–148.

VON KÁRMÁN, T. & BURGERS, J.M. 1935 E. General aerodynamic theory. Perfect fluids. In *Aerodynamic Theory* (ed. W.F. Durand), vol. 2, p. 308. Springer.

KERN, S. & KOUMOUTSAKOS, P. 2006 Simulations of optimized anguilliform swimming. *J. Expl Biol.* **209**, 4841–4857.

KOUMOUTSAKOS, P. & LEONARD, A. 1995 High-resolution simulations of the flow around an impulsively started cylinder using vortex methods. *J. Fluid Mech.* **296**, 1–38.

LAMB, H. 1975 *Hydrodynamics*, 6th edn. Cambridge University Press.

LANDAU, L.D. & LIFSCHITZ, E.M. 1986 *Fluid Mechanics*, 2nd edn., vol. 6. Pergamon Press.

LAUDER, G.V. 2015 Fish locomotion: recent advances and new directions. *Annu. Rev. Mar. Sci.* **7**, 521–545.

LAUDER, G.V. & TYTELL, E.D. 2005 Hydrodynamics of undulatory propulsion. *Fish Physiol.* **23**, 425–468.

LIGHTHILL, J. 1960 Note on the swimming of slender fish. *J. Fluid Mech.* **9** (2), 307–317.

LIGHTHILL, J. 1969 Hydromechanics of aquatic animal propulsion. *Annu. Rev. Fluid Mech.* **1** (1), 413–446.

LIGHTHILL, J. 1970 Aquatic animal propulsion of high hydromechanical efficiency. *J. Fluid Mech.* **44**, 265–301.

LIMACHER, E. 2019 Added mass and vortical impulse: theory and experiment. PhD thesis, University of Calgary (CA).

LIMACHER, E., MORTON, C. & WOOD, D. 2018 Generalized derivation of the added-mass and circulatory forces for viscous flows. *Phys. Rev. Fluids* **2**, 014701.

MAERTENS, A.P., GAO, A. & TRIANTAFYLLOU, M.S. 2017 Optimal undulatory swimming for single fish-like body and for pair of interacting swimmers. *J. Fluid Mech.* **813**, 301–345.

MAERTENS, A.P., TRIANTAFYLLOU, M.S. & YUE, D.K.P. 2015 Efficiency of fish propulsion. *Bioinspir. Biomim.* **10**, 046013.

NOCA, F. 1997 On the evaluation of time-dependent fluid dynamic forces on bluff bodies. PhD thesis, California Institute of Technology.

PANICCIA, D., GRAZIANI, G., LUGNI, C. & PIVA, R. 2021 The relevance of recoil and free swimming in aquatic locomotion. *J. Fluid Struct.* **103**, 103290.

REID, D.A.P., HILDENBRANDT, H., PADDING, J.T. & HEMELRIJK, C.K. 2012 Fluid dynamics of moving fish in a two-dimensional multiparticle collision dynamics model. *Phys. Rev. E* **85**, 021901.

ROSSI, E., COLAGROSSI, A. & GRAZIANI, G. 2015 Numerical simulation of 2d-vorticity dynamics using particle methods. *Comput. Maths Appl.* **69** (12), 1484–1503.

SAFFMAN, P.G. 1967 The self-propulsion of a deformable body in a perfect fluid. *J. Fluid Mech.* **28** (2), 385–389.

SAFFMAN, P.G. 1992 *Vortex Dynamics*. Cambridge University Press.

SCHULTZ, W.W. & WEBB, P.W. 2002 Power requirements of swimming: do new methods resolve old questions? *Integr. Compar. Biol.* **42**, 1018–1025.

SINGH, K. & PEDLEY, T.J. 2008 The hydrodynamics of flexible-body manoeuvres in swimming fish. *Physica* D **237**, 2234–2239.

SMITS, A.J. 2019 Undulatory and oscillatory swimming. *J. Fluid Mech.* **874**, P1.

SPAGNOLIE, S.E. & SHELLEY, M.J. 2009 Shape-changing bodies in fluid: hovering, ratcheting, and bursting. *Phys. Fluids* **21**, 013103.

STEELE, S.C. 2016 Shape change for global vorticity shedding and added mass energy recovery. PhD thesis, Massachusetts Institute of Technology.

TAYLOR, G.I. 1952 Analysis of the swimming of long and narrow animals. *Proc. R. Soc.* A **214** (1117), 158–183.

TYTELL, E.D. 2004 The hydrodynamics of eel swimming: ii effect of swimming speed. *J. Expl Biol.* **207**, 3265–3279.

VIDELER, J. 1993 *Fish Swimming*. Fish and Fisheries Series, vol. 10, Springer Chapman-Hall.

VON KÁRMÁN, T. & GABRIELLI, G. 1950 What price speed? Specific power required for propulsion. *Mech. Engng* **72**, 775–781.

WANG, Z.W., YU, Y.L. & TONG, B.G. 2018 An energetics analysis of fish self-propelled swimming. *Sci. China Phys.* **61** (7), 074721.

WEBB, P. 1975 Hydrodynamics and energetics of fish propulsion. *Bull. Fis. Res. Board Can.* **190**, 1–159.

WOLFGANG, M.J., ANDERSON, J.M., GROSENBAUGH, M.A., YUE, D.K.P. & TRIANTAFYLLOU, M.S. 1999 Near-body flow dynamics in swimming fish. *J. Expl Biol.* **202**, 2303–2327.

WU, J.Z., MA, H.Y. & ZHOU, M.D. 2015 *Vortical Flows*. Springer.

WU, T.Y. 1961 Swimming of a waving plate. *J. Fluid Mech.* **10** (3), 321–344.

WU, T.Y. 2011 Fish swimming and bird/insect flight. *Annu. Rev. Fluid Mech.* **43**, 25–58.

YANG, Y., WU, G.H., YU, Y.L. & TONG, B.G. 2008 Two-dimensional self-propelled fish motion in medium an integrated method for deforming body dynamics and unsteady fluid dynamics. *Chin. Phys. Lett.* **25** (2), 597–600.

ZHANG, D., PAN, G., CHAO, L. & YAN, G. 2018 Mechanisms influencing the efficiency of aquatic locomotion. *Mod. Phys. Lett.* B **32**, 1850299.

ZHANG, J. 2017 Footprints of a flapping wing. *J. Fluid Mech.* **818**, 1–4.

The relevance of recoil and free swimming in aquatic locomotion

Damiano Paniccia [a,*], Giorgio Graziani [a], Claudio Lugni [b,c,d], Renzo Piva [a]

[a] *Department of Mechanical and Aerospace Engineering, University of Rome "La Sapienza", Via Eudossiana, 18 - 00184 Rome, Italy*
[b] *CNR-INM, Marine Technology Research Institute, Rome, Italy*
[c] *NTNU-AMOS, Center for Autonomous Marine Operation Systems, Trondheim, Norway*
[d] *Institute of Marine Hydrodynamics, Harbin Engineering University, Harbin, China*

A B S T R A C T

The study of the free swimming of undulating bodies in an otherwise quiescent fluid has always encountered serious difficulties for several reasons. When considering the full system, given by the body and the unbounded surrounding fluid, the absence of external forces leads to a subtle interaction problem dominated, at least at steady state conditions, by the equilibrium of strictly related internal forces, e.g. thrust and drag, under the forcing of a prescribed deformation. A major complication has been dictated by the recoil motion induced by the non linear interactions, which may find a quite natural solution when considering as unknowns the velocity components of the body center of mass. A simplified two-dimensional model in terms of impulse equations has been used and a fruitful separation of the main contributions due to added mass and to vorticity release is easily obtained. As main results we obtain either the mean locomotion speed and the oscillating recoil velocity components which have a large effect on the overall performance of free swimming. Several constrained gaits are considered to highlight the relevance of recoil for realizing graceful and efficient trajectories and to analyze its potential means for active control.

1. Introduction

The swimming of a deformable body in water, either fish or cetacean, has been studied since the beginning (see e.g. Bainbridge, 1958; Lighthill, 1960; Wu, 1961), by considering the body held in a fixed position under an incoming uniform stream, or tethered with an opposite velocity, to evaluate the performance at steady state conditions. This choice was considered the most favorable for the implementation of simplified mathematical models and instrumental for experimental techniques or for computational solutions. As a consequence, the prevailing attention at the time was given to the resulting thrust which leads, together with the expended power, to the evaluation of the well known Froude efficiency (see e.g. Lighthill, 1960), usually adopted for marine vehicles where the propulsive force is easily separated from the resistive one. Hence, apart from the assigned stream in the forward direction, the other body motions either lateral or angular, perceived as recoil motions, did receive in general a secondary interest or no interest at all. To the best of our knowledge, Lighthill was the first one, at the beginning of the 60s, to emphasize the importance of the recoil, induced by the fluid–body interactions. He did actually pursue, as primary objective of his elongated body theory, the evaluation of thrust and efficiency produced by the prescribed deformation, but he analyzed also the recoil motion as a required

---

correction to satisfy the equilibrium equations. Subsequently, several numerical investigations (see e.g. Maertens et al., 2017) tried to determine by the same procedure the effects of the recoil motion on the overall performance.

Since the animal muscular contractions give rise only to a change of shape relative to the center of mass, the whole body motion including the recoil should be given primarily by the center of mass motion generated by the interaction with the surrounding fluid. To this aim, an approach more suitable for self-propelled swimming was suggested by Saffman (1967) and subsequently adopted in numerical simulations by Carling et al. (1998), Kern and Koumoutsakos (2006), Borazjani and Sotiropoulos (2010), Yang et al. (2008), among others. The free-swimming mode provides as unknowns of the problem the velocity components of the body center of mass under the action of the internal forces exchanged with the otherwise quiescent fluid. Along this line, the motion of a deformable body in an unbounded fluid domain and in the absence of external forces, is analyzed here by imposing the conservation of momentum and of its moment for the entire fluid–body system. The undulatory deformation is usually prescribed, so to conserve linear and angular momenta in the absence of fluid, while the kinematic variables for the body center of mass are obtained by solving the equilibrium equations. Namely, the mean forward velocity in the body frame gives the animal locomotion while the oscillatory angular and lateral velocities are identified as the recoil motions with a significant impact on the swimming performance. The oscillatory part of the forward velocity is also obtained, but, as recognized by many authors (Bale et al., 2014; Smits, 2019), it plays a minor role in most cases.

Recently, several contributions in experimental biology fostered the measurements of the center of mass position, in a frame moving with the mean forward velocity, as a tool for evaluating and comparing different species and different styles of swimming (see e.g. Lauder, 2015; Xiong and Lauder, 2014). Actually, the forward, lateral and angular oscillating velocity components (surge, sway and yaw) are easily obtained with the present model while heave, i.e. the motion in the third direction, is not so important in fish swimming. The numerical values of the oscillating velocities, properly treated by statistical tools, may reveal the main properties of the self propelled locomotion as a signature of the style of swimming.

Purpose of the paper is to define the role of the recoil for a self-propelled body under a prescribed deformation and a non linear interaction with the surrounding fluid. The motion of the body center of mass, in terms of locomotion speed and of oscillating recoil velocities, is the most natural quantity to evaluate. To reduce this subtle problem to its essential features, as suggested by Schultz and Webb (2002) and recently by Akoz et al. (2019), we consider a two-dimensional potential flow model with generation of non-diffusing vorticity and its release from the trailing edge. In this way the related numerical scheme is able to separate the contribution of potential and of vortical impulse, by highlighting their different roles in the time evolution of the unsteady solution. The identification of the added mass term may provide a useful key for a physical interpretation of unsteady phenomena (see e.g. Limacher et al., 2018) while the analysis of the wake evolution, essential to define the asymptotic value of the locomotion speed, allows for the calculation of the energy injected into the fluid (see e.g. Bale et al., 2014). For the well known difficulties to disentangle the internal forces, given by thrust and drag, the standard measures of the efficiency are not easily detectable and we adopt a suitable form of the cost of transport (see e.g. von Kármán and Gabrielli, 1950; Bale et al., 2014) to evaluate the efficiency of the different styles of swimming . Moreover, we discuss with particular care the oscillating velocity components of the center of mass which have a notable importance for understanding different swimming modes and related means for active control.

Among the numerical results, for a better evaluation of free swimming features we analyze in comparison, as originally proposed by Reid et al. (2012), the simulations of constrained motions which are representative of cases where some recoil reactions are prevented. To obtain constrained gaits by the present model it is convenient to annihilate either one or more velocity components in the body frame, among lateral motion and rotation. As a primary result, the efficiency, in terms of the cost of transport, is measured for each one of the above simulations to assess the free swimming performance for aquatic locomotion. A simple tool for the active control of swimming may be obtained by modifying the recoil reaction throughout a sudden variation of the shape. For instance, as suggested by Domenici et al. (2014), the sailfish is able to raise a vertical fin to reduce lateral and angular oscillations with the aim to stabilize the trajectory during a predator–prey interaction. We will see by a crude approximation that an increase of the related components of the fish added mass matrix, consistent with the sail raising, may be instrumental to implement the required pattern control.

2. Material and methods

2.1. Mathematical model

We study the motion of a two-dimensional deformable body within an infinite volume of initially quiescent fluid with constant density. Since no external forces or moments are applied to the fluid–body domain, the self-propelled motion is due to the body undulations. In other words the total linear and angular momenta are conserved for the whole domain, while the forces and moments exchanged between fluid and body appear as internal actions. To express the equations for the fluid–body dynamics we adopt the classical formulation in terms of potential and vortical impulses that overcomes the difficulties to treat an unbounded domain, as largely discussed in the literature (see e.g. Landau and Lifschitz, 1986; Wu et al., 2006), and avoids the evaluation of the pressure on the body contour. Through the impulse formulation we can emphasize the contribution of the acyclic (non circulatory) potential as well as the effects of both the free vorticity and the cyclic part of the bound vorticity. A detailed formulation, though focused on pure potential flow, is given by Kanso (2009) while the extension to generated and released vorticity (see also Eldredge, 2007) is briefly presented here.

The locomotion of the deformable body is obtained by coupling the dynamics of the body and of the surrounding fluid. If we consider the body–fluid system $(\mathcal{V}_b + \mathcal{V}_f)$, in the absence of external forces and moments the linear and angular momenta are conserved as given by

$$\frac{d}{dt}\left[\int_{\mathcal{V}_b} \rho_b\, \mathbf{u}_b\, dV + \int_{\mathcal{V}_f} \rho\, \mathbf{u}\, dV\right] = 0 \tag{1}$$

$$\frac{d}{dt}\left[\int_{\mathcal{V}_b} \rho_b\, \mathbf{x} \times \mathbf{u}_b\, dV + \int_{\mathcal{V}_f} \rho\, \mathbf{x} \times \mathbf{u}\, dV\right] = 0 \tag{2}$$

where $(\rho_b, \mathbf{u}_b)$ and $(\rho, \mathbf{u})$ are the density and the velocity of body and fluid, respectively.

Since forces and moments are not required in the present procedure, we may neglect in the above Eqs. (1)–(2) the time differentiation which would otherwise lead to a subsequent integration to find the kinematics of the body. Hence, by assuming an initial condition of quiescent fluid, we obtain a very efficient solution.

The second term within the square brackets in (1) is the fluid impulse $\mathbf{p}$ which can be expressed, via a well known vector identity, by two contributions due to the field vorticity $\boldsymbol{\omega}$ and to the vortex sheet over the body surface (see e.g. Noca et al., 1999; Wu et al., 2006; Graziani and Bassanini, 2002):

$$\mathbf{p} = \rho\left[\int_{\mathcal{V}_f} \mathbf{x} \times \boldsymbol{\omega}\, dV + \int_{S_b} \mathbf{x} \times (\mathbf{n} \times \mathbf{u})\, dS\right] \tag{3}$$

where S_b is the body contour, $\mathbf{n}$ is the normal vector to S_b pointing into the flow domain and $\mathbf{u}$ is here the limiting value of the fluid velocity on S_b.

Another vector identity, is used for the second integral in (2) yielding an expression for the angular momentum (positive anticlockwise) on the body. Here we consider the moment with respect to a given pole (to be specified later either as the origin of the ground reference frame or as the body center of mass), so $\mathbf{x}$ is the generic distance of the field point from the pole. The angular impulse $\boldsymbol{\pi}$ is defined as:

$$\boldsymbol{\pi} = -\frac{1}{2}\rho\left[\int_{\mathcal{V}_f} |x|^2 \boldsymbol{\omega}\, dV + \int_{S_b} |x|^2 (\mathbf{n} \times \mathbf{u})\, dS\right] \tag{4}$$

The velocity field $\mathbf{u}$ is expressed through the Helmholtz decomposition as the sum of the acyclic component and of the vorticity related one (i.e. wake plus the cyclic part of the bound vortex sheet):

$$\mathbf{u} = \nabla\phi + \nabla \times \boldsymbol{\Psi} = \nabla\phi + \mathbf{u}_w \tag{5}$$

where ϕ and $\boldsymbol{\Psi}$ are referred to as the scalar and the (solenoidal) vector potential, respectively. These are given by the solution of the Laplace/Poisson equation, subject to the impermeable boundary condition on S_b and to a vanishing velocity at infinity.

The fluid impulse $\mathbf{p}$ given by (3) can be expressed in terms of its potential and vortical components, $\mathbf{p}_\phi$ and $\mathbf{p}_v$ respectively, where $\mathbf{p}_v$ is defined by adding the contributions of the released vorticity $\boldsymbol{\omega}$ and of the cyclic part of the bound vorticity $\mathbf{n} \times \mathbf{u}_w$ on S_b:

$$\mathbf{p}_v = \rho\left[\int_{\mathcal{V}_f} \mathbf{x} \times \boldsymbol{\omega}\, dV + \int_{S_b} \mathbf{x} \times (\mathbf{n} \times \mathbf{u_w})\, dS\right]$$

to follow Lighthill's concept of additional vorticity which is given by summing up the field vorticity to the bound vorticity minus its potential part (which is related to the added mass).

The acyclic potential contribution $\mathbf{p}_\phi$, via a renown vector identity, is given by:

$$\mathbf{p}_\phi = \int_{S_b} \mathbf{x} \times (\mathbf{n} \times \nabla\phi)\, dS = -\rho \int_{S_b} \phi\, \mathbf{n}\, dS \tag{6}$$

The expression for the angular momentum can be similarly obtained by separating the potential $\boldsymbol{\pi}_\phi$ and the vortical $\boldsymbol{\pi}_v$ impulses as:

$$\boldsymbol{\pi}_\phi = -\rho \int_{S_b} \phi\, \boldsymbol{x} \times \mathbf{n}\, dS \tag{7}$$

$$\boldsymbol{\pi}_v = -\frac{1}{2}\rho\left[\int_{\mathcal{V}_f} |x|^2 \boldsymbol{\omega}\, dV + \int_{S_b} |x|^2 (\mathbf{n} \times \mathbf{u}_w)\, dS\right] \tag{8}$$

To enforce the conservation of the total impulses, the linear and angular momenta of the body have to be evaluated. To this aim, the location of the body center of mass $\mathbf{x}_{cm}$ and its velocity are defined by:

$$\mathbf{x}_{cm} = \frac{1}{m_b} \int_{\mathcal{V}_b} \rho_b \mathbf{x}_b \, dV \qquad\qquad \mathbf{u}_{cm} = \frac{d}{dt}\mathbf{x}_{cm} = \frac{1}{m_b} \int_{\mathcal{V}_b} \rho_b \mathbf{u}_b \, dV \tag{9}$$

where m_b is the body mass. Consequently, Eq. (1) yields:

$$m_b \, \mathbf{u}_{cm} + \mathbf{p} = 0 \tag{10}$$

Similarly, the angular impulse is recast from Eq. (4) in terms of the distance $\mathbf{x}'$ measured from $\mathbf{x}_{cm}$ as $\pi' = (\boldsymbol{\pi} - \mathbf{x}_o \times \mathbf{p}) \cdot \mathbf{e}_3$ where $\mathbf{x}_o$ is a given reference point. Hence, the angular momentum balance reduces to:

$$I_{zz} \, \Omega + \pi' = 0 \tag{11}$$

where I_{zz} is the moment of inertia with respect to the center of mass and Ω is the angular velocity.

The self-propelled motion of the body is described by the above reported Eqs. (10) and (11) in terms of $\mathbf{u}_{cm}$ and Ω which provide the locomotion speed and the recoil oscillating motions.

By using a Cartesian inertial frame $(\mathbf{e}_1, \mathbf{e}_2, \mathbf{e}_3)$, the body motion occurs in the plane $(\mathbf{e}_1, \mathbf{e}_2)$ and its translation is given by: $\mathbf{x}_o = x_o \mathbf{e}_1 + y_o \mathbf{e}_2$. Moreover, the body may undergo a rotation θ about the axis $\mathbf{e}_3$.

The motion of the body can be expressed as the sum of the prescribed deformation (shape variations with velocity $\mathbf{u}_{sh}$) plus the motion (with translational, $\mathbf{u}_{cm}$, and angular, Ω, velocities) of the center of mass (cm) reference frame. In the ground fixed inertial frame the angular velocity is $\Omega = \dot{\theta} \, \mathbf{e}_3 \equiv \Omega \, \mathbf{e}_3$. The linear velocity is $\mathbf{u}_{cm} = \dot{x}_o \mathbf{e}_1 + \dot{y}_o \mathbf{e}_2$. Thus we can express the body motion as:

$$\mathbf{u}_b = \mathbf{u}_{sh} + \mathbf{u}_{cm} + \Omega \times \mathbf{x}' \tag{12}$$

where $\mathbf{x}'$ is the position vector in the body reference frame, i.e.: $\mathbf{x} = \mathbf{x}_{cm} + \mathbf{x}'$. If Eq. (12) holds, the prescribed deformation has to satisfy:

$$\int_{\mathcal{V}_b} \rho_b \mathbf{u}_{sh} \, dV = 0 \qquad\qquad \int_{\mathcal{V}_b} \rho_b \mathbf{x}' \times \mathbf{u}_{sh} \, dV = 0 \tag{13}$$

Many authors (see e.g. Lighthill, 1970; Borazjani and Sotiropoulos, 2008; Reid et al., 2012; Maertens et al., 2017) adopt a generic deformation $\overline{\mathbf{u}}_{sh}$ which does not generally satisfy Eqs. (13), leading to

$$\int_{\mathcal{V}_b} \rho_b \overline{\mathbf{u}}_{sh} \, dV = m_b \boldsymbol{u}_o \qquad\qquad \int_{\mathcal{V}_b} \rho_b (\mathbf{x}' \times \overline{\mathbf{u}}_{sh}) \cdot \mathbf{e}_3 \, dV = I_{zz} \Omega_o \tag{14}$$

In this case to maintain our approach, the rigid motions given by $\boldsymbol{u}_o$ and Ω_o have to be removed since they should not be imposed on the self-propelled body as deeply analyzed by Bhalla et al. (2013) (see also Singh and Pedley, 2008).

The scalar potential ϕ introduced by the Helmholtz decomposition is further divided as $\phi = \phi_{sh} + \phi_{loc}$, where ϕ_{sh} is given by the imposed deformation velocity $\mathbf{u}_{sh}$ and ϕ_{loc} is given by the combination of the locomotion linear and angular velocity $\mathbf{u}_{cm}$ and Ω, according to the related boundary conditions on S_b

$$\frac{\partial \phi_{sh}}{\partial n} = \boldsymbol{u}_{sh} \cdot \boldsymbol{n} \qquad\qquad \frac{\partial \phi_{loc}}{\partial n} = (\boldsymbol{u}_{cm} + \Omega \times \boldsymbol{x}') \cdot \boldsymbol{n}$$

A similar decomposition holds for both the linear and the angular impulses, i.e. $\boldsymbol{p}_\phi = \boldsymbol{p}_{sh} + \boldsymbol{p}_{loc}$ and $\pi'_\phi = \pi'_{sh} + \pi'_{loc}$. Finally, the locomotion impulses, $\boldsymbol{p}_{loc}$ and π'_{loc}, can be expressed in terms of the added mass coefficients reported in the classical treatises (see e.g. Lamb, 1975). For a body motion given by $\boldsymbol{u}_{cm}$ and Ω, we consider the Kirchhoff base potentials Φ_j to express $\phi_{loc} = u_{cm1}\Phi_1 + u_{cm2}\Phi_2 + \Omega \Phi_3$. When this decomposition is combined with the linear and angular fluid potential impulses, the relevant added mass coefficients m_{ij} appear in the equations of motion.

2.2. Solution procedure

To compute the numerical solution it is convenient to write the locomotion equations in a coordinate frame attached to the body. For the 2D problem under investigation, we consider the ground fixed frame $\{\mathbf{e}_1, \mathbf{e}_2, \mathbf{e}_3\}$ and the body frame $\{\mathbf{b}_1, \mathbf{b}_2, \mathbf{b}_3\}$ whose origin is $\mathbf{x}_o \equiv \mathbf{x}_{cm}$ and $\mathbf{b}_3$ is parallel to $\mathbf{e}_3$. In this frame, the linear velocity $\mathbf{V}_{cm} = V_1 \mathbf{b}_1 + V_2 \mathbf{b}_2$ and the momenta $\mathbf{P}$ and Π are given by:

$$\mathbf{u}_{cm} = \mathbf{R}\,\mathbf{V}_{cm} \qquad\qquad \mathbf{p} = \mathbf{R}\,\mathbf{P} \qquad\qquad \pi' = \Pi \tag{15}$$

where $\mathbf{R}$ is the rotation matrix relating the inertial to the body frame. By starting from Eqs. (10) and (11) and by combining with the decompositions shown in the previous subsection for both potential and vortical impulses, we obtain the system of equations that yields the body motion:

$$\begin{cases} V_1 \, (m_{11} - m_b) + V_2 \, m_{12} + \Omega \, m_{13} = P_{sh1} + P_{v1} \\ V_1 \, m_{21} + V_2 \, (m_{22} - m_b) + \Omega \, m_{23} = P_{sh2} + P_{v2} \\ V_1 \, m_{31} + V_2 \, m_{32} + b\Omega \, (m_{33} - I_{zz}) = \Pi_{sh} + \Pi_v \end{cases} \tag{16}$$

Let us underline that the locomotion unknowns Ω, V_1 and V_2, appearing within the linear and angular impulses, remain on the l.h.s while all the known quantities are shifted to the r.h.s., leading to a well-posed system of equations very suitable for the numerical solutions. A more detailed description of the mathematical aspects supporting the overall procedure is given in Paniccia et al. (2021). The impulses Π_{sh} and $\mathbf{P}_{sh}$ are due to the body deformation, while Π_v and $\mathbf{P}_v$ are the vorticity related quantities. The terms appearing on the l.h.s. in Eq. (16) express the generalized added mass matrix which, together with the body inertial properties, give the coefficient matrix for the locomotion variables. The body mass m_b is assumed to be constant while I_{zz} and m_{ij} change in time according to the shape deformation. In the following, to be consistent with most of the literature on the subject, the velocity components are renamed as $U = -V_1$ and $V = V_2$.

To solve the system of Eqs. (16), we consider an accurate but simplified numerical procedure which does not involve vorticity diffusion (see also Akoz and Moored, 2018). The evaluation of both potential and vortical impulses can be obtained by the discretization of the body surface and by a suitable model for the release of the concentrated vortex sheet via a Kutta condition to mimic the presence of a vanishing viscosity. Let us mention briefly some of the techniques adopted for the numerical results. The linearity of the impulse equations enables to isolate and separate the contribution of the added mass which is correctly evaluated at each time-step and partly located on the l.h.s. driving to a well-posed system of equations.

The flow solution is obtained by using an unsteady potential code which is based on the approach of Hess and Smith (1967) approximating the body by a finite number of panels, each one with a specific source strength, but with a common circulation density. The impermeability condition on each panel together with a suitable unsteady Kutta condition are needed in order to evaluate the source strengths and the uniform circulation density γ. Moreover, according to Kelvin's theorem, any change in circulation about the airfoil results in the release of vorticity by a wake panel attached to the trailing edge (see Basu and Hancock, 1978). At each time step the released wake panel is lumped into a point vortex which is shed into the wake and advected downstream by the flow field. Finally, let us stress that the extension to vorticity diffusion would lead to a classical vortex method (see Chorin, 1973; Koumoutsakos et al., 1994) without substantially changing the adopted numerical procedure. By this extension it would be possible to consider also a release from smooth portions of the body as in the case of the leading edge vortex which plays a very important role in several unsteady maneuvers out of the scope of the present work.

2.3. Swimming kinematics

The swimming fish is represented by an undulating body with a chord length c equal to 1 m and whose shape at rest corresponds to a NACA0012 airfoil. The body undulates according to an artificially designed deformation more suitable for bio-mimetic applications, hereafter referred to as synthetic deformation. This deformation is obtained by assigning the slope β of the body mid-line by the following expression for a traveling wave of constant amplitude $d\beta$ (assumed as $\frac{\pi}{10}$ rad) and a wave number k related to a wavelength (assumed equal to c) along the curvilinear coordinate s

$$\beta(s, t) = d\beta \sin(ks - 2\pi f t) \tag{17}$$

where f is the frequency (assumed equal to $\frac{10}{2\pi}$ s^{-1}). The instantaneous coordinates of the airfoil mid-line in the body-fixed frame are obtained by integrating Eq. (17)

$$x_c(s, t) = \int_0^s \cos\left(\beta(s, t)\right) \, ds \tag{18a}$$

$$y_c(s, t) = \int_0^s \sin\left(\beta(s, t)\right) \, ds \tag{18b}$$

and the resulting configurations are shown in Fig. 1a.

This coordinates are properly corrected consistently with Eq. (13) by removing any rigid linear and angular displacements associated to the center of mass to obtain the mid-line configuration shown in Fig. 1b. Basically, the shape of the body is prescribed with respect to its center of mass and its principal axes of inertia. A further advantage of the synthetic deformation consists in the automatic compliance of the inextensibility condition expressed as

$$\left(\frac{\partial y_c}{\partial s}\right)^2 + \left(\frac{\partial x_c}{\partial s}\right)^2 = 1 \tag{19}$$

which ensures that the length of the body does not change during the motion. Different deformations, closely related to natural styles of swimming, e.g. carangiform and anguilliform, will be considered later for a comparative analysis.

3. Numerical results

3.1. The effects of motion constraints

As anticipated in the previous sections, we are interested in evaluating the effect of both lateral translation and rotation, i.e. the two most relevant recoil motions, accompanying the fish locomotion generated by its shape deformation. To this
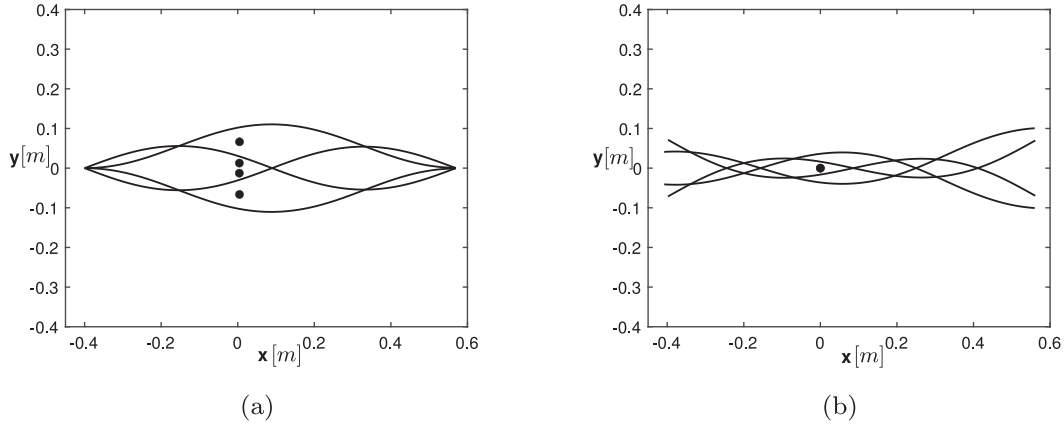
Fig. 1. (1a) Representative mid-line configurations obtained by the direct integration of Eqs. (17) giving an insight of their envelope– (1b) The same for the modified ones to satisfy Eq. (13). The dots represent the center of mass positions.
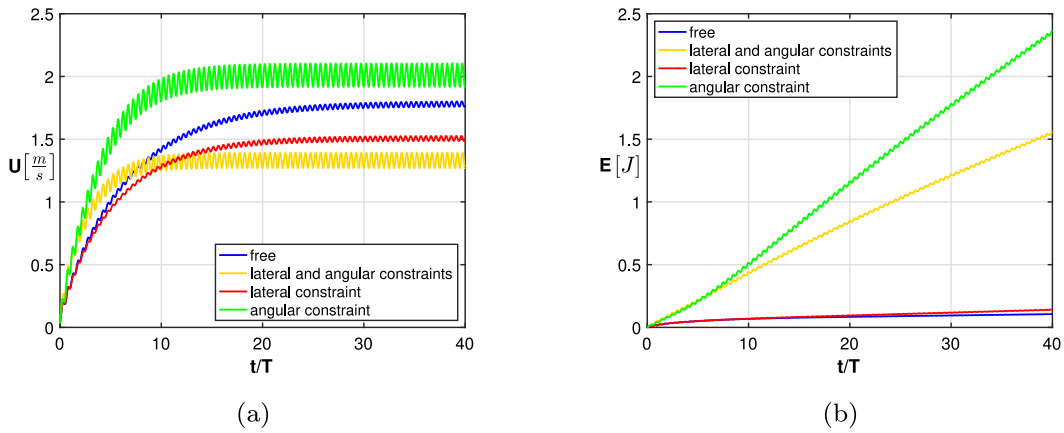
Fig. 2. Time history of (a) the forward velocity and (b) the kinetic energy for free swimming (blue) and constrained gaits: lateral and angular constraints (yellow), lateral constraint (red) and angular constraint (green). (For interpretation of the references to color in this figure legend, the reader is referred to the web version of this article.)

purpose, we consider the comparison between a fish whose recoil motions are allowed and a fish whose lateral and angular recoil motions in the body frame are prevented. This constrained gait implies that the center of mass of the fish is able to move exclusively along the forward direction as it occurs in many experimental investigations. Fig. 2a shows that, in these conditions (yellow curve), the body cannot reach the same asymptotic speed as in the free swimming case (blue curve). Correspondingly, the much larger energy consumption E shown in Fig. 2b, implies a larger cost of transport (COT), defined as the ratio between the mean rate of change of the energy $\bar{\dot{E}}$ and the mean forward velocity U_{loc} (see e.g. Bale et al., 2014; von Kármán and Gabrielli, 1950; Maertens et al., 2015). Consistently, for a certain steady state velocity, if such an unfavorable constraint is imposed, it follows an overestimation of the energy consumption. Let us mention that for the present model it is convenient to evaluate $\bar{\dot{E}}$ as the mean rate of change of the excess energy $\frac{1}{2}\int \mathbf{\Psi} \cdot \boldsymbol{\omega} \, dV$.

At this point, it is also interesting to analyze partial constraints which involve either the lateral or the angular motion while the forward oscillations are expected to have a minor impact on the swimming performance as claimed by many authors (see e.g. Maertens et al., 2017; Smits, 2019). When only the lateral motion is inhibited, the steady-state speed (red curve in Fig. 2a) is slightly lower than for free swimming (blue curve), while the energy consumption is still larger though almost comparable (same colors in Fig. 2b).

Instead, when only the angular motion is prevented, the velocity time history (green curve in Fig. 2a) shows a larger steady-state value together with a shorter transient. However, the energy consumption is even larger, as shown in Fig. 2b, when compared to the fully constrained case.

The bars shown in Fig. 3a represent the peak-to-peak oscillation of the forward, lateral and angular velocity components for the different constrained cases (see Xiong and Lauder, 2014).

It is interesting to note that the angular constrained case, characterized by the largest mean forward velocity, shows larger lateral oscillations to which, in general, is associated a larger thrust force in the forward direction. At the same time, the reduction of the locomotion speed associated with the lateral constraint may be a direct consequence of the suppression of lateral motion. The center of mass displacement is shown in Fig. 3b within a reference frame which moves
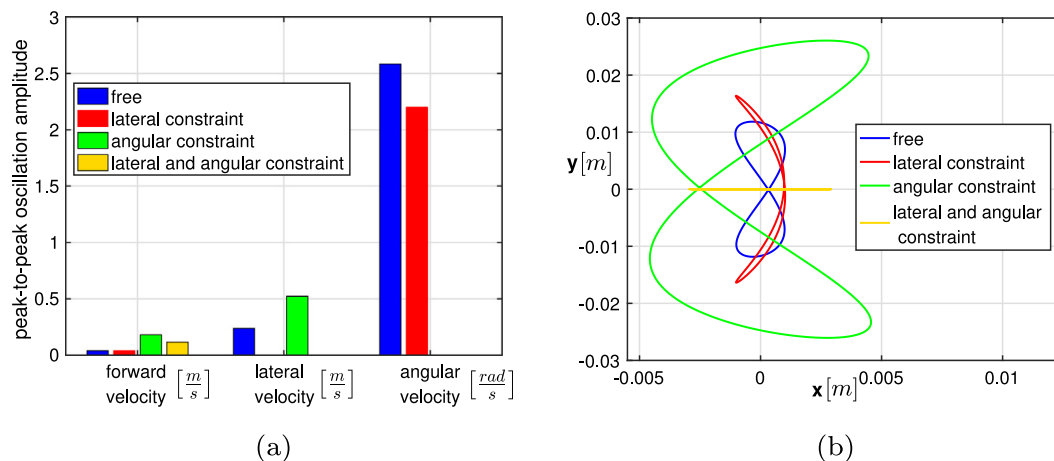
Fig. 3. (a) Amplitude of the peak-to-peak forward, lateral and angular velocity oscillations in the body frame. (b) Center of mass displacement in the locomotion frame for free (blue) and constrained motions: lateral and angular constraints (yellow), lateral constraint (red) and angular constraint (green). (For interpretation of the references to color in this figure legend, the reader is referred to the web version of this article.)
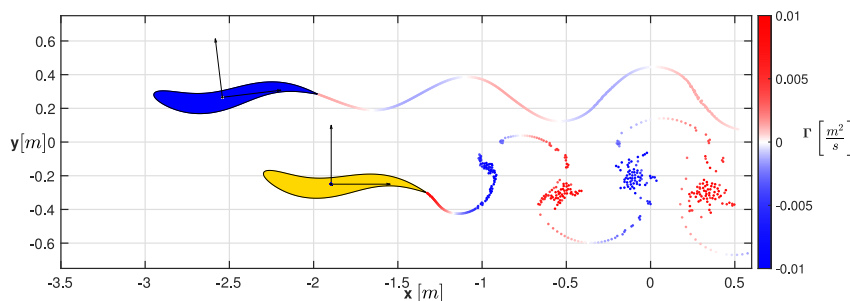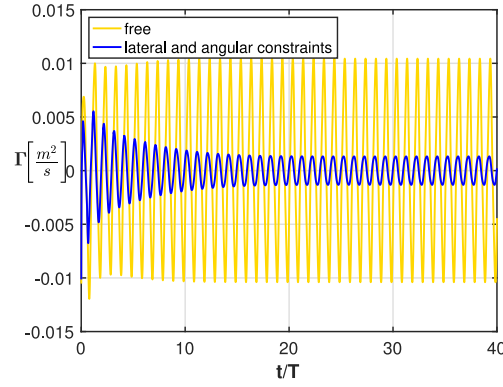

Fig. 4. Comparison at steady-state of the fully constrained (yellow) and the free swimming case (blue) - (animation-link). (For interpretation of the references to color in this figure legend, the reader is referred to the web version of this article.)

with the locomotion velocity, hereafter referred to as locomotion frame. We may notice that in this frame the lateral constrained case is characterized by an orthogonal motion with respect to the swimming direction which leads to a style of swimming quite close to the unconstrained one, as suggested also by the similar energy consumption in Fig. 2b (blue and red curves). Let us stress that large angular oscillations are present both in free swimming and in lateral constrained motions, together with a better energetic performance. Hence, we may consider the angular recoil as a primary form of control to optimize the center of mass trajectory. From the point of view of the expended energy, the lateral recoil motion does not seem as influential as the angular one.

To summarize, when only the lateral motion is constrained, the angular velocity is slightly lower than in free swimming while the associated energy consumption (see red curve in Fig. 2b) is almost the same. On the other hand, when the angular recoil motion is prevented, a huge increase in the energy consumption is observed (see green curve in Fig. 2b). Some of the phenomena related to constrained gaits are poorly intuitive hence, for a quick evaluation of the corresponding motions, we provide an animation (animation-link) with the direct comparison at steady-state of two quite different styles like the fully constrained (yellow case) and the free swimming one (blue case). For the sake of convenience a frame of the video is reported in Fig. 4. We may appreciate the larger speed of the free swimmer together with the stronger vortical wake for the constrained one corresponding to a much larger intensity of the released vortices whose circulation Γ is reported in Fig. 5. The impact of recoil on the swimming performance was also highlighted by other authors, starting from the preliminary work of Reid et al. (2012), limited to the lateral recoil motion, up to the work of Maertens et al. (2017) who clearly showed the importance of recoil for a correct estimation of the overall efficiency. On the same line of reasoning, Yang et al. (2008) reported much larger forces, hence larger power consumption, for the constrained case.

As a further deepening on these constrained motions, let us analyze how the potential and vortical impulses, as introduced in Section 2, cooperate to give the above presented results. To this purpose, we analyze both free swimming and fully constrained motion. We may observe in Fig. 6a how the potential contribution to the forward velocity reaches instantaneously a steady oscillatory state which is going to anticipate and guide the vortical contribution continuously growing in time together with release of new vortices. From the peak-to-peak oscillations shown in Fig. 6b, we may appreciate a larger value of the potential contribution for the constrained case while the value of the vortical one is quite comparable. Finally, a phase shift among the two contributions seems to be responsible for the significantly lower amplitude of the total velocity oscillations for free swimming. This result is confirmed by looking again at Fig. 2a and it seems clearly related to the lower circulation amplitude shown in Fig. 5.

Fig. 5. Time history of the released circulation Γ for the fully constrained (yellow) and free swimming case (blue). (For interpretation of the references to color in this figure legend, the reader is referred to the web version of this article.)

(a)

(b)
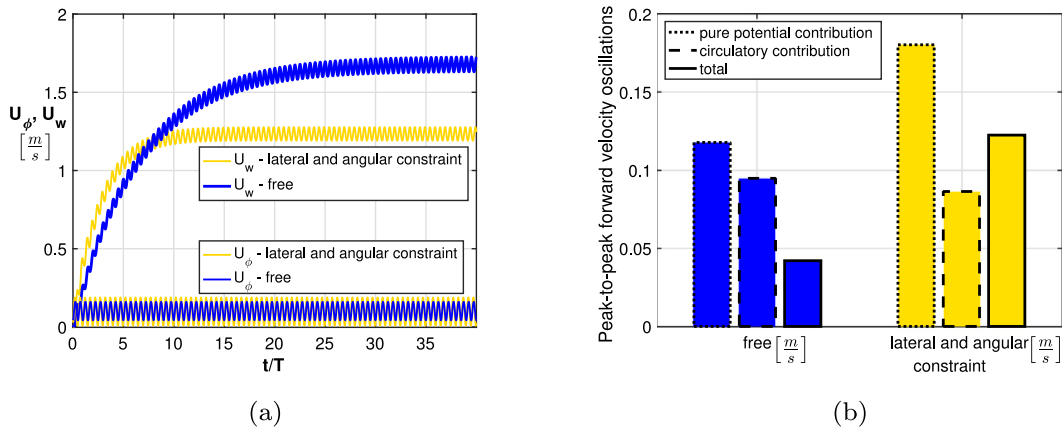
Fig. 6. (a) Time history of the forward velocity potential (U_ϕ) and circulatory (U_w) contributions for free swimming (blue) and fully constrained motion (yellow); (b) peak-to-peak oscillation for U_ϕ, U_w and the total velocity U. (For interpretation of the references to color in this figure legend, the reader is referred to the web version of this article.)

3.2. The impact of shape deformation

The above results has been obtained for the synthetic deformation to have a preliminary account of the constraints. However, in the literature, a large number of different approaches is used to describe different fish species. Most of them are based on analytical expressions for the lateral displacement of the mid-line obtained by fitting data from direct observations. These expressions usually consist of a traveling wave multiplied by a polynomial amplitude modulation $A(x) = ax^2 + bx + c$, whose coefficients are changed according to the fish swimming style. For an anguilliform swimmer, the amplitude modulation of the swimming motion is given by (Tytell and Lauder, 2004)

$$A(x) = 0.1 + 0.0323\,(x - 1) + 0.0310\left(x^2 - 1\right) \tag{20}$$

For a carangiform swimmer, the amplitude modulation is given by (Videler and Hess, 1984)

$$A(x) = 0.1 - 0.0825\,(x - 1) + 0.1625\left(x^2 - 1\right) \tag{21}$$

These prescribed swimming displacements are supposed to represent the real motions of the observed fishes. Nevertheless, in general, they do not satisfy the linear and angular momentum conservation and a recoil correction is required. It follows a substantial change of the final displacement as shown by Fig. 7, where it is possible to appreciate the differences between the prescribed mid-line envelopes and the modified ones accounting for the recoil, hence representing the whole motion. The synthetic deformation introduced here is also shown in the same figure to facilitate the comparison.

Despite the different prescribed deformations, once the recoil motions are considered, the three amplitude envelopes are quite similar, in particular with regard to the bottleneck near the center of mass. As a further strength for this analogy, the effects of constraints on the performance with the experimentally observed deformations are comparable to those discussed for the synthetic one. For instance, Fig. 8 summarizes the results obtained by constraining the anguilliform swimmer. No significant variation with respect to the synthetic deformation (see Fig. 2) appears if we exclude the mean asymptotic forward velocity reached in the case of the angular constraint, which in the present case almost coincides with the free swimming one. An even more significant comparison among the analyzed cases, (all with the same oscillation
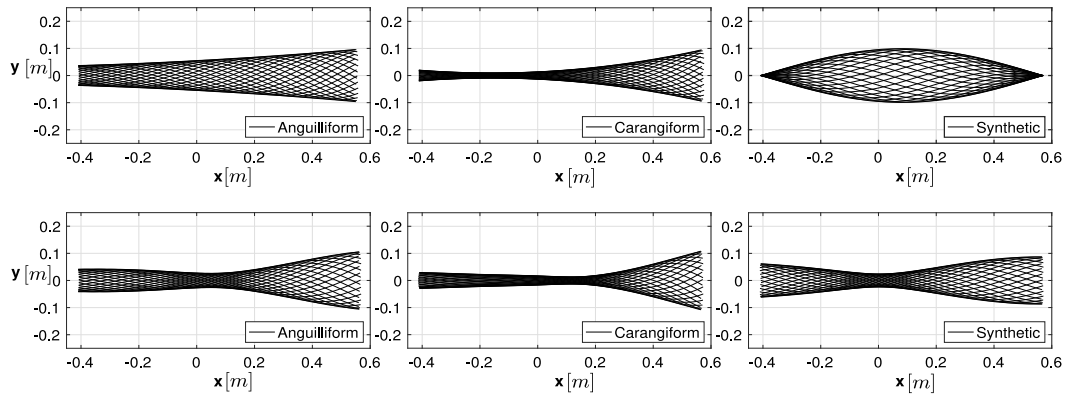
Fig. 7. Envelope of mid-line configurations for several prescribed deformations (top) and their corresponding recoil corrected displacement (bottom).
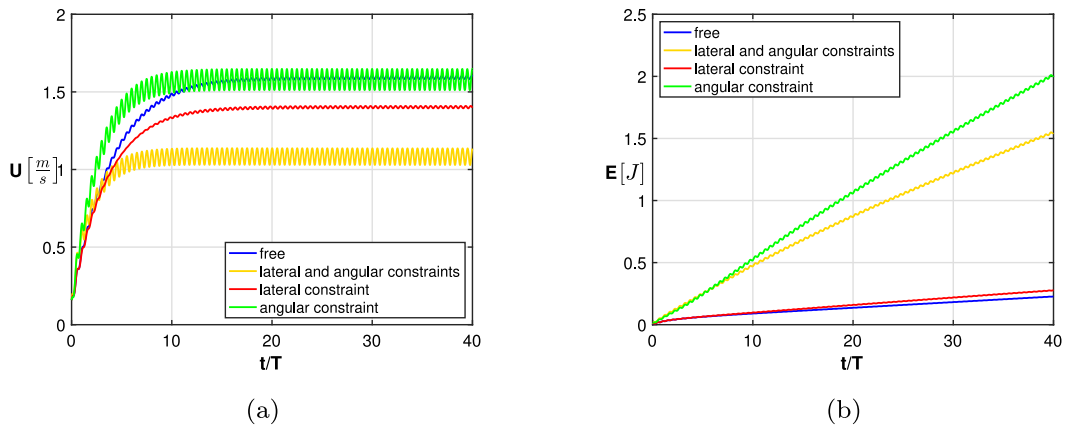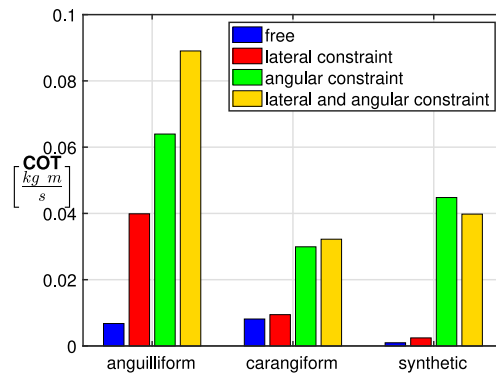

Fig. 8. Anguilliform (a) swimming velocity components and (b) fluid kinetic energy for free swimming (blue) and constrained gaits: lateral and angular constraints (yellow), lateral constraint (red) and angular constraint (green). (For interpretation of the references to color in this figure legend, the reader is referred to the web version of this article.)


Fig. 9. Effects of constraints on the cost of transport for the analyzed different deformations for free swimming (blue) and constrained gaits: lateral and angular constraints (yellow), lateral constraint (red) and angular constraint (green). (For interpretation of the references to color in this figure legend, the reader is referred to the web version of this article.)

frequency and tail-beat amplitude) is given by the cost of transport whose increase (Fig. 9) is mostly affected by the angular constraint.

3.3. A tool for active control

The above reported constrained cases give, as a primary result, interesting information about the effect of the recoil motions on the swimming performance. At the same time, these constraints may represent also the limit case of an active control adopted by the fish through its appendages. For example, the sailfish, is well known to exploit the dorsal fin raising to optimize its performance during the predator–prey interactions. The dorsal fin, i.e. the sail, is kept retracted
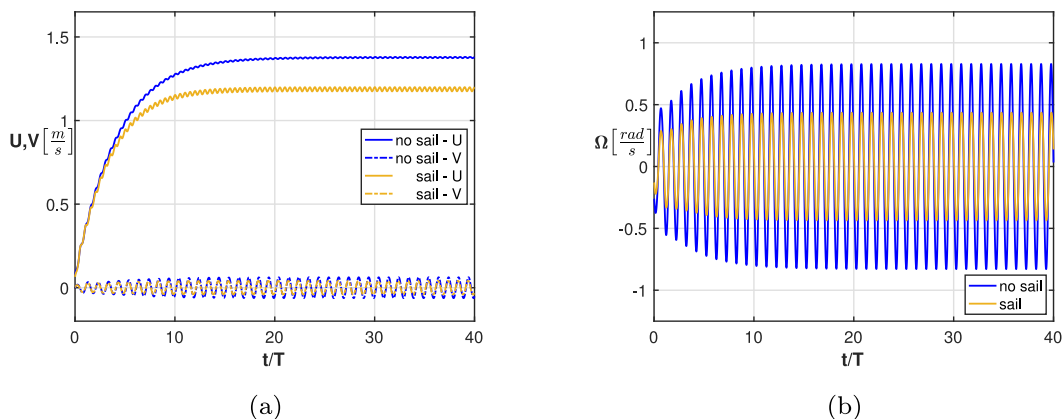
Fig. 10. Sailfish with (orange) and without (blue) the sail model: (a) forward, lateral and (b) angular velocity components. (For interpretation of the references to color in this figure legend, the reader is referred to the web version of this article.)
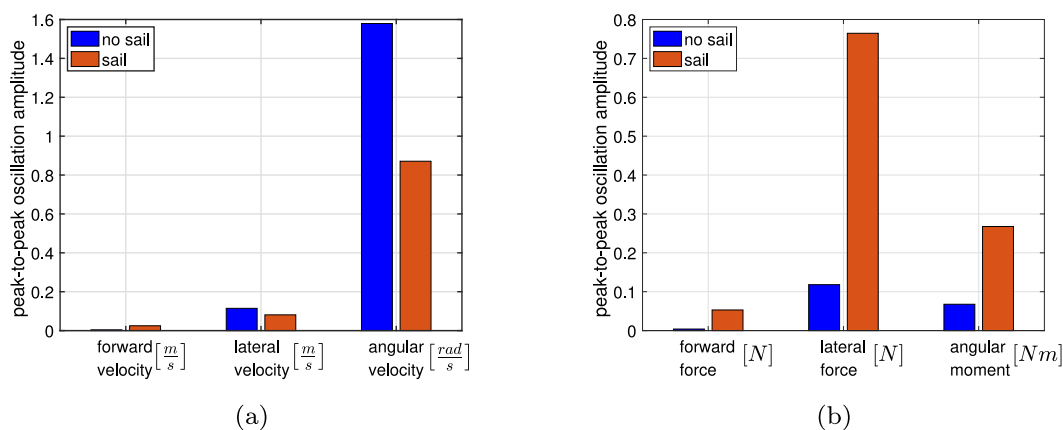
Fig. 11. Amplitude of the peak-to-peak oscillations for the sailfish: (a) forward, lateral and angular velocity and (b) forces and moment with (blue) and without (orange) the sail model. (For interpretation of the references to color in this figure legend, the reader is referred to the web version of this article.)

when cruising or fast swimming to avoid larger energy consumption, while it is extended to increase control during hunting maneuvers. On this subject, Domenici et al. (2014) deeply analyzed the behavior of the sailfish to show how the sail raising may be effective to reduce rotations and lateral translations. By approaching the schooling prey, the sailfish suddenly insert their long bill trying, in the mean time, to minimize any disturbance before slashing. Actually, when the sail is extended, the angular oscillations of the bill are reduced so as to make the bill a stealthy object, not easily detectable, while the approach velocity is reduced to match the prey swimming speed.

To reproduce the effect of the erected dorsal fin, we assumed, as a very crude approximation of a 3D extension, an extra value of the added mass consistent with a rigid flat plate (Faltinsen, 1993). The associated coefficients modify the body mass matrix to take into account the effects of the sail on the linear and angular velocity components.

As shown in Fig. 10, we obtain (as given by the experimental measurements by Domenici et al., 2014; Marras et al., 2015) either a lower swimming speed and the reduction of the angular and lateral oscillations. These are shown in a neat way in Fig. 11a, accompanied by an increase of both the moment and the lateral force experienced by the body (see Fig. 11b), since the larger inertance of the body due to the sail extension leads to a larger power consumption.

4. Final remarks

The locomotion of an undulating, neutrally buoyant, body has been studied either for the steady state and for the transient regime. Due to the involved complex phenomena, a simplified two-dimensional model has been adopted to obtain neat results as proposed by several authors (e.g. Schultz and Webb, 2002; Akoz and Moored, 2018; Akoz et al., 2019) and in a way encouraged by the midbody plane results obtained by Wolfgang et al. (1999) with a three-dimensional numerical model. Apart from the mean forward velocity representing the required locomotion, a particular attention has been given to the oscillating velocity components of the body center of mass which give the recoil motion originally introduced by Lighthill to satisfy the equilibrium equations of the free swimmer. The main points and related results discussed so far are here briefly summarized to highlight the most interesting findings about the relevance of recoil for free swimming performance:

- several constrained gaits have been considered to evaluate the importance of the various velocity components by inhibiting, either singly or jointly, their effect on the overall body motion;
- the locomotion velocity and the related expended energy clearly show the optimal performance of the free swimming with respect to all the considered constrained motions;
- the oscillating velocity components of the body center of mass, corresponding to the recoil motions, may be a simple and efficient tool, as recently proposed by experimental biologists, to understand and classify different styles of swimming;
- the attenuation of the recoil motions, on the other hand, may be seen as a suitable way to control several kinematic and dynamic aspects of the swimmer trajectory, as revealed by well known cases in nature;
- the most typical deformations proper of anguilliform and carangiform swimming styles are analyzed in comparison with the proposed synthetic deformation, with regard to the behavior in presence of recoil.

Some of the above statements, although based on simplified numerical results, give a valuable insight about the importance of recoil for the study of free swimming. Most of the results have been obtained for a synthetic shape deformation of particular interest for bio-mimetic applications and their assessment, through a systematic application to natural swimming styles, is requested. As a final comment, an extension of the methodology to account for vorticity diffusion (see e.g. Graziani et al., 1995; Eldredge, 2007) and for three-dimensional effects (see Wolfgang et al., 1999) should be implemented to deepen the analysis and to better understand further aspects of fish locomotion.

CRediT authorship contribution statement

Damiano Paniccia: Development of the manuscript, Conceptualization, Writing - review & editing. **Giorgio Graziani:** Development of the manuscript, Conceptualization, Writing - review & editing. **Claudio Lugni:** Development of the manuscript, Conceptualization, Writing - review & editing. **Renzo Piva:** Development of the manuscript, Conceptualization, Writing - review & editing.

Declaration of competing interest

The authors declare that they have no known competing financial interests or personal relationships that could have appeared to influence the work reported in this paper.

Acknowledgments

Appendix A. Supplementary data

Supplementary material related to this article can be found online at https://doi.org/10.1016/j.jfluidstructs.2021.103290.

References

Akoz, E., Han, P., Liu, G., Dong, H., Moored, K.W., 2019. Large amplitude intermittent swimming in viscous and inviscid flows. AIAA J..

Akoz, E., Moored, K.W., 2018. Unsteady propulsion by an intermittent swimming gait. J. Fluid Mech. 834.

Bainbridge, R., 1958. The speed of swimming of fish as related to size and to the frequency and amplitude of the tail beat. J. Exp. Biol. 35.

Bale, R., Hao, M., Bhalla, A.P.S., Patankar, N.A., 2014. Energy efficiency and allometry of movement of swimming and flying animals. Proc. Natl. Acad. Sci. USA 111.

Basu, B.C., Hancock, G.J., 1978. The unsteady motion of a two-dimensional aerofoil in incompressible inviscid flow. J. Fluid Mech. 87.

Bhalla, A.P.S., Bale, R., Griffith, B.E., Patankar, N.A., 2013. A unified mathematical framework and an adaptive numerical method for fluid-structure interaction with rigid deforming and elastic bodies. J. Comput. Phys. 250.

Borazjani, I., Sotiropoulos, F., 2008. Numerical investigation of the hydrodynamics of carangiform swimming in the transitional and inertial flow regimes. J. Exp. Biol. 211.

Borazjani, I., Sotiropoulos, F., 2010. On the role of form and kinematics on the hydrodynamics of self-propelled body/caudal fin swimming. J. Exp. Biol. 213.

Carling, J., Williams, T.L., Bowtell, G., 1998. Self-propelled anguilliform swimming simultaneous solution of the two-dimensional Navier-Stokes equations and Newtons laws of motion. J. Exp. Biol. 201.

Chorin, A.J., 1973. Numerical study of slightly viscous flow. J. Fluid Mech. 57, 785–796.

Domenici, P., Wilson, A.D.M., Kurvers, R.H.J.M., Marras, S., Herbert-Read, J.E., Steffensen, J.F., Krause, S., Viblanc, P.E., Krause, P.C.J., 2014. How sailfish use their bills to capture schooling prey. Proc. R. Soc. B 281.

Eldredge, J.D., 2007. Numerical simulation of the fluid dynamics of 2D rigid body motion with the vortex particle method. J. Comput. Phys. 221 (2), 626–648.

Faltinsen, O., 1993. Sea Loads on Ships and Offshore Structures. Cambridge Univ. Press.

Graziani, G., Bassanini, P., 2002. Unsteady viscous flows about bodies: Vorticity release and forces. Meccanica 37.

Graziani, G., Ranucci, M., Piva, R., 1995. From a boundary integral formulation to a vortex method for viscous flows. Comput. Mech. 15.

Hess, J.L., Smith, A.M.O., 1967. Calculation of potential flow about arbitrary bodies. Prog. Aerosp. Sci. 8.

Kanso, E., 2009. Swimming due to transverse shape deformations. J. Fluid Mech. 631.

von Kármán, T., Gabrielli, G., 1950. What price speed? Specific power required for propulsion. Mech. Eng. 72, 775–781.

Kern, S., Koumoutsakos, P., 2006. Simulations of optimized anguilliform swimming. J. Exp. Biol. 209.

Koumoutsakos, P., Leonard, A., Pepin, F., 1994. Boundary conditions for viscous vortex methods. J. Comput. Phys. 113 (1), 52–61.

Lamb, H., 1975. Hydrodynamics, sixth ed. Cambridge Univ. Press.

Landau, L.D., Lifschitz, E.M., 1986. Fluid Mechanics, Vol. 6, second ed. Pergamon Press.

Lauder, G.V., 2015. Fish locomotion: Recent advances and new directions. Annu. Rev. Mar. Sci. 7.

Lighthill, J., 1960. Note on the swimming of slender fish. J. Fluid Mech. 9.

Lighthill, J., 1970. Aquatic animal propulsion of high hydromechanical efficiency. J. Fluid Mech. 44, 265–301.

Limacher, E., Morton, C., Wood, D., 2018. Generalized derivation of the added-mass and circulatory forces for viscous flows. Phys. Rev. Fluids 2.

Maertens, A.P., Gao, A., Triantafyllou, M.S., 2017. Optimal undulatory swimming for single fish-like body and for pair of interacting swimmers. J. Fluid Mech. 813.

Maertens, A.P., Triantafyllou, M.S., Yue, D.K.P., 2015. Efficiency of fish propulsion. Bioinspir. Biomim. 10.

Marras, S., Noda, T., Steffensen, J.F., Svendsen, M.B., Krause, J., Wilson, A.D., Kurvers, R.H., Herbert-Read, J., Boswell, K.M., Domenici, P., 2015. Not so fast: Swimming behavior of sailfish during predator–prey interactions using high-speed video and accelerometry. Integr. Comp. Biol. 55.

Noca, F., Shiels, D., Jeon, D., 1999. A comparison of methods for evaluating time-dependent fluid dynamic forces on bodies, using only velocity fields and their derivatives. J. Fluids Struct. 13.

Paniccia, D., Graziani, G., Lugni, C., Piva, R., 2021. On the role of added mass and vorticity release for self propelled aquatic locomotion. J. Fluid Mech. (in press).

Reid, D.A.P., Hildenbrandt, H., Padding, J.T., Hemelrijk, C.K., 2012. Fluid dynamics of moving fish in a two-dimensional multiparticle collision dynamics model. Phys. Rev. E 85.

Saffman, P.G., 1967. The self-propulsion of a deformable body in a perfect fluid. J. Fluid Mech. 28 (2).

Schultz, W.W., Webb, P.W., 2002. Power requirements of swimming: Do new methods resolve old questions?. Integr. Comp. Biol. 42.

Singh, K., Pedley, T.J., 2008. The hydrodynamics of flexible-body manoeuvres in swimming fish. Physica D 237, 2234–2239.

Smits, A.J., 2019. Undulatory and oscillatory swimming. J. Fluid Mech. 874.

Tytell, E.D., Lauder, G.V., 2004. The hydrodynamics of eel swimming: I wake structure. J. Exp. Biol. 207.

Videler, J., Hess, F., 1984. Fast continuous swimming of two pelagic predators saithe (pollachius virens): and mackerel (scomber scombrius). a kinematic analysis. J. Exp. Biol. 109.

Wolfgang, M.J., Anderson, J.M., Grosenbaugh, M.A., Yue, D.K.P., Triantafyllou, M.S., 1999. Near-body flow dynamics in swimming fish. J. Exp. Biol. 202.

Wu, T.Y., 1961. Swimming of a waving plate. J. Fluid Mech. 10.

Wu, J.Z., Ma, H.Y., Zhou, M.D., 2006. Vorticity and Vortex Dynamics. Springer.

Xiong, G., Lauder, G.V., 2014. Center of mass motion in swimming fish: effects of speed and locomotor mode during undulatory propulsion. Zoology 117.

Yang, Y., Wu, G.H., Yu, Y.L., Tong, B.G., 2008. Two-dimensional self-propelled fish motion in medium an integrated method for deforming body dynamics and unsteady fluid dynamics. Chin. Phys. Lett. 25.

scientific reports

OPEN

The performance of a flapping foil for a self-propelled fishlike body

Damiano Paniccia[1,2]✉, Luca Padovani[1,2], Giorgio Graziani[1,2] & Renzo Piva[1,2]

Several fish species propel by oscillating the tail, while the remaining part of the body essentially contributes to the overall drag. Since in this case thrust and drag are in a way separable, most attention was focused on the study of propulsive efficiency for flapping foils under a prescribed stream. We claim here that the swimming performance should be evaluated, as for undulating fish whose drag and thrust are severely entangled, by turning to self-propelled locomotion to find the proper speed and the cost of transport for a given fishlike body. As a major finding, the minimum value of this quantity corresponds to a locomotion speed in a range markedly different from the one associated with the optimal efficiency of the propulsor. A large value of the feathering parameter characterizes the minimum cost of transport while the optimal efficiency is related to a large effective angle of attack. We adopt here a simple two-dimensional model for both inviscid and viscous flows to proof the above statements in the case of self-propelled axial swimming. We believe that such an easy approach gives a way for a direct extension to fully free swimming and to real-life configurations.

The self-propulsion of certain fishes may be reduced to the study of the oscillatory motion of the caudal fin. For instance, a tunniform swimmer uses the tail to generate most of the propulsive force, while the anterior part of the body provides essentially a viscous resistance. In these cases since it is possible, as a first approximation, to separate drag and thrust, in the past it was considered more convenient to study the tail as an isolated flapping foil, i.e. with a combined heave and pitch motion. Actually, most of the attention was paid to the study of a flapping foil under a uniform incoming stream to evaluate the fluid-induced thrust which is able to counteract the unavoidable body resistance. Hence, the Froude efficiency $\eta = TU/P$ (T thrust, P input power and U inflow velocity) was used as a measure for the performance of the propulsion system, repeatedly analyzed in many contributions either analytical[1,2], numerical[3,4] or experimental[5,6]. However, the primary interest remains the evaluation of self-propelled swimming properties like the locomotion speed and the energy consumption hence we propose here to recover the approach properly adopted when the whole body is cooperating for the generation of the required thrust. This is the case of undulatory swimming, where a wave travelling from head to tail is involving a significant part of the body consistently with the fish's shape and swimming style (e.g. anguilliform, carangiform, etc.). For these reasons, a clear identification of the propulsive efficiency is prevented[7–9] and, after a few initial studies with a prescribed stream[10,11], the self-propelled locomotion velocity was obtained by leaving the fish completely free to swim according to the forces exchanged with the surrounding fluid[12–15]. When at steady state thrust and drag balance exactly, the Froude efficiency loses its meaning and a proper concept like the cost of transport $COT = P/U$, or its inverse as introduced by von Kármán and Gabrielli[16], should be considered instead[17,18]. By proceeding in an analogous way for oscillatory swimming, we intend to investigate the axial self-propulsion of a flapping foil pushing a fishlike body which, in a way passive with respect to the thrust, may be approximated by defining only its mass and its resistance, i.e. a virtual body as proposed by Akoz[19]. These assumptions, due to the known resistance and to the axial motion of the virtual body, allow for the evaluation of the cost of transport as a measure for the self-propelled swimming performance, but also for a clear-cut evaluation of the Froude efficiency providing an easy comparison between the optimal conditions for the two performance measures. By following other suggestions from the seminal work of Schultz and Webb[20] and later by Gazzola et al.[21], we prefer to concentrate our attention on two dimensional simulations to achieve a sharp understanding of the complex phenomena just described. A cartoon for the virtual body and its tail propulsor with a sketch representing the exchanged forces and the oscillatory trajectory for the tail pivot point is reported in Fig. 1. The animation reported in the Supplementary Video online gives a first glance insight of the swimming fishlike model and of the related vortex wake.

[1]Department of Mechanical and Aerospace Engineering, University of Rome "La Sapienza", Rome, Italy. [2]These authors contributed equally: Damiano Paniccia, Luca Padovani, Giorgio Graziani and Renzo Piva. ✉email: damiano.paniccia@uniroma1.it
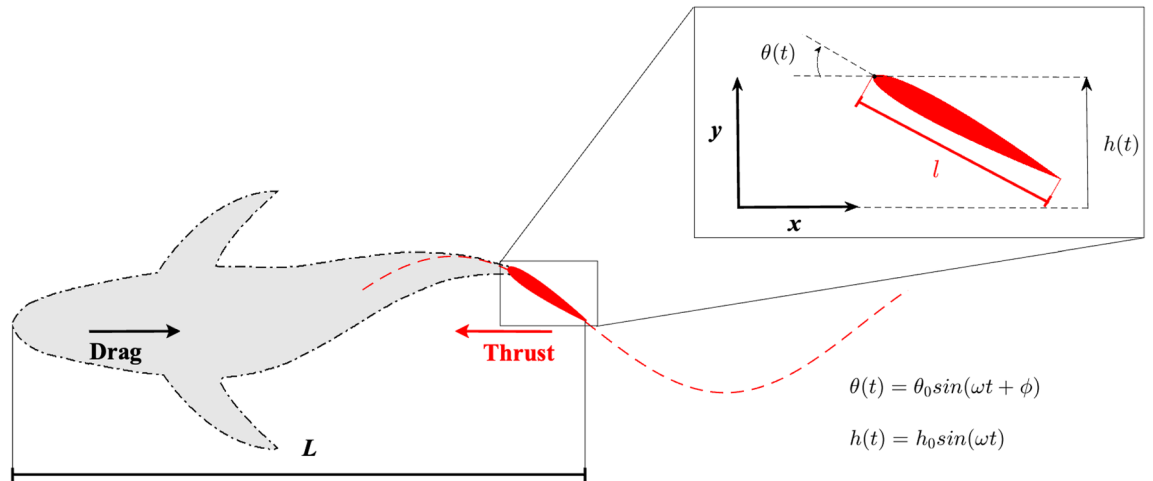
Figure 1. A cartoon for the virtual body (gray) and the tail propulsor (red) with a sketch of the exchanged forces and the oscillatory trajectory of the tail pivot point. The details of the flapping motion are reported in the inset. See also the animation of the swimming fishlike model and the related vortex wake in the Supplementary Video online.

Results and discussion

A test for zero resistance. As a preliminary step, we like to consider the self-propelled axial motion of a virtual body having zero resistance[22–25], a sort of ideal case, to highlight in the most simple and neat way the possible analogies with the undulatory swimming mode. For instance, we like to understand if an asymptotic locomotion velocity occurs also for a flapping foil and how to find a good approximation of its value. This is feasible if the pitch motion about the leading edge, with an angular frequency ω and a small amplitude θ_0, anticipates the heave motion, with amplitude h_0, by a phase angle $\phi = \pi/2$. With these assumptions, we may express the flapping motion of a foil with chord l as

$$y(x,t) = h_0 \sin(\omega t) - x \sin(\theta(t)) \approx h_0 \sin(\omega t) - \theta_0 x \cos(\omega t) \quad 0 \leq x \leq l \tag{1}$$

which may be assimilated to an undulatory motion of amplitude A and wavenumber k.

When the wavelength $\lambda = 2\pi/k \gg l$, this motion may be expressed as

$$y(x,t) = A \sin(\omega t - kx) \approx A \sin(\omega t) - Akx \cos(\omega t) \quad 0 \leq x \leq l \tag{2}$$

and, by identifying the single terms of (1) and (2), we obtain for the phase velocity

$$c = \frac{\omega}{k} \approx \omega \frac{h_0}{\theta_0} \tag{3}$$

Intuitively, if $\lambda \gg l$, the foil itself acts as a small portion of the wave whose undulating motion is perceived, instantaneously, as a local oscillation given by the heave and pitch motions.

Consistently with the assumption of small θ_0, the above analogy becomes more and more accurate as the wavelength λ is greater than the tail length. This phase velocity gives us the opportunity to recall the proportional-feathering parameter $\Theta = \theta_0 U / \omega h_0$, as ingeniously suggested by Lighthill[26], to qualify the propulsive performance of flapping foils. Actually, the expression for Θ results to be the ratio between the locomotion velocity U and the phase velocity c given by (3), to match the concept of slip velocity usually adopted in undulatory swimming[27].

For the analysis of the numerical results in the self-propelled case, since both the Strouhal number $St = \omega l A_{TE}/(2\pi U)$ and the reduced frequency $k_r = \omega l/U$ contain the forward velocity U which is part of the solution, we should select new parameters strictly based on the assigned data. To this purpose, we introduce the non-dimensional trailing edge peak-to-peak oscillation amplitude A_{TE} in terms of the foil chord l and the pure heave non-dimensional peak-to-peak amplitude defined as $A_h = 2h_0/l$. For a given value A_{TE}, which for small values of θ_0 may be approximated by $\sqrt{(2\theta_0)^2 + A_h^2}$, the ratio A_h/A_{TE} is the parameter that we are going to use to analyze the results. It represents the fraction of the trailing edge amplitude due to heave, so as $A_h/A_{TE} = 0$ for pure pitch and 1 for pure heave.

The time history of the forward locomotion velocity obtained by a standard inviscid numerical procedure for the zero resistance virtual body is reported in fig.2a for $A_{TE} = 1$ and three different values of A_h/A_{TE}. From the figure we may appreciate how the acceleration during the transient is increasing with the heave amplitude to reach anyhow, even in the absence of a viscous resistance, an asymptotic velocity which is going to infinity for pure heave. We like to notice that the forward velocity oscillations appearing in the figure are very small and their global effect on swimming performance is quite negligible as assumed in a previous work on recoil motions[28] and confirmed by a present simulation reported in the Supplementary Material (see also[17] and[29]). The

2
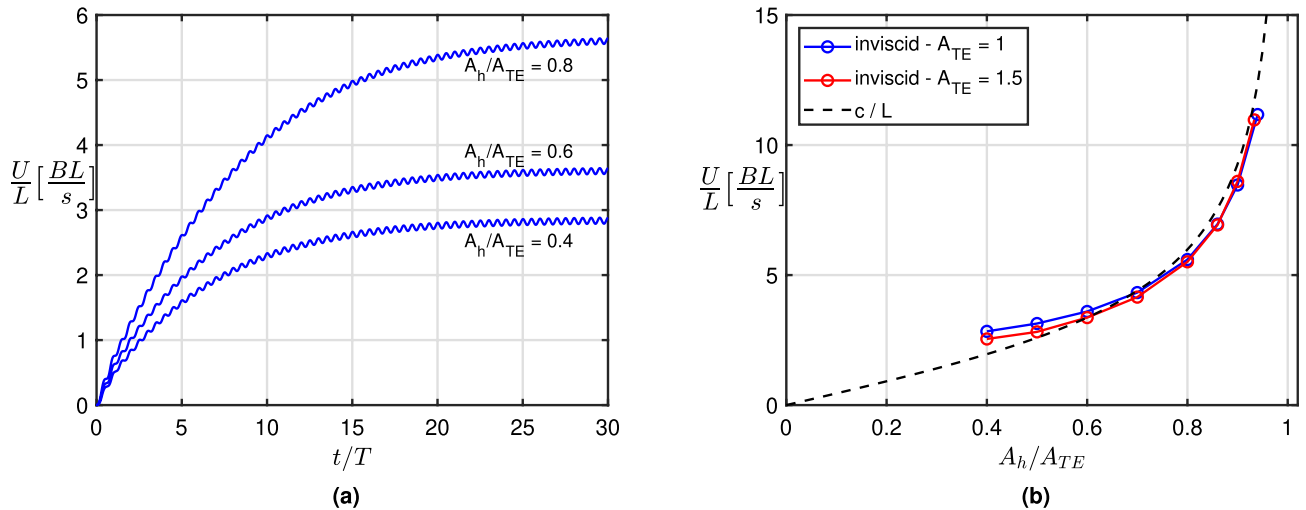
Figure 2. (**a**) Time history of the locomotion speed for $A_{TE} = 1$ and three different values of A_h/A_{TE}. (2b) Mean steady state swimming velocity U/L and phase velocity c/L (dashed line) against A_h/A_{TE} for different peak-to-peak trailing edge oscillation amplitudes ($A_{TE} = 1$ and 1.5). Inviscid numerical results for zero resistance of the virtual body.

mean forward velocity at the steady state, for A_{TE} equal to 1 and 1.5, is plotted against A_h/A_{TE} in Fig. 2b together with the phase velocity c which is only a function of the ratio A_h/A_{TE}. Let us remark that the selected values of A_{TE} correspond nearly to $0.15 - 0.2$ in terms of the ratio between the tail-beat amplitude and the body length L, as frequently observed in nature[30]. As anticipated above, for small pitch angles, i.e. for A_h/A_{TE} going to one, the prediction of the asymptotic velocity equal to c is confirmed by the numerical results which also show how the locomotion speed is practically independent of the trailing edge amplitude A_{TE}, as for undulatory swimming in the specific case of inviscid flows[31]. For zero resistance, the Froude efficiency continuously decreases up to a null value at steady state where the net thrust is going to vanish. At the same time, the cost of transport is decreasing towards steady state but it reaches an asymptotic finite value resulting extremely low due to a reduced expended energy and a very large locomotion speed in absence of viscous resistance. This expected behaviour is properly modified when introducing a non zero virtual body resistance leading to intermediate values of both COT and η with respect to the above extreme conditions. At steady state the efficiency is not zero anymore since the thrust reaches a finite value able to counterbalance the imposed drag and the cost of transport gains a value consistent with a reduced locomotion speed together with an increase of the expended power. As shown by the numerical results in the following section, it is easy to understand the primary role of the body resistance to qualify the overall performance of the swimming fish.

The role of the body resistance. As anticipated before, the concept of virtual body introduced to estimate the performance of the fishlike body, requires an assumption for the drag coefficient C_D as close as possible to expected real values which may be selected from experimental evidence[32].

The mean forward velocity is shown in Fig. 3a for viscous and inviscid flows together with the phase velocity c. We may notice a general reduction of the velocity values with respect to Fig. 2b clearly due to the extra virtual body resistance and their dependence on the peak-to-peak trailing edge amplitude A_{TE}, as expected in the presence of viscous resistance[33]. A contained difference is appreciable when comparing viscous and inviscid results, in particular for larger values of A_h/A_{TE}, essentially related to the viscous resistance of the propulsor which increases with the locomotion speed to give a sensible difference between the two approaches[34]. The whole body performance given by the cost of transport is shown in Fig. 3b with a very satisfactory agreement between viscous and inviscid results. A clear evidence of the classical U-shaped form for the COT curves[35,36] is obtained and a minimum value appears in a quite small range about $A_h/A_{TE} = 0.7$. The presence of a virtual body allows also for the calculation of the propulsor efficiency since the thrust, balancing the known drag at cruising speed, is now available[37,38]. Interestingly, the range where we find the maximum efficiency of the propulsor, reported in Fig. 3c, is clearly different from the one where the minimum COT for the whole body occurs. Specifically, the range corresponding to the maximum value of the efficiency η is found for larger values of A_h/A_{TE}. Let us mention that other authors, by making different choices, may obtain different results which however are perfectly compatible with the present ones. For instance, Akoz et al.[19], by forcing a constant self-propelled locomotion speed for a defined body via a change of frequency, interestingly find the cost of transport as the inverse of the propulsor efficiency. Instead, if a constant speed is prescribed without caring for the self-propelled conditions consistent with a given body resistance[3,4,6], the attention is only focused on the generic properties of the propulsor as clearly underlined by Anderson et al.[5].

For the sake of completeness, we illustrate in Fig. 4a the values of cost of transport and efficiency also in terms of the more commonly used Strouhal number that was previously set apart for its dependence on the unknown locomotion velocity. The figure confirms the results previously discussed about the substantial difference of the
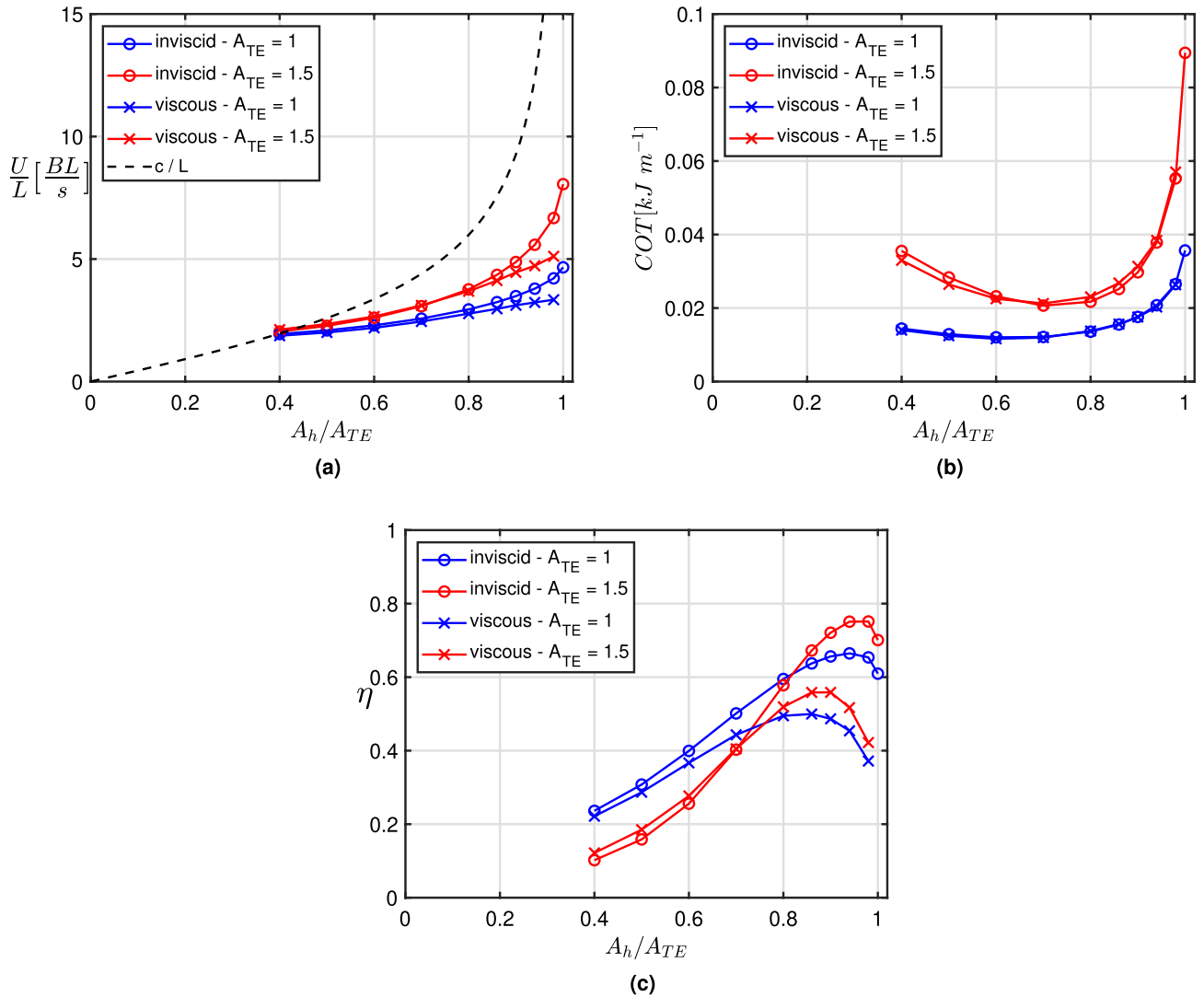
Figure 3. (**a**) Mean steady state swimming velocity U/L and phase velocity c/L (dashed line), (**b**) cost of transport of the whole body and (**c**) efficiency of the propulsor against A_h/A_{TE} for different peak-to-peak trailing edge oscillation amplitudes ($A_{TE} = 1$ and 1.5). Viscous and inviscid numerical solutions for a prescribed virtual body resistance.
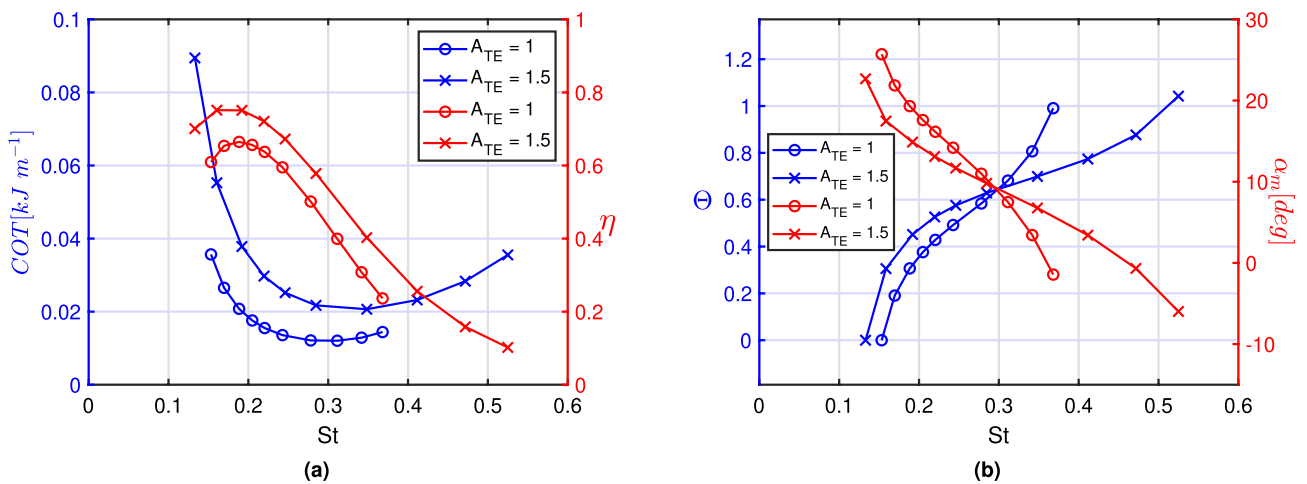
Figure 4. (**a**) Cost of transport of the whole body (blue) and efficiency of the propulsor (red) as function of the Strouhal number St. (**b**) Feathering parameter Θ (blue) and maximum angle of attack α_m (red) for the inviscid case as function of the Strouhal number. Comparison between $A_{TE} = 1$ and 1.5 for the inviscid case.

optimal ranges for the two performance measures. Within this context it is worth stressing how the optimal values of COT and η are related to a couple of very significant parameters i.e. the proportional-feathering Θ and the maximum effective angle of attack α_m. Following Anderson et al.[5], we recall the definition of α_m as

$$\alpha_m = \arctan \frac{\omega h_0}{U} - \theta_0 \approx \frac{\omega h_0}{U} - \theta_0 \qquad (4)$$

where the approximation holds for small values of the pure heave incidence angle $\omega h_0 / U$. If this is the case, the following simple relation between α_m and Θ holds

$$\frac{\alpha_m}{\theta_0} = \frac{1 - \Theta}{\Theta} \qquad (5)$$

whose physical meaning is very clear: as the feathering parameter is tending to one, i.e. the locomotion velocity is approaching the phase velocity c, the value of α_m tends to zero. From Fig. 4b we may easily deduce that the maximum propulsor efficiency occurs for very large values of α_m while the minimum of the cost of transport for the whole body occurs for large values of Θ. The corresponding values of the parameters α_m and Θ are well reproducing results proposed in the literature for the search of optimal performance conditions. Namely, several findings confirm that fish select cruising speed usually very close to the phase velocity (i.e. Θ within $0.7 - 0.8$) when they have to cover large distances[26,27]. On the opposite, large values of the angle of attack, within $15° - 25°$, are associated with higher propulsor efficiency[5] and are more favorable when a large locomotion speed is required for escape-like gaits.

Final remarks

When studying flapping airfoils under an incoming uniform flow, the focus is usually on the ability of the propulsor to generate a large thrust to balance the resistance, together with a high propulsive efficiency. Obviously, if the thrust of the propulsor prevails over the body drag an acceleration follows leading to different operating conditions. Once a certain body has been selected, a constant drag coefficient is prescribed hence it is more comfortable to adopt a self-propulsion approach which, by assuring the force balance, leads to a straightforward evaluation of the energy consumption together with the proper locomotion speed. In this way, we recover the procedure usually adopted in undulatory swimming governed by the phase velocity of a traveling wave. This choice is encouraged by the analogy illustrated before which introduces an asymptotic velocity also in the case of oscillatory swimming. The presence of a virtual body with its prescribed resistance allows, in the frame of a self-propulsion procedure, to evaluate also a well-defined propulsor efficiency to be contrasted with the cost of transport of the whole body. The results clearly indicate two different optimal swimming conditions: the first, characterized by a large locomotion velocity and a large angle of attack, is associated with the maximum propulsive efficiency; the second, associated with the minimum cost of transport, is characterized by a lower locomotion velocity and a quite large value of the feathering parameter. The contemporary observation of these different measures and the understanding of their validity for different swimming demands overcomes the conflicting opinions appearing in the literature about the best procedure to evaluate swimming performance[39]. In line with the overall discussion, we support here the use of a self-propulsion approach for the study of oscillatory swimming to obtain a direct evaluation of the performance, either for cruising long-range motions or for fast escape-like gaits. As a further point, the self-propelled axial motion is propaedeutic for the extension to lateral and angular degrees of freedom which drive the performance[28] and better represents the swimming gaits observed in nature. To this purpose, the study of a swimming body under a prescribed uniform flow is not suitable, since no recoil motion may be accounted for, and the fully free locomotion is confirmed as the natural approach to obtain meaningful results.

Materials and methods

The self-propelled axial motion of a swimming body with velocity $\mathbf{u}_b$ is analyzed by considering a two-dimensional body $\mathscr{B}$ within an unbounded fluid domain $\mathscr{V}_\infty$. No external forces are applied, hence only internal actions are exchanged between the deformable body and the surrounding fluid, otherwise quiescent. To the purpose, we adopt the classical impulse formulation[40,41] for the linear fluid momentum which is expressed by two terms representing the field vorticity $\boldsymbol{\omega}$ and the vortex sheet over the body surface as

$$\mathbf{p} = \int_{V_\infty} \rho\, \mathbf{x} \times \boldsymbol{\omega}\, dV + \int_{\partial\mathscr{B}} \rho\, \mathbf{x} \times (\mathbf{n} \times \mathbf{u}^+)\, dS \qquad (6)$$

where $\boldsymbol{n}$, the normal to the body surface $\partial\mathscr{B}$, points into the fluid domain V_∞ and ρ is the fluid density. A Helmholtz decomposition may be now applied to express the velocity field as the sum of the acyclic and vorticity related components:

$$\mathbf{u}^+ = \boldsymbol{\nabla}\phi + \boldsymbol{\nabla} \times \boldsymbol{\Psi} = \boldsymbol{\nabla}\phi + \mathbf{u}_w \qquad (7)$$

where ϕ and $\boldsymbol{\Psi}$ are referred to as the scalar and the (solenoidal) vector potential, and are given by the solution of the Laplace/Poisson equation, subject to the impermeable boundary condition on $\partial\mathscr{B}$, i.e. $\boldsymbol{\nabla}\phi \cdot \boldsymbol{n} = \boldsymbol{u}_b \cdot \boldsymbol{n}$ and $(\boldsymbol{\nabla} \times \boldsymbol{\Psi}) \cdot \boldsymbol{n} = 0$ respectively, and to the vanishing velocity at infinity. It follows that the total impulse $\boldsymbol{p}$, which does not suffer the poor convergence of the momentum over an unbounded domain[42,43] and whose time derivative gives the forces exchanged between the body and the surrounding fluid, may be expressed as the sum of the potential and vortical impulses, $\boldsymbol{p}_\phi$ and $\boldsymbol{p}_v$, as

$$\mathbf{p}_{\phi} = -\rho \int_{\partial \mathscr{B}} \phi \, \mathbf{n} \, dS \quad \mathbf{p}_{\nu} = \int_{V_{\infty}} \rho \, \mathbf{x} \times \boldsymbol{\omega} dV \, + \int_{\partial \mathscr{B}} \rho \, \mathbf{x} \times (\mathbf{n} \times \mathbf{u}_w) \, dS \tag{8}$$

where the bound vorticity due to $\mathbf{u}_w$, properly added to the released vorticity $\boldsymbol{\omega}$, gives the additional vorticity introduced by Lighthill. The mathematical model, described in detail for undulatory free swimming in Paniccia et al.[31], has been partially reported in the Supplementary Material and properly reshaped for the axial oscillatory swimming given by a flapping foil in the presence of a virtual body. The flow solutions are obtained by a simple inviscid procedure easily extendable to a classical vortex method by introducing the diffusion of the vorticity as detailed in a previous paper[44]. In the present work, a standard viscous solver, validated against the one used by Lin et al.[25], has been used to provide a comparison of the results and an overall assessment of the inviscid procedure.

The sinusoidal heave and pitch motions with amplitudes h_0 and θ_0, respectively, are characterized by an angular oscillation frequency $\omega = 10\pi \; rad/s$ and are separated in phase by an angle $\phi = \pi/2$ (pitch leading). The ratio A_h/A_{TE} between the non-dimensional peak-to-peak trailing edge amplitude for pure heave motion and for combined heave and pitch motions is varied in the range $0.4 \sim 0.98$ and the pitch oscillation amplitude θ_0 follows to maintain the prescribed A_{TE}. Finally, for the virtual body, the drag coefficient C_D is set equal to 0.25 and the mass m of the total body, i.e. virtual body plus propulsor, is set equal to 4.5 kg. For the details about the numerical procedures and choice of the parameters, see the Supplementary Material.

References

1. Garrick, I. E. *Propulsion of a Flapping and Oscillating Airfoil*, vol. 567 of *National Advisory Committee for Aeronautics: Report* (NACA, 1936).
2. Fernandez-Feria, R. Note on optimum propulsion of heaving and pitching airfoils from linear potential theory. *J. Fluid Mech.* **826**, 781–796 (2017).
3. Jones, K. & Platzer, M. Numerical computation of flapping-wing propulsion and power extraction. *AIAA Paper* **97**, 0826 (1997).
4. Young, J. & Lai, J. C. S. Mechanisms influencing the efficiency of oscillating airfoil propulsion. *AIAA J.* **45**, 1695–1702 (2007).
5. Anderson, J. M., Streitlien, K., Barrett, D. S. & Triantafyllou, M. S. Oscillating foils of high propulsive efficiency. *J. Fluid Mech.* **360**, 41–72 (1998).
6. Floryan, D., Van Buren, T., Rowley, C. W. & Smits, A. J. Scaling the propulsive performance of heaving and pitching foils. *J. Fluid Mech.* **822**, 386–397 (2017).
7. Gray, J. Studies in animal locomotion i. *J. Experim. Biol.* **10**, 88–104 (1933).
8. Bale, R., Hao, M., Bhalla, A. P. S., Patel, N. & A.Patankar, N. Gray's paradox a fluid mechanical perspective. *Sci. Rep.* **4**, 5904 (2014).
9. Lucas, K. N., Lauder, G. V. & Tytell, E. D. Airfoil-like mechanics generate thrust on the anterior body of swimming fishes. *PNAS* **117**, 10585–10592 (2020).
10. Lighthill, J. Note on the swimming of slender fish. *J. Fluid Mech.* **9**, 305–317 (1960).
11. Wu, T. Y. Swimming of a waving plate. *J. Fluid Mech.* **10**, 321–344 (1961).
12. Carling, J., Williams, T. L. & Bowtell, G. Self-propelled anguilliform swimming simultaneous solution of the two-dimensional Navier–Stokes equations and newtons laws of motion. *J. Experim. Biol.* **201**, 3143–3166 (1998).
13. Kern, S. & Koumoutsakos, P. Simulations of optimized anguilliform swimming. *J. Experim. Biol.* **209**, 4841–4857 (2006).
14. Yang, Y., Wu, G. H., Yu & Tong, B. G. Two-dimensional self-propelled fish motion in medium: An integrated method for deforming body dynamics and unsteady fluid dynamics. *Chin. Phys. Lett.* **25**, 597–600 (2008).
15. Borazjani, I. & Sotiropoulos, F. On the role of form and kinematics on the hydrodynamics of self-propelled body-caudal fin swimming. *J. Experim. Biol.* **213**, 89–107 (2010).
16. Gabrielli, G. & von Kármán, T. What price speed? Specific power required for propulsion. *J. Am. Soc. Naval Eng.* **63**, 188–200 (1951).
17. Bale, R., Hao, M., Bhalla, A. P. S. & Patankar, N. A. Energy efficiency and allometry of movement of swimming and flying animals. *PNAS* **111**, 7517–7521 (2014).
18. Smits, A. J. Undulatory and oscillatory swimming. *J. Fluid Mech.* **874**, 1–70 (2019).
19. Akoz, E. & Moored, K. W. Unsteady propulsion by an intermittent swimming gait. *J. Fluid Mech.* **834**, 149–172 (2018).
20. Schultz, W. W. & Webb, P. W. Power requirements of swimming: Do new methods resolve old questions?. *Integr. Comp. Biol.* **42**, 1018–25 (2002).
21. Gazzola, M., Argentina, M. & Mahadevan, L. Energy gait and speed selection in slender inertial swimmers. *PNAS* **112**, 3874–3879 (2015).
22. Alben, S. & Shelley, M. Coherent locomotion as an attracting state for a free flapping body. *PNAS* **102**, 11163–11166 (2005).
23. X, Zhang, Ni Wang, S. & He, G. Effects of geometric shape on the hydrodynamics of a self-propelled flapping foil. *Phys. Fluids* **21**, 103302 (2009).
24. Arora, N., Gupta, A., Sanghi, S., Aono, H. & Shyy, W. Flow patterns and efficiency-power characteristics of a self-propelled, heaving rigid flat plate. *J. Fluid Struct.* **66**, 517–542 (2016).
25. Lin, X., Wu, J. & Zhang, T. Performance investigation of a self-propelled foil with combined oscillating motion in stationary fluid. *Ocean. Eng.* **174**, 33–49 (2019).
26. Lighthill, J. Aquatic animal propulsion of high hydromechanical efficiency. *J. Fluid Mech.* **44**, 265–301 (1970).
27. Wu, T. Y. Fish swimming and bird/insect flight. *Annu. Rev. Fluid Mech.* **43**, 25–58 (2011).
28. Paniccia, D., Graziani, G., Lugni, C. & Piva, R. The relevance of recoil and free swimming in aquatic locomotion. *J. Fluids Struct.* **103**, 103290. https://doi.org/10.1016/j.jfluidstructs.2021.103290 (2021).
29. Maertens, A. P., Gao, A. & Triantafyllou, M. S. Optimal undulatory swimming for single fish-like body and for pair of interacting swimmers. *J. Fluid Mech.* **813**, 301–345 (2017).
30. Bainbridge, R. The speed of swimming of fish as related to size and to the frequency and amplitude of the tail beat. *J. Experim. Biol.* **35**, 109–133 (1958).
31. Paniccia, D., Graziani, G., Lugni, C. & Piva, R. On the role of added mass and vorticity release for self propelled aquatic locomotion. *J. Fluid Mech.* **918**, A45. https://doi.org/10.1017/jfm.2021.375 (2021).
32. White, C. H., Lauder, G. V. & Bart-Smith, H. Tunabot flex: a tuna-inspired robot with body flexibility improves high-performance swimming. *Bioinspir. Biomim.* **16**, 026019 (2021).

33. Zhang, D., Pan, G., Chao, L. & Yan, G. Mechanisms influencing the efficiency of aquatic locomotion. *Mod. Phys. Lett. B* **32**, 1850299 (2018).
34. Floryan, D., Van Buren, T. & Smits, A. J. Efficient cruising for swimming and flying animals is dictated by fluid drag. *PNAS* **115**, 8116–8118 (2018).
35. Di Santo, V., Kenaley, C. P. & Lauder, G. V. High postural costs and anaerobic metabolism during swimming support the hypothesis of a u-shaped metabolism-speed curve in fishes. *PNAS* **114**, 13048–13053 (2017).
36. Zhu, J. *et al.* Tuna robotics: A high-frequency experimental platform exploring the performance space of swimming fishes. *Sci. Robot.* **4**, eaax4615 (2019).
37. Li, N., Liu, X. & Su, Y. Numerical study on the hydrodynamics of thunniform bio-inspired swimming under self-propulsion. *PLOS One* **12**, e0174740 (2017).
38. Akoz, E., Han, P., Liu, G., Dong, H. & Moored, K. W. Large-amplitude intermittent swimming in viscous and inviscid flows. *AIAA J.* **57**, 1–8 (2019).
39. Van Buren, T., Floryan, D., Wei, N. & Smits, A. J. Flow speed has little impact on propulsive characteristics of oscillating foils. *Phys. Rev. Fluids* **3**, 013103 (2018).
40. Noca, F. *On the evaluation of time-dependent fluid dynamic forces on bluff bodies*. Ph.D. thesis, California Institute of Technology (1997).
41. Wu, J. Z., Ma, H. Y. & Zhou, M. D. *Vortical Flows* (Springer, 2015).
42. Landau, L. D. & Lifschitz, E. M. *Fluid Mechanics*, vol. 6 (Pergamon Press, 1986), 2 edn.
43. Childress, S. *An Introduction to Theoretical Fluid Dynamics* (Courant Lecture Notes, vol. 19, AMS, 2009).
44. Graziani, G., Ranucci, M. & Piva, R. From a boundary integral formulation to a vortex method for viscous flows. *Comput. Mech.* **15**(4), 301–314 (1995).

Acknowledgements

Author contributions

D.P., L.P., G.G and R.P contributed equally to this work.

Competing interests

The authors declare no competing interests.

Additional information

Supplementary Information The online version contains supplementary material available at https://doi.org/10.1038/s41598-021-01730-4.

Correspondence and requests for materials should be addressed to D.P.

Reprints and permissions information is available at www.nature.com/reprints.

Publisher's note Springer Nature remains neutral with regard to jurisdictional claims in published maps and institutional affiliations.

SUPPLEMENTARY MATERIAL - The performance of a flapping foil for a self-propelled fishlike body.

Damiano Paniccia[1,*,+], **Luca Padovani**[1,+], **Giorgio Graziani**[1,+], **and Renzo Piva**[1,+]

[1]Dept. of Mechanical and Aerospace Engineering, Univ. of Rome "La Sapienza", Rome, Italy
[*]damiano.paniccia@uniroma1.it
[+]these authors contributed equally to this work

1 The model for axial motion

As illustrated in the main text, we intend to study the axial motion of a swimming body $\mathscr{B}$ which is moving with a velocity $\mathbf{u}_b$ within an unbounded fluid domain $\mathscr{V}_\infty$. To this purpose we assume an unbounded 2D incompressible flow field, with constant density ρ, whose velocity vanishes at the far field boundary. We report below the main steps of the procedure to obtain the final equation to be solved for the numerical results.

The locomotion is obtained by coupling the body dynamics and the actions exchanged with the fluid. If we consider the body-fluid system $(\mathscr{B} + \mathscr{V}_\infty)$, no external forces are present and therefore the linear momentum is conserved:

$$\frac{d}{dt} \int_{\mathscr{B}} \rho_b \mathbf{u}_b \, dV + \frac{d\mathbf{p}}{dt} = 0 \tag{S1}$$

where the time derivative of the total impulse $\boldsymbol{p}$ gives the force acting on the body and ρ_b is the body density. Let us now divide the whole body into an active part $\mathscr{B}_T$ given by the tail and a completely passive one, named virtual body $\mathscr{B}_V$, whose presence is attested only by its mass and its viscous drag in the axial direction. By using a Cartesian frame of reference $(\mathbf{e}_1, \mathbf{e}_2, \mathbf{e}_3)$ and by isolating the unknown locomotion speed $\mathbf{u}_0 = U \mathbf{e}_1$, the total motion of the entire body may be split into

$$\mathbf{u}_b = \begin{cases} \mathbf{u}_0 + \bar{\mathbf{u}} & \text{if } x \in \mathscr{B}_V \\ \mathbf{u}_0 + \mathbf{u}_T & \text{if } x \in \mathscr{B}_T \end{cases} \tag{S2}$$

where $\mathbf{u}_T$ is given by the prescribed heave and pitch motion of the tail

$$\mathbf{u}_T = V \mathbf{e}_2 + (\mathbf{x} - \mathbf{x}_0) \times \Omega \mathbf{e}_3 \quad \mathbf{x} \in \mathscr{B}_T \tag{S3}$$

where $\mathbf{x}_0$ is the position of the pivot point and V and Ω are the lateral and angular heave and pitch velocity, respectively. Since "... *the fish's muscular contractions can only determine changes in its shape relative to the centre of gravity.*" (Lighthill '70[1]), the velocity of the virtual body $\bar{\mathbf{u}}$ is taken to satisfy the conservation of linear and angular momenta for the entire body system, including the prescribed movement of the tail.

By combining (S1) and (S2) we obtain

$$\frac{d}{dt}(m_b \mathbf{u}_0) + \frac{d\mathbf{p}}{dt} = 0 \tag{S4}$$

The surface integrals appearing within the total impulse $\mathbf{p}$ may be decoupled into the contribution from the tail and that from the virtual body. By taking the component of (S4) along $\mathbf{e}_1$ to solve for the locomotion along the axial direction, we assume the virtual body contribution to be represented by its overall resistance D, leading to

$$\frac{d}{dt}(m_b U) + \frac{dp}{dt} + D = 0 \tag{S5}$$

where the axial component p of the impulse contains the contribution from the tail. By assuming zero initial conditions, (S5) gives:

$$m_b U + p = -\int_0^t D \, dt \tag{S6}$$

The scalar potential introduced by the Helmholtz decomposition is evaluated according to the related boundary conditions on the tail boundary

$$\frac{\partial \phi}{\partial n} = \boldsymbol{u}_b \cdot \boldsymbol{n}\bigg|_T$$

Finally, the potential impulse may be expressed in terms of the added mass coefficients introduced in the classical treatises (see e.g.[2]) that, for completeness, are reported below. For a foil motion with unknown axial velocity U and prescribed lateral and angular velocity V and Ω respectively, we consider the Kirchhoff base potentials Φ_1, Φ_2 and Φ_3 defined through the boundary conditions

$$\frac{\partial \Phi_1}{\partial n} = \mathbf{n} \cdot \mathbf{e}_1 \qquad \frac{\partial \Phi_2}{\partial n} = \mathbf{n} \cdot \mathbf{e}_2 \qquad \frac{\partial \Phi_3}{\partial n} = (\mathbf{x} - \mathbf{x}_0) \times \mathbf{n} \cdot \mathbf{e}_3 \tag{S7}$$

to have $\phi = U\Phi_1 + V\Phi_2 + \Omega\Phi_3$. It follows for the added mass coefficients in the axial direction m_{1j} the expression

$$m_{1j} = \rho \int_{\partial \mathscr{B}_T} \frac{\partial \Phi_1}{\partial n} \Phi_j \, dS \tag{S8}$$

The prescribed lateral and angular tail velocities within p_ϕ, which are multiplied by m_{12} and m_{13} respectively, can be shifted to the r.h.s. to yield the equation for the axial body motion:

$$U\,(m_{11} - m_b) = -V\,m_{12} - \Omega\,m_{13} + p_v + \int_0^t D\,dt \tag{S9}$$

The drag term appearing on the r.h.s. of (S9) is expressed as $D = \frac{1}{2}\rho U^2 L C_D$, where L is the body length and C_D is the prescribed drag coefficient. The numerical solution of the equation, quite trivial at steady state, requires a simple numerical treatment to manage the transient phase of the locomotion velocity.
As a final remark, the input power P is evaluated as

$$P = f \int_{t+1/f} (LV + M\Omega)\,dt \tag{S10}$$

where the lift is $L = \frac{d\boldsymbol{p}}{dt} \cdot \boldsymbol{e}_2$ and the moment is $M = \frac{d\boldsymbol{\pi}}{dt} \cdot \boldsymbol{e}_3$ with the angular impulse about the tail leading edge defined as

$$\boldsymbol{\pi} = -\frac{1}{2}\left[\int_{V_\infty} \rho\,|x|^2 \boldsymbol{\omega}\,dV + \int_{\partial \mathscr{B}_T} \rho\,|x|^2 (\boldsymbol{n} \times \boldsymbol{u}^+)\,dS\right] \tag{S11}$$

2 Techniques and data for the simulations

A flapping foil acting as the propulsor of a fishlike body has been studied by a well-known inviscid numerical procedure with the aim to suggest a neat and simple way to investigate the performance of oscillatory swimming fish. The flow solutions about the flapping airfoil are obtained by a potential code based on Hess and Smith[3] approach together with a suitable unsteady Kutta condition and a proper evolution of the wake behind the airfoil as indicated by Basu and Hancock[4]. Finally, the locomotion of the whole-body (airfoil + virtual body) is obtained by satisfying the conservation of total momentum in the forward direction. Further details on the adopted methodology can be found in Paniccia et al.[5], where also lateral and angular directions are considered.

With regard to the viscous results reported in the manuscript, the flow solutions have been obtained by using a CFD solver for
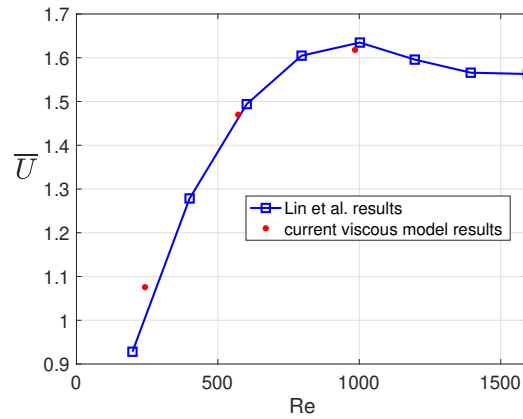
Figure S1. Comparison between the current viscous model results and the ones by Lin et al.[8] for a self-propelled heaving and pitching foil.

the Navier-Stokes equations based on an immersed boundary method. The numerical code has been developed by Popinet[6] and it was already successfully adopted in the field of self-propelled fish locomotion by[7] among others. The forward locomotion of the whole-body follows from the evaluation of the axial force exerted by the surrounding fluid and from the solution of the Newton's second law in the axial direction only. The current viscous solver results are validated against the ones obtained by Lin et al.[8] for the same heaving and pitching conditions as shown in fig.S1.

Let us now describe in more details the parameters we selected for the flapping foil and for the virtual body in front of it. We assume the body length $L = 1\ m$ and the tail length l, here taken as the reference length, equal to $1/7\ L$, ratio frequently observed in nature for real tuna. The presence of the virtual body is only attested by its mass m_b and its resistance in terms of a prescribed drag coefficient C_D. The values of m_b is based on a NACA0018 airfoil geometry with chord length equal to $6l$ and unit density, i.e. $m_b \approx 4.4\ kg$, and the value of $C_D \approx 0.25$ has been selected as the mean value of the experimental data by White et al.[9] for their robotic tuna. Finally, the flapping foil representing the tail is modeled as a NACA0012 airfoil of chord length l with mass m_t equal to $0.08\ kg$, leading to a total mass of the whole-body $m = m_b + m_t \approx 4.5\ kg$. For further geometrical details, fig.S2 reports the sketch of the tail from the inset of fig.1 in the main text where the whole-body is shown.
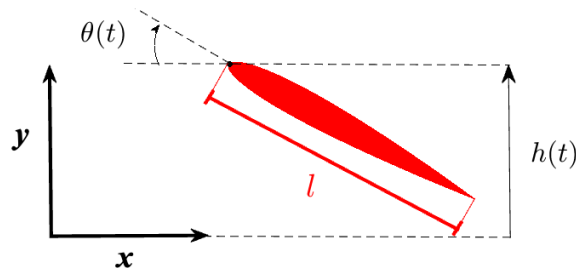
Figure S2. Sketch of the tail from the inset of fig.(1) in the main text.

The heave motion of the tail is defined as

$$h(t) = h_0 \sin(\omega t) \tag{S12}$$

where h_0 is the heave amplitude and ω is the oscillation angular frequency which is equal to $10\pi\ rad/s$ in the present case. The pitch motion is defined as

$$\theta(t) = \theta_0 \sin(\omega t + \phi) \tag{S13}$$

where θ_0 is the pitch amplitude and the phase angle ϕ is equal to $\pi/2$. For pitch motions about the leading edge and for sufficiently small θ_0 it is possible to approximate the value of the non-dimensional peak-to-peak trailing edge amplitude with the following analytical expression (see also[10])

$$A_{TE} = \sqrt{(2\theta_0)^2 + A_h^2} \tag{S14}$$

where $A_h = 2h_0/l$ is the non-dimensional amplitude for a pure heave motion. Two different trailing edge amplitudes have been considered, namely $A_{TE} = 1.0$ and $A_{TE} = 1.5$, for the ratio A_h/A_{TE} ranging within $0.4 \sim 0.98$ while the pitch amplitude θ_0 follows directly from (S14). For the sake of completeness, we summarize in Tab.S1 below all the input data used in our study.

	A_{TE}=1.0			A_{TE}=1.5	
$\frac{h_0}{l}$	$\frac{A_h}{A_{TE}}$	θ_0	$\frac{h_0}{l}$	$\frac{A_h}{A_{TE}}$	θ_0
0.2000	0.4000	0.4583	0.3000	0.4000	0.6874
0.2500	0.5000	0.4330	0.3750	0.5000	0.6495
0.3000	0.6000	0.4000	0.4500	0.6000	0.6000
0.3500	0.7000	0.3571	0.5250	0.7000	0.5356
0.4000	0.8000	0.3000	0.6000	0.8000	0.4500
0.4300	0.8600	0.2551	0.6450	0.8600	0.3827
0.4500	0.9000	0.2179	0.6750	0.9000	0.3269
0.4700	0.9400	0.1706	0.7050	0.9400	0.2559
0.4900	0.9800	0.0995	0.7350	0.9800	0.1492

Table S1. Values of $\frac{h_0}{l}$, $\frac{A_h}{A_{TE}}$ and θ_0 for A_{TE}=1.0 (left) and A_{TE}=1.5 (right).

3 The effect of forward oscillations

To proof that the oscillations in the forward velocity give a negligible contribution on large scale parameters like the cost of transport and the locomotion velocity we should realize a self-propelled motion with an axial velocity constrained to be perfectly constant, i.e. without the implicit oscillations. However, since the axial velocity is the unknown of the problem, we cannot make any constraint on this variable as we may do with the lateral and angular motions where it is quite easy to annihilate the values of the corresponding velocities (see[11]). To overcome this conundrum we report here for comparison the results obtained by a self propelled approach and the ones obtained by the prescribed uniform stream. Figure (S3a) shows the forward velocity obtained by the self-propelled fishlike body for $h_0 = 0.6$ and $A_{TE} = 1.5$. To compare this self-propelled case against an axial location fixed swimming case, we selected the mean forward velocity reached at steady state of the first case as the prescribed constant speed for the second one. It follows the same drag coefficient in both cases within the approximation obtained for the other variables. In fig.(S3b) we report the input power time evolution in one oscillation period for both the self-propelled and the fixed swimming cases. From the comparison we may appreciate a very small difference, less than 2%, between the two mean values that, in a first approximation, is quite negligible. This fact, explains why for the axial swimming, and exclusively in this case, each single result in one point of the parameter space may be indifferently obtained by the two mentioned approaches. Obviously, this is not true anymore for fully free swimming in presence of all the recoil motion components.

As an ultimate comment, when using the one or the other approach to explore the parameter space, the routes to find the optimal swimming performance are completely different. In fact, by taking the flapping foil data as a running parameter for the analysis, we may fix either the velocity, as in the prescribed stream approach, or the body drag coefficient, as in the self propulsion approach and this last procedure, in our opinion, is certainly preferable since the aim is to find these results for a certain fishlike body.
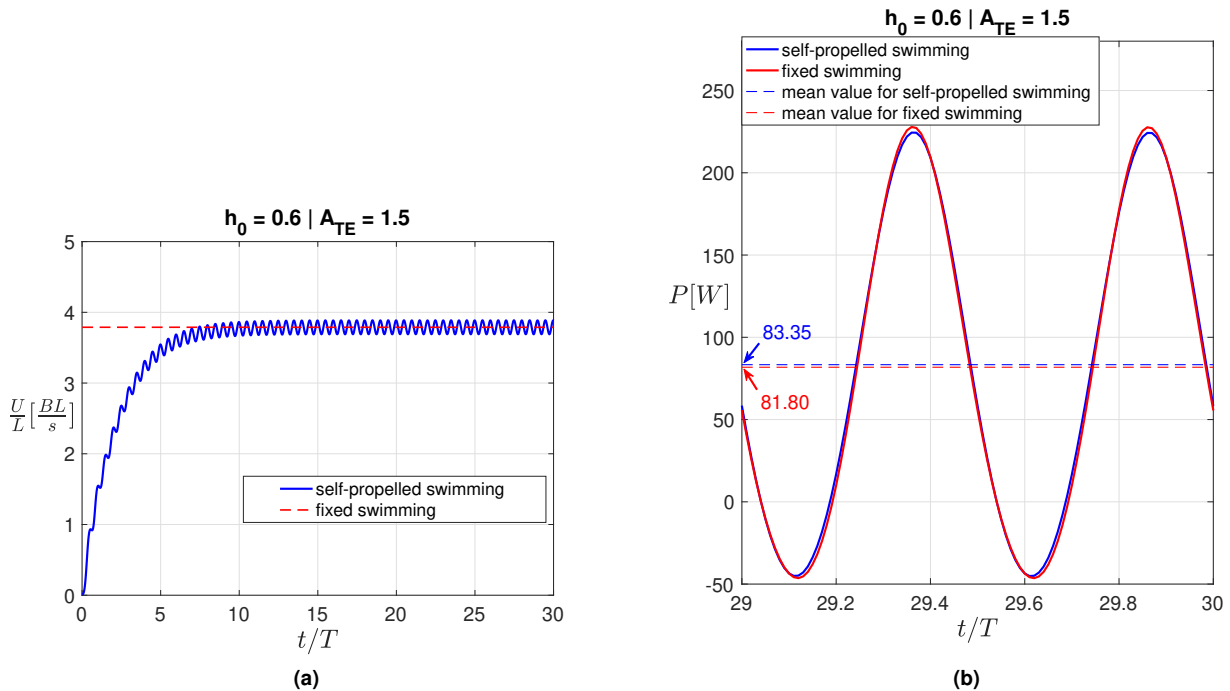
Figure S3. (S3a) Forward velocity for the self-propelled swimming case. The steady state mean value has been selected as the prescribed value for the fixed swimming case. (S3b) Comparison between the input power for the self-propelled swimming case and for the fixed swimming case. The two different mean values are reported in blue and red respectively.

Supplementary Video Legend

Animation of the swimming fishlike model and the related vortex wake. The appearing deformation of the virtual body (gray) is not effective, but instrumental to make a smooth and nice connection with the oscillating tail (red).

References

1. Lighthill, J. Aquatic animal propulsion of high hydromechanical efficiency. *J. Fluid Mech.* **44**, 265–301 (1970).

2. Lamb, H. *Hydrodynamics* (Cambridge Univ. Press, 1975), 6 edn.

3. Hess, J. L. & Smith, A. M. O. Calculation of potential flow about arbitrary bodies. *Prog. Aerosp. Sci.* **8**, 1–138 (1967).

4. Basu, B. C. & Hancock, G. J. The unsteady motion of a two-dimensional aerofoil in incompressible inviscid flow. *J. Fluid Mech.* **87**, 159–178 (1978).

5. Paniccia, D., Graziani, G., Lugni, C. & Piva, R. On the role of added mass and vorticity release for self propelled aquatic locomotion. *J. Fluid Mech.* **918**, A45, DOI: 10.1017/jfm.2021.375 (2021).

6. Popinet, S. Gerris: a tree-based adaptive solver for the incompressible euler equations in complex geometries. *J. Comput. Phys.* **190**, 572–600 (2003).

7. Wang, L. & Wu, C. J. An adaptive version of ghost-cell immersed boundary method for incompressible flows with complex stationary and moving boundaries. *Sci. China* **53**, 923–932 (2010).

8. Lin, X., Wu, J. & Zhang, T. Performance investigation of a self-propelled foil with combined oscillating motion in stationary fluid. *Ocean. Engin.* **174**, 33–49 (2019).

9. White, C. H., Lauder, G. V. & Bart-Smith, H. Tunabot flex: a tuna-inspired robot with body flexibility improves high-performance swimming. *Bioinspir. Biomim.* **16**, 026019 (2021).

10. Young, J. *Numerical simulation of the unsteady aerodynamics of flapping airfoils*. Ph.D. thesis, School of Aerosp. Civil and Mech. Engin. Univ. New South Wales, AUS (2005).

11. Paniccia, D., Graziani, G., Lugni, C. & Piva, R. The relevance of recoil and free swimming in aquatic locomotion. *J. Fluids Struct.* **103**, 103290, DOI: 10.1016/j.jfluidstructs.2021.103290 (2021).

Bioinspiration & Biomimetics

PAPER

Locomotion performance for oscillatory swimming in free mode

D Paniccia* , L Padovani, G Graziani and R Piva

Department of Mechanical and Aerospace Engineering, Sapienza University, Rome, Italy
* Author to whom any correspondence should be addressed.

E-mail: damiano.paniccia@uniroma1.it

Abstract

Oscillatory swimming of a fishlike body, whose motion is essentially promoted by the flapping tail, has been studied almost exclusively in axial mode under an incoming uniform stream or, more recently, self-propelled under a virtual body resistance. Obviously, both approaches do not consider the unavoidable recoil motions of the real body which have to be necessarily accounted for in a design procedure for technological means. Actually, once combined with the prescribed kinematics of the tail, the recoil motions lead to a remarkable improvement on the resulting swimming performance. An inviscid impulse model, linear in both potential and vortical contributions, is a proper tool to obtain a deeper comprehension of the physical events with respect to more elaborated flow interaction models. In fact, at a first look, the numerical results seem to be quite entangled, since their trends in terms of the main flapping parameters are not easy to be identified and a fair interpretation is obtained by means of the model capability to separate the effects of added mass and vortex shedding. Specifically, a prevailing dependence of the potential contribution on the heave amplitude and of the vortical contribution on the pitch amplitude is instrumental to unravel their combined action. A further aid for a proper interpretation of the data is provided by accounting separately for a geometrical component of the recoil which is expected to follow from the annihilation of any spurious rigid motion in case no fluid interactions occur. The above detailed decomposition of the recoil motions shows, through the numerical results, how the single components are going to influence the main flapping parameters and the locomotion performance as a guide for the design of biomimetic swimmers.

1. Introduction

Several fish species, like tunafish, are assumed to produce their locomotion almost exclusively by oscillating their caudal fin while the rest of the body should essentially contribute to both inertial and viscous resistance. The performance of these oscillatory swimmers has been usually evaluated by the Froude efficiency of the flapping foil propulsor, with assigned heave and pitch motions, under a prescribed uniform stream [1–6] or by the cost of transport for the whole body, consisting of a flapping foil plus a resistant virtual body, self-propelled in axial mode [7, 8]. A comparative analysis of the above two parameters for evaluating the swimming performance has been deeply analyzed to prove their suitability for different swimming gaits [9, 10]. The above

procedures are both very convenient for experimental and numerical investigations, but unable to account for the actual motion of the fishlike body in free swimming mode and for its presumed impact on the overall performance [11–14]. In fact, as firmly stated by Lighthill [15], the locomotion is necessarily accompanied by some recoil motions whose effect has to be accounted for to satisfy the equilibrium equations. The recoil velocity components have been shown to modify, for undulatory swimming, the resulting kinematics to reach a favorable effect on the overall efficiency while for constrained or tethered cases, where their influence is neglected, different results are obtained for both locomotion speed and expended energy so to experience a poorer swimming performance [16–20]. The focus of the present work is on the analysis of the recoil motions for oscillatory

swimming with the purpose to find whether they play a similar role also in this case. In fact, the deformation is now essentially limited to the rear end of the body and one could expect rather small recoil reactions with a presumably low impact on the overall performance [21]. In spite of this common belief, we claim here that the recoil induced modifications of the flapping tail parameters cannot be neglected and even more they produce an overall improvement of the swimming performance. For a better comprehension of these large scale effects, we intend, as a proper way, to analyze separately the different components of the recoil motions and their influence on the fish dynamics. Specifically, the potential and vortical contributions given by the interaction with the surrounding fluid and the geometrical component of the recoil which instead is an *a priori* requirement to satisfy the equilibrium of the fishlike body for any given deformation.

The reported numerical results are obtained by a simple impulse model which is able to isolate the added mass and the vortex-shedding contributions without using more elaborated simulations which might obscure the essence of the problem. A detailed analysis of the inviscid results for different values of the prescribed kinematic parameters is instrumental to devise the influence of the recoil motion for a suitable design procedure of free swimming biomimetic means.

2. Materials and methods

2.1. Mathematical model
The self-propelled motion of an impermeable, flexible body $\mathcal{B}$ with bounding surface $\partial\mathcal{B}$ is modeled by assuming a two-dimensional incompressible flow in an unbounded fluid domain $\mathcal{V}$ with density ρ. Only internal actions are exchanged between the swimming body and the surrounding fluid, whose velocity vanishes at the far field boundary.

By adopting the impulse formulation (see e.g. [22–24]) for both linear and angular fluid momenta and assuming $\boldsymbol{n}$ as the normal to $\partial\mathcal{B}$ pointing into the fluid domain $\mathcal{V}$, the force $\boldsymbol{F}_{\mathrm{b}}$ and the moment $\boldsymbol{M}_{\mathrm{b}}$ acting on the body are obtained as the time derivatives of the linear impulse, $\boldsymbol{p}$, and angular impulse, $\boldsymbol{\pi}$:

$$
\begin{aligned}
\boldsymbol{F}_{\mathrm{b}} &= -\frac{d\boldsymbol{p}}{dt} \\
&= -\frac{d}{dt}\left[\int_{\mathcal{V}}\rho\boldsymbol{x}\times\boldsymbol{\omega}\,dV + \int_{\partial\mathcal{B}}\rho\boldsymbol{x}\times(\boldsymbol{n}\times\boldsymbol{u})dS\right] \\
\boldsymbol{M}_{\mathrm{b}} &= -\frac{d\boldsymbol{\pi}}{dt} \\
&= \frac{d}{dt}\frac{1}{2}\left[\int_{\mathcal{V}}\rho|\boldsymbol{x}|^2\,\boldsymbol{\omega}\,dV + \int_{\partial\mathcal{B}}\rho|\boldsymbol{x}|^2(\boldsymbol{n}\times\boldsymbol{u})\,dS\right]
\end{aligned}
\tag{1}
$$

where $\boldsymbol{\omega}$ is the vorticity and $\boldsymbol{u}$ stays for the limiting value of the fluid velocity on $\partial\mathcal{B}$.

The fluid velocity field is expressed through a Helmholtz decomposition as

$$
\boldsymbol{u} = \boldsymbol{\nabla}\phi + \boldsymbol{\nabla}\times\boldsymbol{\Psi} = \boldsymbol{\nabla}\phi + \boldsymbol{u}_{\mathrm{w}}
\tag{2}
$$

where the scalar potential ϕ and the (solenoidal) vector potential $\boldsymbol{\Psi}$ are easily obtained by imposing the impermeable boundary condition on $\partial\mathcal{B}$ and vanishing velocity at infinity. According to this decomposition, we express the linear impulse $\boldsymbol{p}$ in terms of its potential and vortical contributions as $\boldsymbol{p} = \boldsymbol{p}_\phi + \boldsymbol{p}_{\mathrm{v}}$, where the potential impulse $\boldsymbol{p}_\phi$ and the vortical impulse $\boldsymbol{p}_{\mathrm{v}}$ are given by (see [25] for further details)

$$
\begin{aligned}
\boldsymbol{p}_\phi &= -\rho\int_{\partial\mathcal{B}}\phi\,\boldsymbol{n}\,dS \\
\boldsymbol{p}_{\mathrm{v}} &= \int_{\mathcal{V}}\rho\,\boldsymbol{x}\times\boldsymbol{\omega}\,dV + \int_{\partial\mathcal{B}}\rho\,\boldsymbol{x}\times(\boldsymbol{n}\times\boldsymbol{u}_{\mathrm{w}})\,dS.
\end{aligned}
\tag{3}
$$

The same decomposition may be used for the angular impulse which, by using appropriate vector identities, can be split into its potential and vortical parts as $\boldsymbol{\pi} = \boldsymbol{\pi}_\phi + \boldsymbol{\pi}_{\mathrm{v}}$, where

$$
\begin{aligned}
\boldsymbol{\pi}_\phi &= -\rho\int_{\partial\mathcal{B}}\boldsymbol{x}\times\phi\boldsymbol{n}\,dS \\
\boldsymbol{\pi}_{\mathrm{v}} &= -\frac{1}{2}\int_{\mathcal{V}}\rho|x|^2\,\boldsymbol{\omega}\,dV \\
&\quad - \frac{1}{2}\int_{\partial\mathcal{B}}\rho|x|^2(\boldsymbol{n}\times\boldsymbol{u}_{\mathrm{w}})\,dS.
\end{aligned}
\tag{4}
$$

By combining the Newton laws with equation (1) and by eliminating the time derivatives, we obtain, for null initial conditions, the conservation of the linear and angular momenta as

$$
\begin{aligned}
\int_{\mathcal{B}}\rho_{\mathrm{b}}\boldsymbol{u}_{\mathrm{b}}\,dV + \boldsymbol{p} &= 0 \\
\int_{\mathcal{B}}\rho_{\mathrm{b}}\boldsymbol{x}\times\boldsymbol{u}_{\mathrm{b}}\,dV + \boldsymbol{\pi} &= 0.
\end{aligned}
\tag{5}
$$

The body velocity $\boldsymbol{u}_{\mathrm{b}}$ is given by the sum of the prescribed deformation velocity $\boldsymbol{u}_{\mathrm{sh}}$ plus the unknown rigid motion of the body-fixed frame with origin in the centre-of-mass (translational, $\boldsymbol{u}_{cm}$, and rotational, $\boldsymbol{\Omega}$, velocity):

$$
\boldsymbol{u}_{\mathrm{b}} = \boldsymbol{u}_{\mathrm{sh}} + \boldsymbol{u}_{\mathrm{cm}} + \boldsymbol{\Omega}\times\boldsymbol{x}'
\tag{6}
$$

where $\boldsymbol{x}'$ is the position vector in the body frame, i.e. $\boldsymbol{x} = \boldsymbol{x}_{\mathrm{cm}} + \boldsymbol{x}'$.

As a mandatory requirement for equation (6) to be valid, since no rigid motions are allowed for an isolated body, the body deformation velocity have to satisfy the following two conditions

$$
\int_{\mathcal{B}}\rho_{\mathrm{b}}\boldsymbol{u}_{\mathrm{sh}}\,dV = 0 \qquad \int_{\mathcal{B}}\rho_{\mathrm{b}}\boldsymbol{x}'\times\boldsymbol{u}_{\mathrm{sh}}\,dV = 0
\tag{7}
$$

so as the net linear and angular momenta of the imposed kinematics are equal to zero. Finally, by

combining equations (5) and (6) with the above conditions (7), we obtain:

$$m_b \boldsymbol{u}_{cm} + \boldsymbol{p} = 0$$
$$I_{zz}\Omega + \pi' = 0 \qquad (8)$$

where the angular impulse is recast in terms of the distance $\boldsymbol{x}'$ as $\pi' = (\boldsymbol{\pi} - \boldsymbol{x}_{cm} \times \boldsymbol{p}) \cdot \boldsymbol{e}_3$ and $\boldsymbol{x}_{cm} = x_{cm}\boldsymbol{e}_1 + y_{cm}\boldsymbol{e}_2$ is the position of the body center of mass.

In the most general case, especially when designing a prescribed deformation kinematics $\overline{\boldsymbol{u}}_{sh}$, equation (7) are very unlikely to be satisfied and they read as

$$\int_{\mathcal{B}} \rho_b \overline{\boldsymbol{u}}_{sh} \, dV = m_b \boldsymbol{u}_0 \qquad \int_{\mathcal{B}} \rho_b \boldsymbol{x}' \times \overline{\boldsymbol{u}}_{sh} \, dV = I_{zz}\Omega_0 \qquad (9)$$

where m_b and I_{zz} are the mass and the moment of inertia of the body respectively and $\boldsymbol{u}_0$ and Ω_0 represent spurious rigid motion embedded in the prescribed kinematics. In the present approach, to obtain directly the velocity of the body center of mass [26, 27], $\overline{\boldsymbol{u}}_{sh}$ should be properly modified by accounting for a corrective motion able to counterbalance and to annihilate $\boldsymbol{u}_0$ and Ω_0. We refer to this motion as geometrical recoil correction, essential to ensure that any deformation assigned to the body is actually viable in the absence of the interactions with the surrounding fluid.

The expended energy is obtained in terms of the fluid kinetic energy released into the flow field [28] as

$$E = \frac{1}{2}\int_S \phi \frac{\partial \phi}{\partial n} \, dS + \frac{1}{2}\int_S (\boldsymbol{u}_w \times \boldsymbol{\psi}) \cdot \boldsymbol{n} \, dS$$
$$+ \frac{1}{2}\int_V \boldsymbol{\psi} \cdot \boldsymbol{\omega} \, dV \qquad (10)$$

where the last term is commonly known as the excess energy while the first two integrals are usually quite negligible at steady state conditions.

2.2. Solution procedure
Going back to the Helmholtz decomposition introduced by equation (2), the scalar potential may be further divided as $\phi = \phi_{sh} + \phi_{loc}$ [29], so as

$$\frac{\partial \phi_{sh}}{\partial n} = \boldsymbol{u}_{sh} \cdot \boldsymbol{n} \qquad \frac{\partial \phi_{loc}}{\partial n} = (\boldsymbol{u}_{cm} + \boldsymbol{\Omega} \times \boldsymbol{x}') \cdot \boldsymbol{n} \quad (11)$$

where ϕ_{sh} and ϕ_{loc} are associated to the prescribed deformation velocity $\boldsymbol{u}_{sh}$ and to the locomotion (linear and angular) velocity respectively, according to the related boundary conditions on S_b. It follows that the linear and angular impulses may be also split as

$$\boldsymbol{p}_\phi = \boldsymbol{p}_{sh} + \boldsymbol{p}_{loc} \qquad \pi'_\phi = \pi'_{sh} + \pi'_{loc} \qquad (12)$$

accordingly with the above decomposition.

In line with classical treatises (see e.g. [30]), we may express $\boldsymbol{p}_{loc}$ and π'_{loc} by defining the added mass coefficients m_{ij} as

$$m_{ij} = -\rho \int_{\partial \mathcal{B}} \Phi_i \frac{\partial \Phi_j}{\partial n} \, dS \qquad (13)$$

where the Kirchhoff base potentials Φ_j are defined through the boundary conditions

$$\frac{\partial \Phi_1}{\partial n} = \boldsymbol{n} \cdot \boldsymbol{e}_1 \qquad \frac{\partial \Phi_2}{\partial n} = \boldsymbol{n} \cdot \boldsymbol{e}_2 \qquad \frac{\partial \Phi_3}{\partial n} = \boldsymbol{x}' \times \boldsymbol{n} \cdot \boldsymbol{e}_3 \qquad (14)$$

to finally have

$$\phi_{loc} = \dot{x}_{cm}\Phi_1 + \dot{y}_{cm}\Phi_2 + \Omega\Phi_3. \qquad (15)$$

By using equations (12) and (15), the final system of equations is obtained by recasting equation (8) in a reference frame fixed to the body center of mass. With the use of capital letters for the unknowns linear (V_1, V_2) and angular (Ω) velocities in this frame, we may bring to the right hand side only the known terms due to shape deformation and released vorticity, so to obtain the system

$$\begin{cases} V_1(m_{11} + m_b) + V_2 m_{12} + \Omega m_{13} = -P_{sh1} - P_{v1} \\ V_1 m_{21} + V_2(m_{22} + m_b) + \Omega m_{23} = -P_{sh2} - P_{v2} \\ V_1 m_{31} + V_2 m_{32} + \Omega(m_{33} + I_{zz}) = -\Pi_{sh} - \Pi_v \end{cases} \qquad (16)$$

to be solved at each time step for the unknown velocity components. In the previous sections, to lighten the reading, the velocity components have been renamed as $U = -V_1$ and $V = V_2$, while the mean steady-state value of the forward velocity U will be referred to as the locomotion velocity U_{loc} which identifies the locomotion frame of reference, i.e. a reference frame moving with the locomotion velocity itself. The remaining lateral and angular velocity components V and Ω together with the forward velocity fluctuations U', define the body-fixed frame motion within the locomotion frame and will be referred to as fluid recoil motions. Many authors (see e.g. [17, 18, 31]), by following Lighthill's first definition of recoil [32] as the motion to be added to a prescribed deformation to satisfy the linear and angular momentum conservation laws, do not distinguish between the geometrical recoil correction and the one resulting only from the fluid-body interaction, i.e. the fluid recoil. Although this approach substantially differs from the one proposed here, it is equally suitable to obtain the correct solution [26]. However, we favour our methodology since it is able to reveal the role of both contributions and may provide a useful insight for the design of optimal deformation gaits.

Finally, due to the linearity of the present model, the system of equation (16) is solved by splitting the unknown velocity components (U, V, Ω) into their potential contributions $(U_\phi, V_\phi, \Omega_\phi)$ and their vortical contributions (U_v, V_v, Ω_v). The potential ones

are obtained by solving the system only for the potential impulses associated to the shape deformation $\boldsymbol{P}_{\text{sh}}$ and Π_{sh}, while the vortical contributions are obtained by solving for the vortical impulses $\boldsymbol{P}_{\text{v}}$ and Π_{v}.

The flow solutions are obtained by a simple 2D inviscid model with concentrated vorticity, which allow for neat and physically intuitive results. Specifically, we used an unsteady potential code based on the Hess and Smith approach [33], while the vortex shedding is treated by following the procedure described in [34]. This well-known numerical procedure has been extensively used in the literature to study rigid bodies like airfoils moving with a fully prescribed motion [2, 4, 35–37]. Since in the present application the linear and angular rigid body velocities are unknown for free swimming of a deformable body (see also [11, 12]), the coupling between its dynamics and the flow solution implies a much larger complexity.

2.3. Caudal fin shape and kinematics

The anterior part of the two-dimensional body is represented by a NACA0012 hydrofoil with length l_{b} while the caudal fin is represented by a NACA0004 with length l_{t}. The tail length l_{t}, illustrated in figure 1, is equal to 1/7 of the total body length $L = l_{\text{b}} + l_{\text{t}}$, as frequently observed in nature for oscillatory swimmers like tuna.

The caudal fin kinematics is fully prescribed and its flapping motion is given by the combination of a heaving motion of the peduncle $y_{\text{p}}(t)$ and a pitching motion about the peduncle itself given by $\theta(t)$. The pitch motion $\theta(t)$ has a phase angle $\phi = -\pi/2$ with respect to the heave motion, so to have

$$y_{\text{p}}(t) = h_0 \sin(2\pi f t)$$
$$\theta(t) = \theta_0 \sin(2\pi f t + \phi) \quad (17)$$

where h_0 is the maximum heave amplitude, θ_0 is the maximum pitch angle and f is the oscillation frequency. The phase shift ϕ between these motions has been chosen to be consistent with many observations either in nature or in experimental investigations. According to these assumptions, the lateral motion of the caudal fin is finally given as

$$y_f(s_f, t) = y_{\text{p}}(t) - s_f \sin(\theta(t)) \quad (18)$$

where s_f goes from 0 to l_{t}, i.e. from the peduncle to the trailing edge of the tail, and $\theta(t)$ is taken positive in the clockwise direction.

With regard to the prescribed body deformation, we followed a path similar to the one suggested by Li *et al* [38] for a pure oscillation of the rear-end of the anterior body, but we consider a proper undulatory motion to better represent the shape deformations observed in real fish. The procedure to obtain the body kinematics, which is both fitting the flapping motion of the caudal fin and satisfying the inextensibility condition, is described in the appendix.
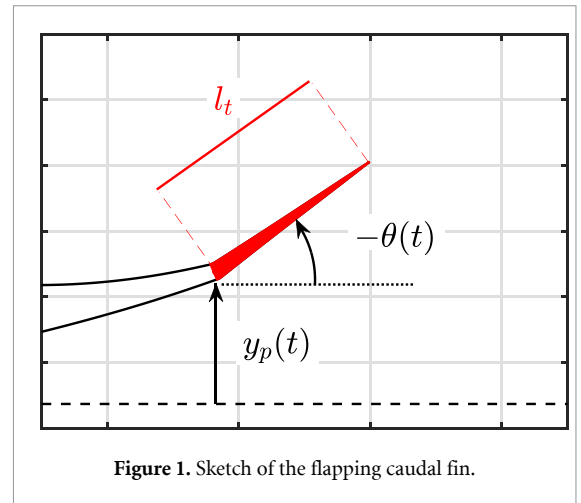

Figure 1. Sketch of the flapping caudal fin.

It is interesting to compare the flapping motion under consideration with an undulatory motion to look for possible similarities concerning the existence of a phase velocity also in the present case. By considering sufficiently small values of the maximum pitch angle θ_0, the flapping motion of the tail given by equation (18) may be approximated as

$$y(x, t) \approx h_0 \sin(2\pi f t) - \theta_0 x \cos(2\pi f t) \quad 0 \leqslant x \leqslant l_{\text{t}} \quad (19)$$

where s_f has been confused with the abscissa x. This approximated expression may be assimilated to the one for an undulatory motion of amplitude h_0 with a wavelength $\lambda \gg l_{\text{t}}$

$$y(x, t) = h_0 \sin\left(2\pi f t - \frac{2\pi}{\lambda} x\right)$$
$$\approx h_0 \sin(2\pi f t) - \frac{2\pi}{\lambda} h_0 x \cos(2\pi f t) \quad 0 \leqslant x \leqslant l_{\text{t}} \quad (20)$$

and, by equating the coefficients of (19) and (20), we may evaluate the phase velocity of the flapping motion as

$$c = f\lambda \approx 2\pi f \frac{h_0}{\theta_0}. \quad (21)$$

In other words, if $\lambda \gg l_{\text{t}}$, the flapping tail itself may be seen as a small portion of the longer wave whose undulating motion is perceived, instantaneously, as a local oscillation given by the heave and pitch motions.

The above derived equation (21) for the phase velocity associated to the tail reminds in some way the proportional-feathering parameter $\Theta = \theta_0 \, U_{\text{loc}}/2\pi f h_0$, ingeniously suggested by Lighthill [32] to qualify the propulsive performance of flapping foils. It is straightforward to obtain the expression of Θ in this case simply as the ratio between the locomotion velocity U_{loc} and the phase velocity given by equation (21), usually identified as the slip velocity [39].

One of the main parameters characterizing the flapping motion of the caudal fin is the peak-to-peak oscillation amplitude of the trailing edge A_{te} which, for small values of the θ_0, may be approximated by using the following expression:

$$A_{te} \approx 2\sqrt{h_0^2 + 2\,h_0\,l_t\theta_0\cos(\phi) + l_t^2\,\theta_0^2} \qquad (22)$$

valid for any value of the phase-lag. In the present case, since the phase angle ϕ is equal to $-\pi/2$, equation (22) reads as

$$A_{te} \approx \sqrt{A_h^2 + 4\,l_t^2\,\theta_0^2} \qquad (23)$$

where the peak-to-peak heave amplitude A_h has been defined as $A_h = 2\,h_0$. By combining equations (21) and (23), it follows

$$c \approx 2\pi f l_t \frac{A_h/A_{te}}{\sqrt{1 - (A_h/A_{te})^2}} \qquad (24)$$

where it can be appreciated how the phase velocity depends only on the ratio between A_{te} and the maximum excursion of the peduncle A_h. In other words, if A_h/A_{te} is fixed, the phase velocity would be constant no matter the value of A_{te}. From equation (24), it is interesting to note how the phase velocity is rapidly increasing for A_h/A_{te} going to one.

To restrict in a reasonable way the parameter space to be analyzed, we fixed the value of the design trailing edge oscillation amplitude A_{te} that is usually taken to be approximately 0.2 from well-known experimental evidence [40].

3. Results

We consider a fishlike body self-propelled by an oscillating caudal fin in free swimming mode with no viscous resistance. This ideal case is shown to be very useful to understand how the recoil is combined with the prescribed caudal fin motion to obtain the resulting flapping kinematics.

As a first step, the time history of the forward velocity and of the fluid kinetic energy (see equation (10)) for different values of the design parameters in free swimming condition are reported in figures 2(a) and (b), respectively. After an initial transient, the forward velocity reaches a steady-state condition characterized by fluctuations around a mean value classically identified as the locomotion velocity U_{loc}. By looking at both figures 2(a) and (b), we may observe how the kinetic energy transferred to the fluid (see section 2) increases for larger oscillation amplitude of the forward velocity, i.e. for increasing values of the design pitch amplitude θ_0. At the same time, due to the fixed value of the design parameter A_{te}, a decrease of θ_0 is accompanied by an increase of the heave amplitude h_0, which may be associated to larger value of the locomotion velocity.

At this point it is instructive to discuss how the phase velocity and the asymptotic locomotion speed are related to the main parameters h_0 and θ_0.

A simple gait representation is given by figure 3(a) which has been constructed by reporting a few successive configurations of the entire body in free swimming mode to highlight, with their envelope, the wave-like character of the caudal fin motion. We may observe how the tail trajectory follows a sinusoidal path characterized by a wavelength λ obtained with a good approximation as

$$\lambda = \frac{c}{f} \approx 2\pi \frac{h_0}{\theta_0} \qquad (25)$$

where the phase velocity c has been evaluated by using equation (21) with the flapping parameters h_0 and θ_0 obtained in free swimming condition. From the same figure and even better from the related animation (see the movie in the supplementry material online), it appears that the caudal fin motion drives the swimming gait along a traveling wave, while the anterior body seems to have a neutral role with respect to the illustrated motion. More specifically, figure 3(b) reports a comparison between the forward locomotion speed and the estimated phase velocity c both for the case of a swimmer not accounting for any recoil motion, from now on referred to as no-recoil swimmer, and for the case of a fully free swimmer characterized by the same initial design parameters. In both cases the estimated value of the phase velocity, through equation (24) with the proper values of the parameters, is quite close to the actual value of the locomotion speed, though a large difference is observed between the two swimming conditions. The mean power consumption P_m is reported in figure 3(c) to show the different trends with respect to design value of A_h/A_{te}. While P_m is decreasing as A_h/A_{te} goes to one for the free swimmer, the opposite is occurring for the no-recoil swimmer. It follows a markedly better performance in terms of cost of transport when the fish is able to exploit the recoil motions to line up its body to the fluid flowing about, with a resulting more streamlined swimming style. The focus of the paper is on the analysis of the above differences in locomotion speed and expended power which are clearly due to the recoil motions accounted for only in the free mode. A careful investigation on its effects is still not available in the literature for oscillatory free swimming and a further deepening on the subject is certainly due. To this purpose, the adopted impulse model allows for the separation of the recoil in its geometrical, potential and vortical components whose different impact on the tail flapping parameters in free swimming mode are going to be presented below and carefully discussed in the next section.

Figure 4(a) shows the excursion ΔA_h of the peak-to-peak heave amplitude induced by the different recoil motions for all the cases under investigation. Both the geometrical and the potential recoil
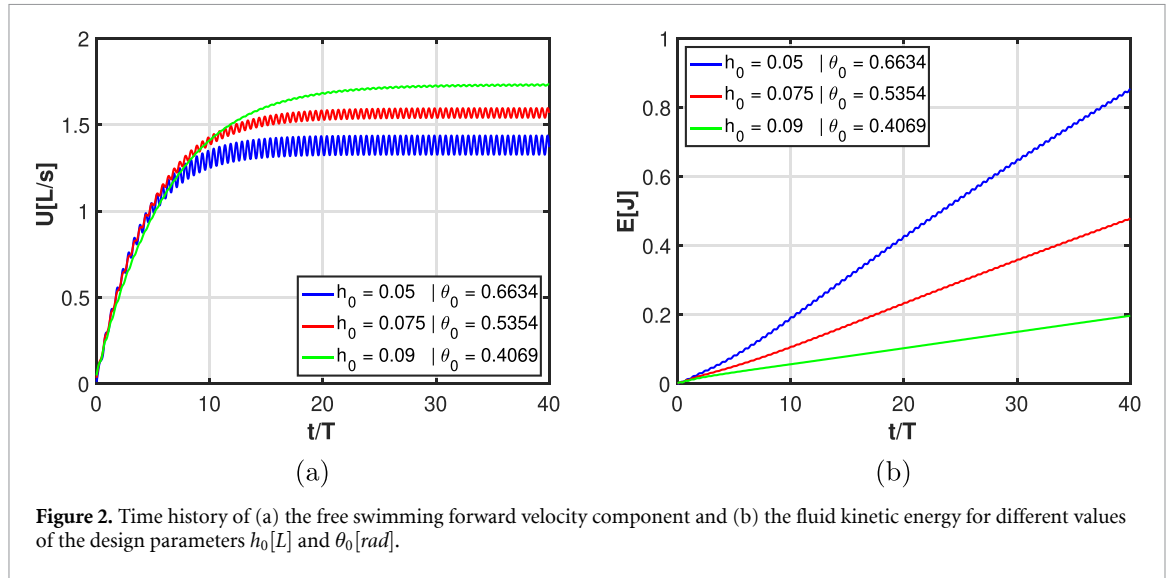
Figure 2. Time history of (a) the free swimming forward velocity component and (b) the fluid kinetic energy for different values of the design parameters $h_0[L]$ and $\theta_0[rad]$.
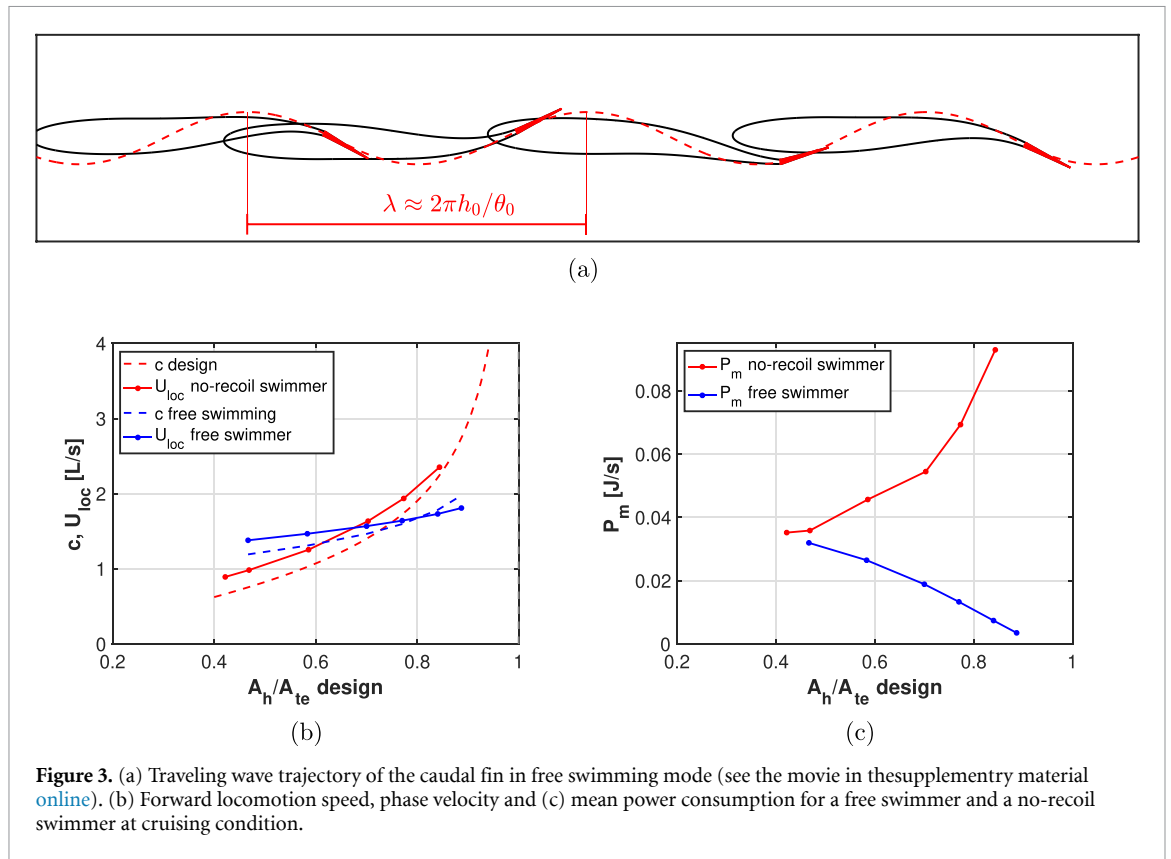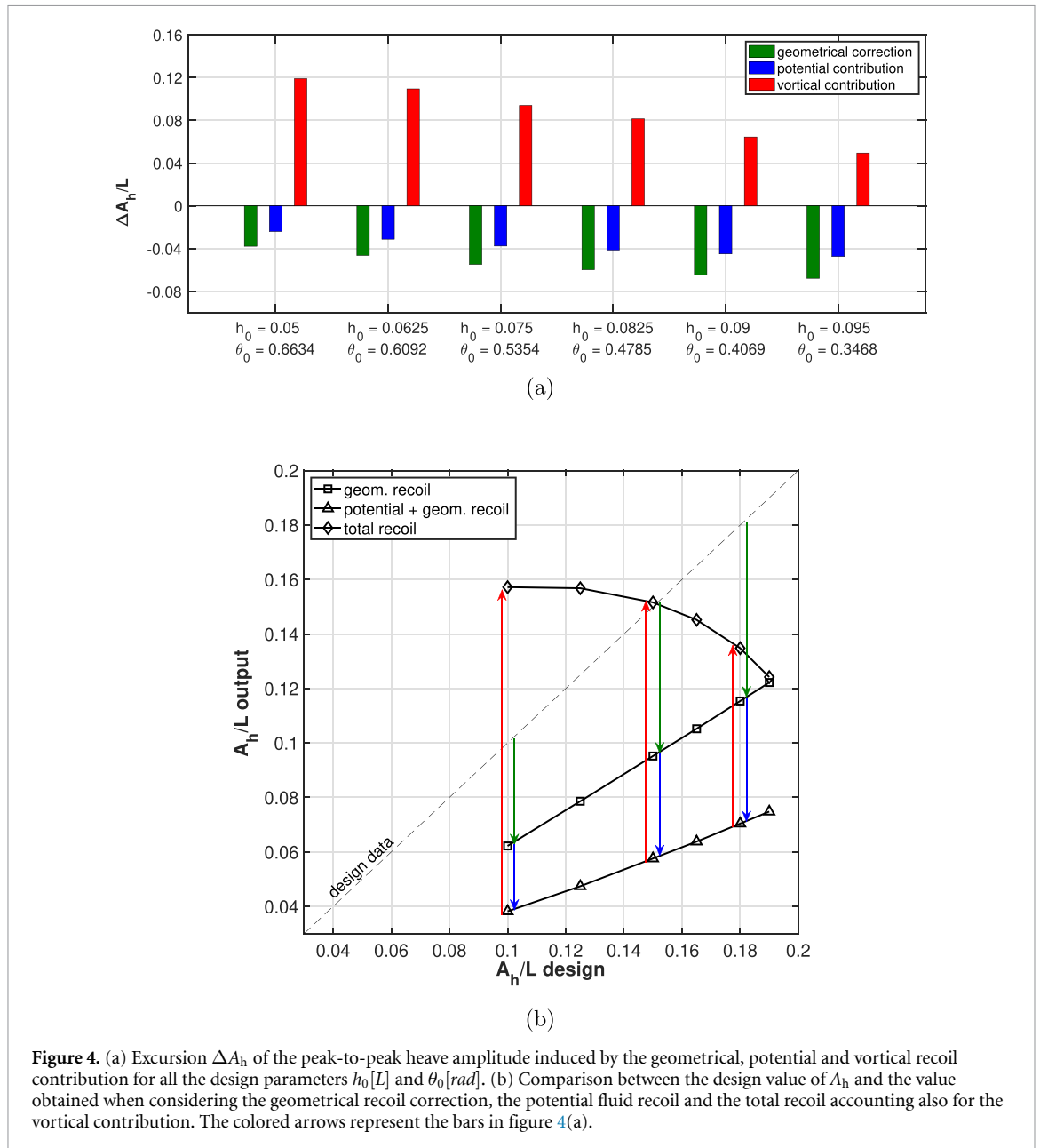

Figure 3. (a) Traveling wave trajectory of the caudal fin in free swimming mode (see the movie in thesupplementry material online). (b) Forward locomotion speed, phase velocity and (c) mean power consumption for a free swimmer and a no-recoil swimmer at cruising condition.

contributions are always negative and are increasing in their absolute value for larger design value of h_0, consequently leading to a reduction of the free swimming peak-to-peak peduncle amplitude A_h. On the other hand, the vortical contribution to ΔA_h given by the vortex shedding in the wake, shows exactly the opposite behaviour by decreasing with the prescribed h_0, i.e. increasing with θ_0 according to equation (23), and by showing a clear tendency to enhance the heave amplitude A_h, whose large values are commonly associated to a great propulsive capability. The final value of A_h may be obtained by

starting from its design value and summing up all the different contributions as reported in figure 4(b) where the colored arrows are representative of the bars in figure 4(a). By looking at the data obtained in free swimming condition in comparison with the prescribed ones, in some cases we notice an increase while in others a decrease of the heave amplitude, resulting in a quite unclear trend for the variation induced by the total recoil motions. However, by isolating the geometrical, potential and vortical contributions, a monotonic behaviour is clearly obtained for each component. Specifically, the geometrical recoil
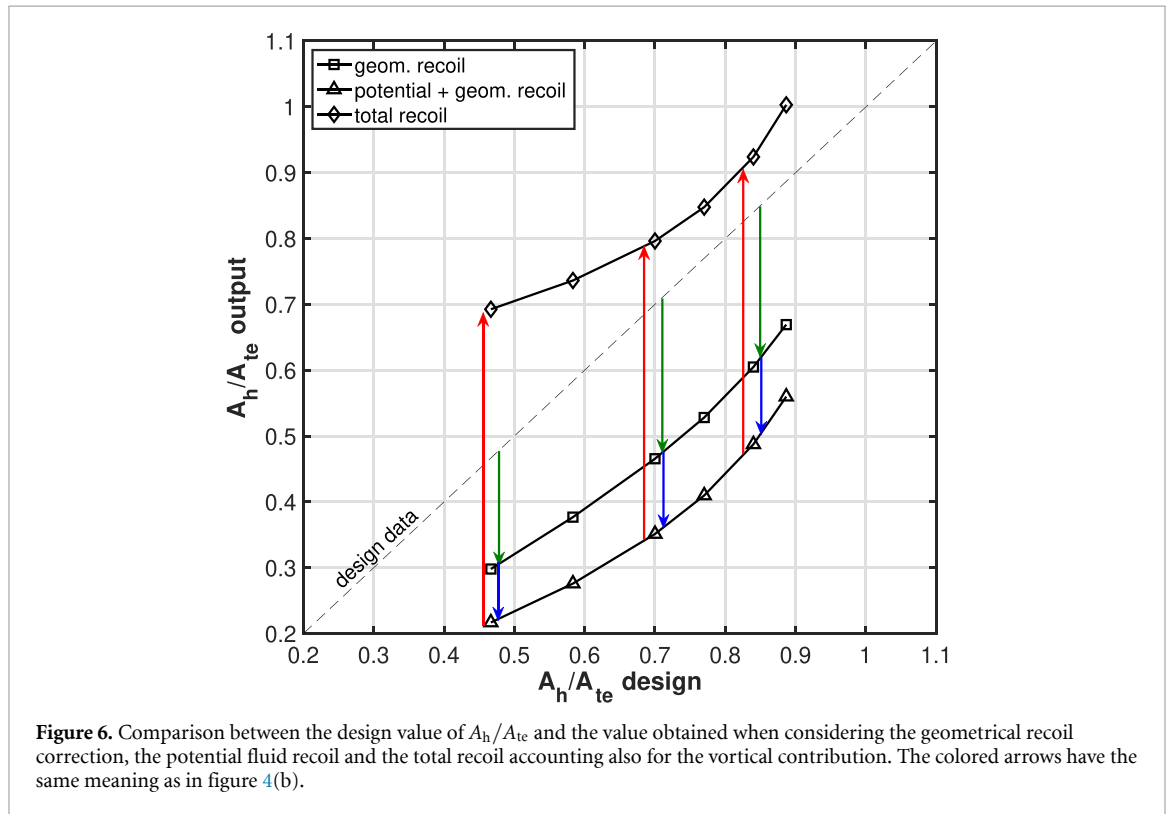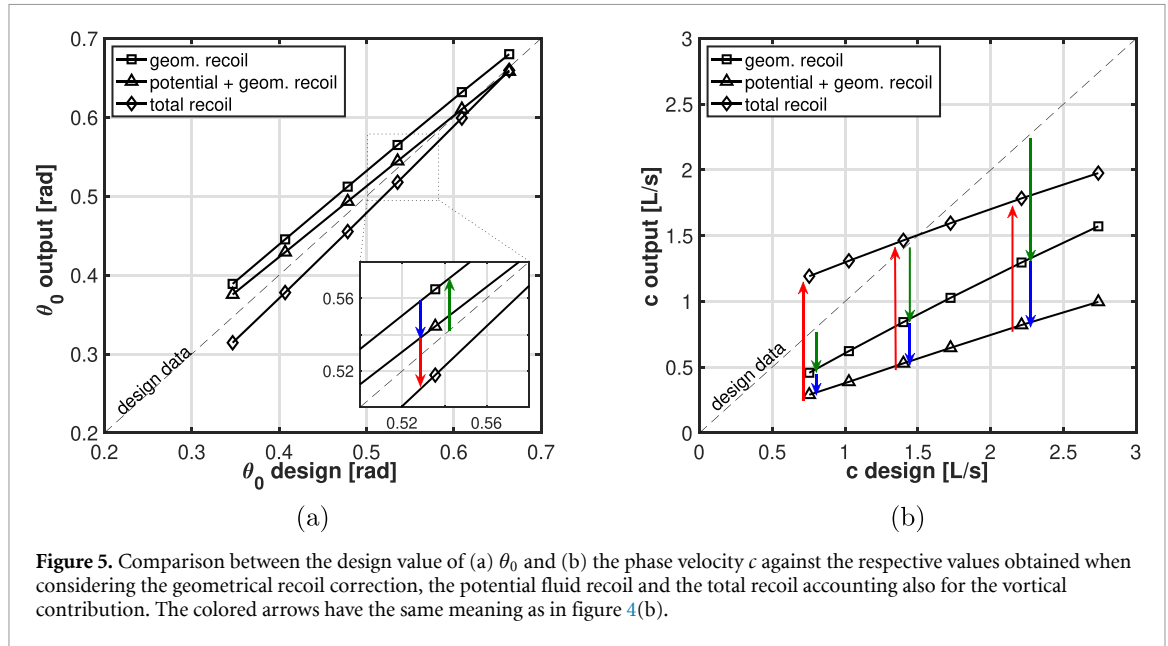
(a)

(b)

Figure 4. (a) Excursion ΔA_h of the peak-to-peak heave amplitude induced by the geometrical, potential and vortical recoil contribution for all the design parameters $h_0[L]$ and $\theta_0[rad]$. (b) Comparison between the design value of A_h and the value obtained when considering the geometrical recoil correction, the potential fluid recoil and the total recoil accounting also for the vortical contribution. The colored arrows represent the bars in figure 4(a).

correction is always giving a decrease in the peak-to-peak heave amplitude, followed by a further decrease due to the pure potential flow. The final value of A_h is reached when we consider also the vortical contribution, which always leads to its increase with respect to the potential case.

By adopting the same representation used for A_h (figure 4(b)), we observe how for the pitch angle θ_0, reported in figure 5(a), the influence of recoil motions seems to be quite negligible. Actually, the final θ_0 values, obtained once the total fluid recoil motions are considered, do not show a significant variation with respect to the design values. Nevertheless, it should be noticed that in this case the geometrical correction is going to increase the value of θ_0, while both fluid contributions have an opposite effect. The estimated phase velocity c and the ratio A_h/A_{te} reported in figures 5(b) and 6 show the same behaviour observed in figure 4(b) for A_h. Namely, the vortical fluid recoil is always contrasting the deterioration generated by the geometrical recoil correction and by the potential fluid recoil to enhance the values of the peak-to-peak values A_h/A_{te} and of the phase velocity c driving the asymptotic locomotion speed.

By comparing figures 5(b) and 6, it appears that even if the free swimming value of the ratio A_h/A_{te} is always increasing with respect to its design value, the same is not true for the phase velocity, whose trend follows closely the one observed in figure 4(b) for A_h. For the sake of consistency, this is not conflicting with the increase in the phase velocity with A_h/A_{te} suggested by equation (24) which is strictly valid for prescribed swimming with a phase lag between the

Figure 5. Comparison between the design value of (a) θ_0 and (b) the phase velocity c against the respective values obtained when considering the geometrical recoil correction, the potential fluid recoil and the total recoil accounting also for the vortical contribution. The colored arrows have the same meaning as in figure 4(b).

Figure 6. Comparison between the design value of A_h/A_{te} and the value obtained when considering the geometrical recoil correction, the potential fluid recoil and the total recoil accounting also for the vortical contribution. The colored arrows have the same meaning as in figure 4(b).

peduncle heave motion and the pitch of the caudal fin equal to $-\pi/2$, condition which is not usually verified in the free swimming mode under investigation in the present paper.

4. Discussion

As theoretically discussed in section 2, the deformation resulting from the geometrical parameters prescribed in a design procedure, in general, does not satisfy the equilibrium equations in the absence of fluid interactions as required to guarantee its feasibility in this condition. Figure 7(a) reports an extremely simplified sketch of a flapping fishlike body to attack such a subtle issue, frequently underestimated in the literature. The first frame on the left illustrates the body in its straight and undeformed configuration, while the second one illustrates a deformed one where the body rear-end representative of the tail is flexed by a clockwise angle β. For a fixed anterior body, the rotation of the tail is going to induce a downward motion of the body center of mass CM and a clockwise rotation of the inertia principal axes. However,
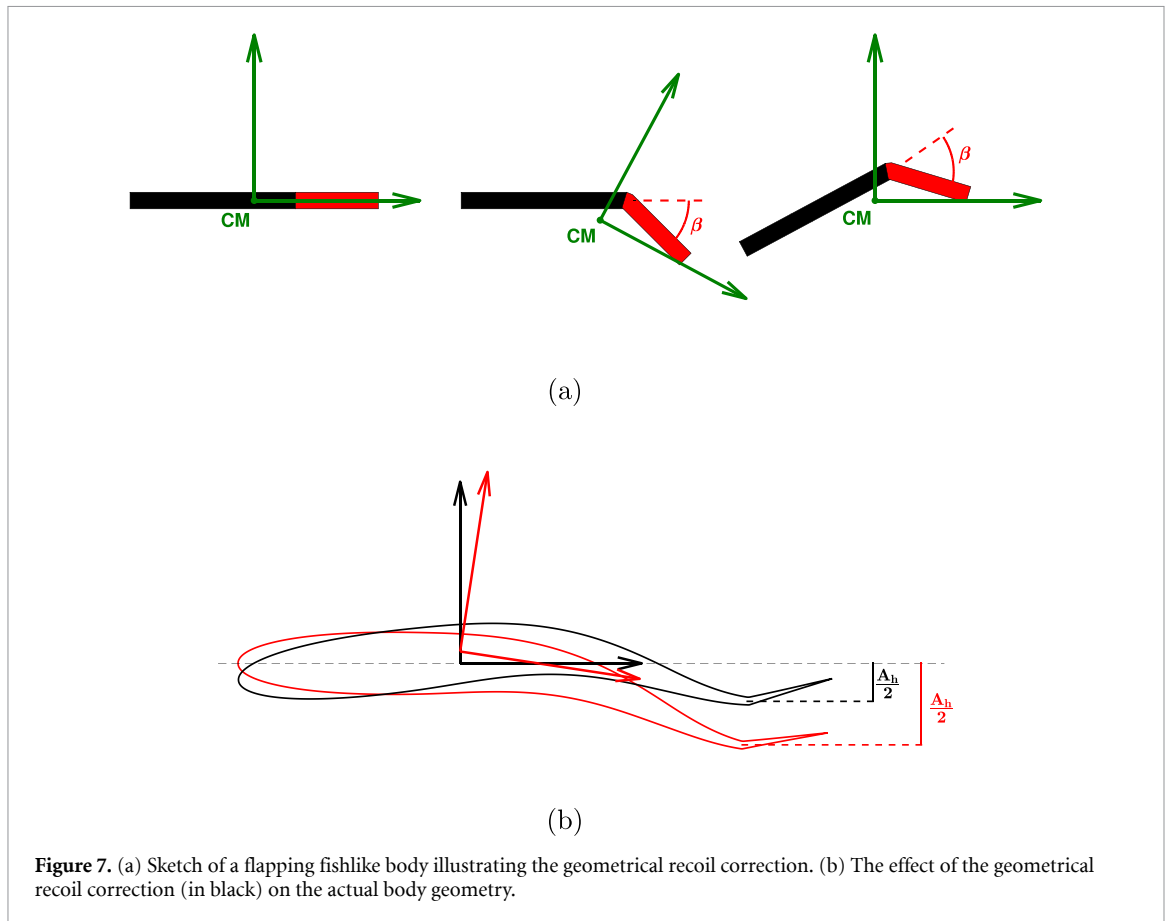
Figure 7. (a) Sketch of a flapping fishlike body illustrating the geometrical recoil correction. (b) The effect of the geometrical recoil correction (in black) on the actual body geometry.

for an isolated body, neither the translation of its center of mass nor the rotation of its principal axes are allowed since no external actions are applied. In this condition, the geometrical recoil correction is the motion required to make this configuration feasible, i.e. the motion required to go from the central frame in figure 7(a) to the last frame on the right, where the center of mass and the principal axes perfectly match the ones for the undeformed configuration. In this way, any spurious rigid motion introduced in the design procedure is annihilated by the geometrical recoil, whose impact on the actual body geometry is illustrated by figure 7(b) that gives a qualitative insight on its overall effects on the prescribed deformation. The results reported in the previous section show how the geometrical correction presents a general tendency to reduce all the relevant data but the pitch angle θ_0, whose variation is very small. As a consequence, the large reduction of the peduncle heave amplitude A_h leads to a smaller value of the asymptotic phase velocity c, hence to a lower performance in terms of the related locomotion speed. It follows that the geometrical recoil correction is definitely negative for the fish propulsive capability and it should be minimized, at least, for fully constrained motions [19, 20] to avoid such an evident deterioration of the performance. This last consideration is probably the reason for the bad reputation erroneously gained

in the past by the recoil with regard to swimming performance. Actually, the concept of recoil correction was initially introduced by Lighthill as a unique rigid motion, not distinguishing between the correction due to the interaction with the surrounding fluid and the geometrical one, which led subsequently to contradictory opinions on the subject. To this regard, a typical consideration is that some fish species have evolved deep and heavy head to counterbalance the rapid motions of the light caudal fin so to reduce lateral and angular oscillations about the center of mass to avoid performance deterioration, which is consistent, in the framework of our model, with the results reported in the previous section for the geometrical recoil.

Going now to the fluid recoil contributions, as illustrated in the section 2, the linearity of the present model allows for the separation of the potential-induced velocity components $(U_\phi, V_\phi, \Omega_\phi)$ from the vortical-induced velocity components (U_v, V_v, Ω_v) which, once combined, give the total fishlike body kinematics. This particular property of the model led to the results reported in figures 4–6 which clearly show how, even though the potential recoil gives another negative effect, the vortical recoil contribution is always leading to a consistent improvement of the flapping parameters. The opposite behaviour of the vortical contribution with respect
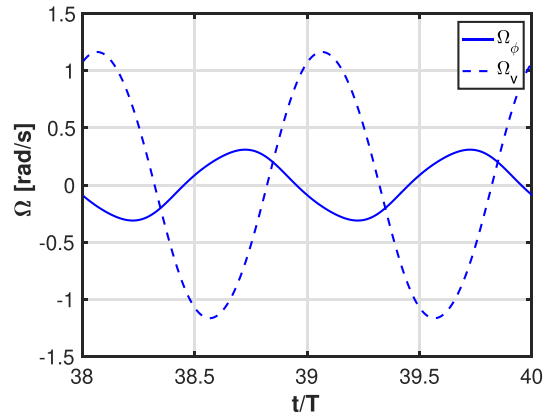
Figure 8. Comparison between the time history of the potential, Ω_ϕ, and vortical, Ω_v, contributions to the body angular velocity.

(a)   (b)
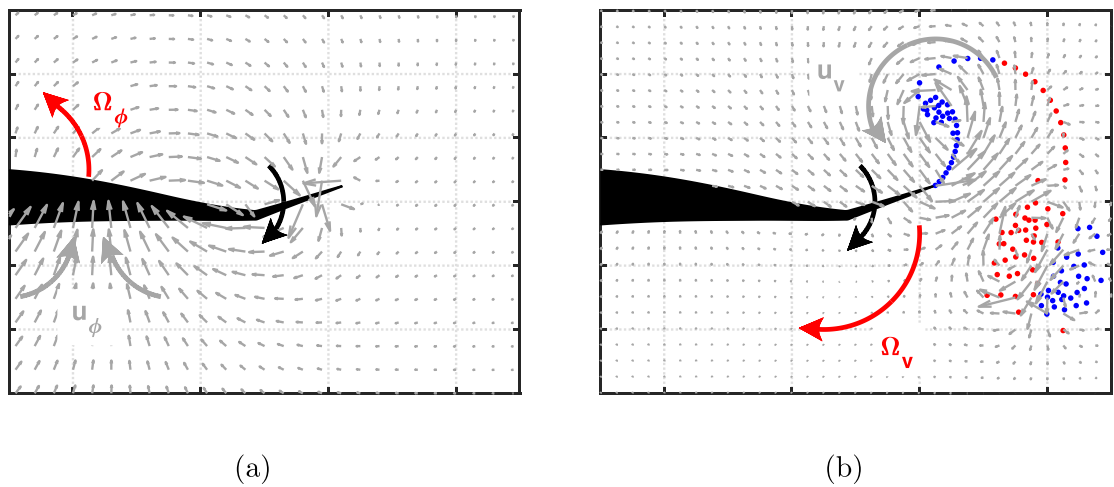
Figure 9. Flow field sketches for (a) the potential fluid recoil and (b) the vortical fluid recoil.

to the potential one is observable from the comparison between the time history of the potential-induced angular velocity Ω_ϕ with the vortical-induced angular velocity Ω_v reported in figure 8 for one sample case. The potential contribution Ω_ϕ has an opposite phase with respect to the vortical one Ω_v. This behaviour is perfectly consistent with the physical meaning of the two contributions related to the added mass and to the vortex shedding, respectively. The sample flow fields reported in figure 9, inspired by previous analyses [41, 42], may give a simple idea to understand their counteracting role. As illustrated in figure 9(a), the potential acyclic field $\boldsymbol{u}_\phi$ generated by the caudal fin downstroke leads to a counterclockwise angular velocity Ω_ϕ in the opposite direction with respect to tail motion. It follows that the potential recoil contribution, increasing with the body deformation (see figures 4–6), tends to counterbalance and to attenuate the tail oscillation. On the other hand, the vortical field reported in figure 9(b) shows an opposite behaviour since the fluid vortical velocity $\boldsymbol{u}_v$ induced by the vortex cluster just released

by the body is going to enhance the tail motion via the angular recoil velocity Ω_v, as it may easily result from figure 4(a).

As a general comment, it is worth to underline the tendency of the fluid recoil to enhance the heave amplitude up to a value strictly comparable with the trailing edge excursion A_{te} as shown by the increase of the ratio A_h/A_{te} which represents the fraction of the trailing edge amplitude due to the heave motion of the peduncle. The more A_h/A_{te} approaches unity, the more the caudal fin is flat at its maximum lateral position, so to lay, together with the anterior body, on the sinusoidal trajectory and to obtain a good swimming performance [9, 43]. Actually, the relationship between a high swimming performance and a flat tail excursion was already envisaged in the early sixties by Lighthill [15] who suggested to annihilate the slope of the midline amplitude modulation to maximize the swimming efficiency. Interestingly for the no-recoil swimmer, since the body is not able to align with the flow, the expended energy keeps increasing with A_h/A_{te} as shown in figure 3(c).

5. Concluding remarks

The different style of swimming proper of different fish species brought, in the past, to several specific approximations, which in most cases are not anymore strictly required [44]. For instance, oscillatory swimming, classically investigated in axial motion to look for the best propulsive efficiency of the caudal fin, should be analyzed by considering the free mode of the whole body, as commonly done for undulatory swimming. In fact, the free self-propulsion reveals the importance of the recoil rigid motions, given by the fluid interaction, which are essential to guarantee the overall equilibrium and may drastically modify the kinematics of the caudal fin with respect to the prescribed one, to finally obtain a better swimming performance. The recoil reaction and the locomotion speed are obtained here by a simple impulse model able to highlight the added mass and the released vorticity contributions, together with their coupling terms which are especially important in transient conditions [45]. This model allows to understand the capability of the potential terms to attenuate the recoil reaction continuously forced by the vortex shedding which is directly related to the wasted energy. Since the input deformation prescribed in a design procedure usually is not satisfying the equilibrium equations to guarantee null rigid motions of the body in the absence of fluid interaction, the induced spurious rigid displacements are removed by a geometrical recoil correction. The direct application of the impulse model to such corrected shape deformation helps the physical interpretation of the results since it provides a more clear pattern from the input to the output values of the caudal fin parameters. In fact, by combining the fluid recoil with both heave and pitch motions modified by the geometrical recoil, the actual features of the caudal fin in the inertial frame are identified together with the associated phase velocity which drives the locomotion speed in inviscid flows. In a few words, the illustrated simple model may give helpful suggestions to figure out the free motion of a biomimetic body in water and to select a deformation able to generate the desired swimming performance for biomimetic technological means.

Data availability statement

All data that support the findings of this study are included within the article (and any supplementary files).

Acknowledgments

Appendix. Anterior body deformation

For the prescribed deformation of the anterior body, we followed a path similar to the one suggested by Li *et al* [38] for a pure oscillation up the peduncle, but we consider a proper undulatory motion with wavelength λ to better represent the shape deformations observed in real fish and to better fit the flapping motion of the caudal fin. In details, the first third of the anterior body midline is fixed and the remaining rear-end of length $l_r = l_b - 1/3$ is divided into N segments of length l_i. For a given penduncle oscillation amplitude h_0, the lateral motion $y_i(t)$ of the left edge of each segment is defined as

$$\begin{cases} y_1(s_1,t) = 0 \\ y_i(s_i,t) = h_i \sin\left(2\pi f t - \dfrac{2\pi}{\lambda} s_i\right) & i = 2, ..., N \\ y_p(t) = h_p \sin\left(2\pi f t - \dfrac{2\pi}{\lambda} l_r\right) & \text{for the peduncle} \end{cases} \tag{.1}$$

where the coefficients h_i is the maximum lateral displacement of the *ith* segment and s_i is a curvilinear abscissa going from 0 to 1, i.e. from the first third of the body to the penducle. The coefficients h_i and the instantaneous inclination of each segment Ψ_i may be obtained as follows

$$\begin{cases} h_1 = 0 \\ h_i = h_0 \left(\dfrac{\sum_{j=1}^{i-1} l_j}{l_r}\right)^2 & i = 2, ..., N \end{cases} \tag{.2}$$

$$\begin{cases} \Psi_i(s_i,t) = \arcsin \dfrac{y_{i+1}(s_{i+1},t) - y_i(s_i,t)}{l_i} & i = 1, ..., N-1 \\ \Psi_N(s_N,t) = \arcsin \dfrac{y_p(t) - y_N(s_N,t)}{l_N}. \end{cases} \tag{.3}$$

ORCID iDs

D Paniccia ⬤ https://orcid.org/0000-0002-1154-2783
G Graziani ⬤ https://orcid.org/0000-0002-7522-6755

References

[1] Garrick I E 1936 Propulsion of a flapping and oscillating airfoil *National Advisory Committee for Aeronautics: Report (NACA)* vol 567
[2] Jones K and Platzer M 1997 Numerical computation of flapping-wing propulsion and power extraction *AIAA Paper* vol 97 p 0826

[3] Anderson J M, Streitlien K, Barrett D S and Triantafyllou M S 1998 Oscillating foils of high propulsive efficiency *J. Fluid Mech.* **360** 41–72

[4] Young J and Lai J C S 2007 Mechanisms influencing the efficiency of oscillating airfoil propulsion *AIAA J.* **45** 1695–702

[5] Floryan D, Van Buren T, Rowley C W and Smits A J 2017 Scaling the propulsive performance of heaving and pitching foils *J. Fluid Mech.* **822** 386–97

[6] Fernandez-Feria R 2017 Note on optimum propulsion of heaving and pitching airfoils from linear potential theory *J. Fluid Mech.* **826** 781–96

[7] Akoz E and Moored K W 2018 Unsteady propulsion by an intermittent swimming gait *J. Fluid Mech.* **834** 149–72

[8] Akoz E, Han P, Liu G, Dong H and Moored K W 2019 Large-amplitude intermittent swimming in viscous and inviscid flows *AIAA J.* **57** 1–8

[9] Paniccia D, Padovani L, Graziani G and Piva R 2021 The performance of a flapping foil for a self-propelled fishlike body *Sci. Rep.* **11** 22297

[10] Li G, Liu H, Muller U K, Voesenek C J and van Leeuwen J L 2021 Fishes regulate tail-beat kinematics to minimize speed-specific cost of transport *Proc. R. Soc.* B **288** 20211601

[11] Carling J, Williams T L and Bowtell G 1998 Self-propelled anguilliform swimming simultaneous solution of the two-dimensional navier-stokes equations and newtons laws of motion *J. Exp. Biol.* **201** 3143–66

[12] Kern S and Koumoutsakos P 2006 Simulations of optimized anguilliform swimming *J. Exp. Biol.* **209** 4841–57

[13] Yang Y, Wu G H, Yu Y-L and Tong B G 2008 Two-dimensional self-propelled fish motion in medium an integrated method for deforming body dynamics and unsteady fluid dynamics *Chin. Phys. Lett.* **25** 597–600

[14] Borazjani I and Sotiropoulos F 2010 On the role of form and kinematics on the hydrodynamics of self-propelled body-caudal fin swimming *J. Exp. Biol.* **213** 89–107

[15] Lighthill J 1960 Note on the swimming of slender fish *J. Fluid Mech.* **9** 305–17

[16] Li G, Muller U K, van Leeuwen J L and Liu H 2012 Body dynamics and hydrodynamics of swimming fish larvae: a computational study *J. Exp. Biol.* **215** 4015–33

[17] Reid D A P, Hildenbrandt H, Padding J T and Hemelrijk C K 2012 Fluid dynamics of moving fish in a two-dimensional multiparticle collision dynamics model *Phys. Rev.* E **85** 021901

[18] Maertens A P, Gao A and Triantafyllou M S 2017 Optimal undulatory swimming for single fish-like body and for pair of interacting swimmers *J. Fluid Mech.* **813** 301–45

[19] Paniccia D, Graziani G, Lugni C and Piva R 2021 The relevance of recoil and free swimming in aquatic locomotion *J. Fluids Struct.* **103** 103290

[20] Sohn S 2021 A computational model of the swimming dynamics of a fish-like body in two dimensions *Phys. Fluids* **33** 121902

[21] Lighthill J 1971 Large-amplitude elongated body theory of fish locomotion *Proc. R. Soc.* B **179** 126–38

[22] Noca F 1997 On the evaluation of time-dependent fluid dynamic forces on bluff bodies *PhD Thesis* California Institute of Technology

[23] Graziani G and Bassanini P 2002 Unsteady viscous flows about bodies: Vorticity release and forces *Meccanica* **37** 283–303

[24] Wu J Z, Ma H Y and Zhou M D 2015 *Vortical Flows* (Berlin: Springer)

[25] Paniccia D, Graziani G, Lugni C and Piva R 2021 On the role of added mass and vorticity release for self propelled aquatic locomotion *J. Fluid Mech.* **918** A45

[26] Bhalla A P S, Bale R, Griffith B E and Patankar N A 2013 A unified mathematical framework and an adaptive numerical method for fluid-structure interaction with rigid deforming and elastic bodies *J. Comput. Phys.* **250** 446–76

[27] Singh K and Pedley T J 2008 The hydrodynamics of flexible-body manoeuvres in swimming fish *Physica* D **237** 2234–9

[28] Kanso E 2009 Swimming due to transverse shape deformations *J. Fluid Mech.* **631** 127–48

[29] Saffman P G 1967 The self-propulsion of a deformable body in a perfect fluid *J. Fluid Mech.* **28** 385

[30] Lamb H 1975 *Hydrodynamics* 6th edn (Cambridge: Cambridge University Press)

[31] Borazjani I and Sotiropoulos F 2008 Numerical investigation of the hydrodynamics of carangiform swimming in the transitional and inertial flow regimes *J. Exp. Biol.* **211** 1541–58

[32] Lighthill J 1970 Aquatic animal propulsion of high hydromechanical efficiency *J. Fluid Mech.* **44** 265–301

[33] Hess J L and Smith A M O 1967 Calculation of potential flow about arbitrary bodies *Prog. Aerosp. Sci.* **8** 1–138

[34] Basu B C and Hancock G J 1978 The unsteady motion of a two-dimensional aerofoil in incompressible inviscid flow *J. Fluid Mech.* **87** 159–78

[35] Jones K D, Dohring C M and Platzer M F 1998 Experimental and computational investigation of the knoller-betz effect *AIAA J.* **36** 1240–6

[36] Young J 2005 Numerical simulation of the unsteady aerodynamics of flapping airfoils *PhD Thesis* The University of New South Wales

[37] Platzer M F, Jones K D, Young J and Lai J C S 2008 Flapping wing aerodynamics: progress and challenges *AIAA J.* **46** 2136–49

[38] Li N, Liu X and Su Y 2017 Numerical study on the hydrodynamics of thunniform bio-inspired swimming under self-propulsion *PLoS One* **12** e0174740

[39] Wu T Y 2011 Fish swimming and bird/insect flight *Annu. Rev. Fluid Mech.* **43** 25–58

[40] Bainbridge R 1958 The speed of swimming of fish as related to size and to the frequency and amplitude of the tail beat *J. Exp. Biol.* **35** 109–33

[41] Pollard B and Tallapragada P 2019 Passive appendages improve the maneuverability of fishlike robots *IEEE/ASME Trans. Mechatronics* **24** 1586–96

[42] Hang H, Heydari S, Costello J H and Kanso E 2022 Active tail flexion in concert with passive hydrodynamic forces improves swimming speed and efficiency *J. Fluid Mech.* **932** A35

[43] Ayancik F, Fish F and Moored K 2020 Three-dimensional scaling laws of cetacean propulsion characterize the hydrodynamic interplay of flukes' shape and kinematics *J. R. Soc. Interface* **17** 20190655

[44] Di Santo V, Goerig E, Wainwright D, Akanyeti O, Liao J, Castro-Santos T and Lauder G 2021 Convergence of undulatory swimming kinematics across a diversity of fishes *Proc. Natl Acad. Sci.* **118** e2113206118

[45] Paniccia D, Graziani G, Lugni C and Piva R 2022 The fish ability to accelerate and suddenly turn in fast maneuvers *Sci. Rep.* **12** 4946

scientific reports

OPEN

The fish ability to accelerate and suddenly turn in fast maneuvers

Damiano Paniccia[1,5✉], Giorgio Graziani[1,5], Claudio Lugni[2,3,4,5] & Renzo Piva[1,5]

Velocity burst and quick turning are performed by fish during fast maneuvers which might be essential to their survival along pray–predator encounters. The parameters to evaluate these truly unsteady motions are totally different from the ones for cruising gaits since a very large acceleration, up to several times the gravity, and an extreme turning capability, in less than one body length, are now the primary requests. Such impressive performances, still poorly understood, are not common to other living beings and are clearly related to the interaction with the aquatic environment. Hence, we focus our attention on the water set in motion by the body, giving rise to the relevant added mass and the associated phenomena in transient conditions, which may unveil the secret of the great maneuverability observed in nature. Many previous studies were almost exclusively concentrated on the vortical wake, whose account, certainly dominant at steady state, is not sufficient to explain the entangled transient phenomena. A simple two-dimensional impulse model with concentrated vorticity is used for the self-propulsion of a deformable body in an unbounded fluid domain, to single out the potential and the vortical impulses and to highlight their interplay induced by recoil motions.

The aquatic motion of fish is characterized by paths of long term cruising swimming and by very fast maneuvers during pray–predator encounters, either for escaping or for foraging needs. Such maneuvers, for instance the so called C-start characterized by a C shape bending, give rise to a sudden change of the swimming direction together with a huge acceleration leading the fish to follow a proper path to survive or to capture the desired pray[1]. Their purpose is very different from the one for standard cruising and the usual performance parameter, i.e. the cost of transport given by the ratio between expended power and locomotion speed[2,3], is no longer a priority so that different measures are needed to search for optimal performances. The most common fast start swimming gaits were largely described in a survey paper by Domenici and Blake[4] with a large set of experimental data, very useful for understanding the relevant phenomena. In particular, both C-start and S-start maneuvers are deeply analyzed, but we will concentrate here only on the first one since, in our opinion, it is more rich of interesting aspects like the sudden change of the swimming direction. Anyhow, a full comprehension of many facets of the physical behavior is still not available and a satisfactory account of all the reasons for such unique achievements is still missing. Some recent and very interesting contributions[5–7] investigated a problem, in a way related to the present one, concerning the peculiar acceleration properties of the octopus that is propelled by a water jet expelled by the body itself, which in the mean time experiences a simultaneous reduction of its volume. The reported results for this case show a dominant effect of the added mass reduction which acts as a substantial improvement of the propulsion due to the water jet. Along with the proper differences essentially due to the unavoidable recoil motions[8–10], the C-start under investigation may be brought back to the above problem since the added mass and its variability may play a central role for the maneuver's performance. For the analysis, we have to consider the full system of the evolution equations for the kinetic variables pertaining to the body center of mass. Since the numerical results may be quite involved, we consider a simple impulse model with concentrated vorticity, so to isolate the potential and the vortical contributions as a *conditio sine qua non* for a proper physical interpretation of the results. As a major goal, we intend to confirm the added mass and its variability to be key items during the transient phase though the release of vorticity is always significant to definitely prevail at the end of the maneuver. Other interesting contributions analyzed the C-shape deformation accompanied by a traveling wave from head to tail to show, by numerical results, a more impressive performance[11–14]. Also in this case, we

[1]Department of Mechanical and Aerospace Engineering, University of Rome "La Sapienza", Rome, Italy. [2]CNR-INM, Marine Technology Research Institute, Rome, Italy. [3]Institute of Marine Hydrodynamics, Harbin Engineering University, Harbin, China. [4]NTNU-AMOS, Center for Autonomous Marine Operation Systems, Trondheim, Norway. [5]These authors contributed equally: Damiano Paniccia, Giorgio Graziani, Claudio Lugni and Renzo Piva. ✉email: damiano.paniccia@uniroma1.it

t/T = 0	t/T = 0.25	t/T = 0.5	t/T = 0.75	t/T = 1
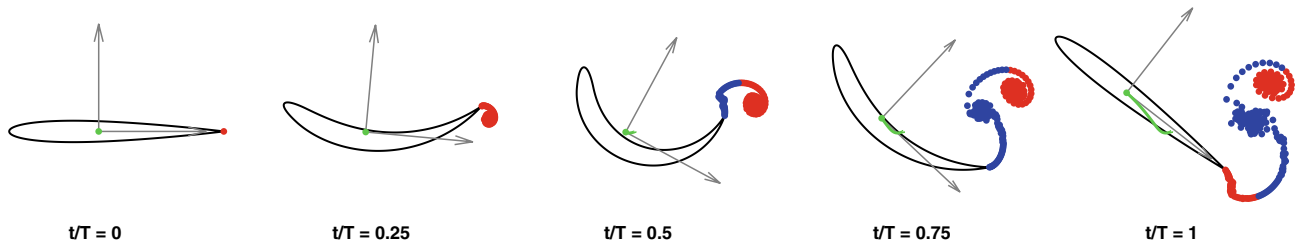
Figure 1. Snapshots of the C-start maneuver of a neutrally buoyant fish from the numerical simulation. The relative animation is reported in Movie S1.
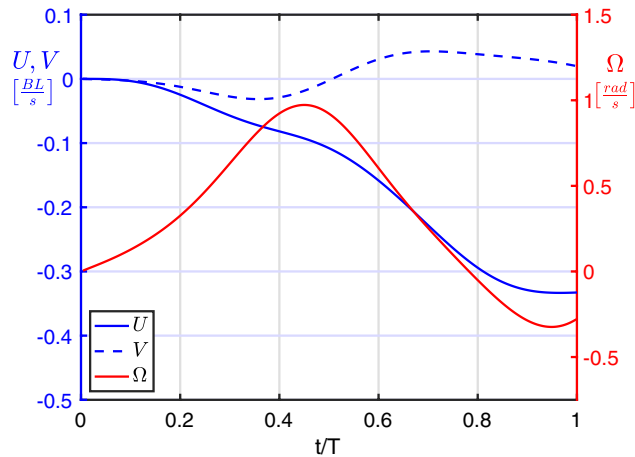
Figure 2. Velocity components for the C-start maneuver of a neutrally buoyant fish.

intend to provide the proper reasons for the increased efficiency of the maneuver. In the following sections we report and discuss a few numerical results for a deeper understanding of fast start swimming maneuvers whose comprehension, beyond a basic value per se, may provide a technical contribution to the design of biomimetic fishlike robots for particular applications requiring excellent maneuverability.

Results

As a first step, let us make a short description of the C like fast start just to recall by a few snapshots (see Fig. 1 and the related animation reported in Movie S1) the main phases of this pretty elaborated maneuver which obeys to the conservation of both linear and angular momenta, since no external actions are applied. The fish willing to suddenly accelerate and change its swimming direction initiates a preparatory phase via a rotation of its tail which induces a simultaneous opposite rotation of the body fixed frame.

The successive propulsive phase, corresponding to the rapid return of the tail to the position aligned with the forward axis, gives rise to a substantial velocity boost in the same direction while the whole motion is accompanied by a significant release of vorticity. The kinematic performance of the C-start maneuver for a neutrally buoyant fish may be furtherly appreciated by the velocity components reported in Fig. 2 where we see that during the preparatory phase, i.e. for $0 \leq t/T < 0.5$ when the tail is raised towards the head (see Fig. 1), the body fixed frame starts to counter-rotate with an angular velocity Ω whose maximum occurs approximately for $t/T = 0.5$. A relatively small forward velocity U from right to left (i.e. negative in sign) is also obtained halfway, but a much larger forward speed is finally achieved at the end of the propulsive phase when the tail is pushed back. No comments are made about the lateral velocity component V since, in a first approximation, its presence is quite negligible.

The literature on the subject was mostly focused on the study of the vortex shedding and of the vortical wake geometry as a potential source of comprehension, while a little attention was given to the added mass that we consider instead of primary importance for the maneuver. For a quantitative evaluation of all these contributions, we rely on the conservation of the linear impulse along the forward direction:

$$(m + m_{11}) \, U = \mathcal{P}_1 \tag{1}$$

where m is the body mass and m_{11} is the added mass coefficient as properly defined when deriving the full system of equations (12) reported in the Methods section. Namely, Eq. (1) represents the first equation of the system once all the contributions but the one containing the unknown forward velocity U are grouped together within a single term $\mathcal{P}_1 = -P_{v1} - P_{sh1} - m_{12} V - m_{13} \Omega$ to ease the interpretation of the results. Specifically $\mathcal{P}_1$, beyond the component P_{v1} associated to the shed vortices and P_{sh1} associated to the shape deformation, includes
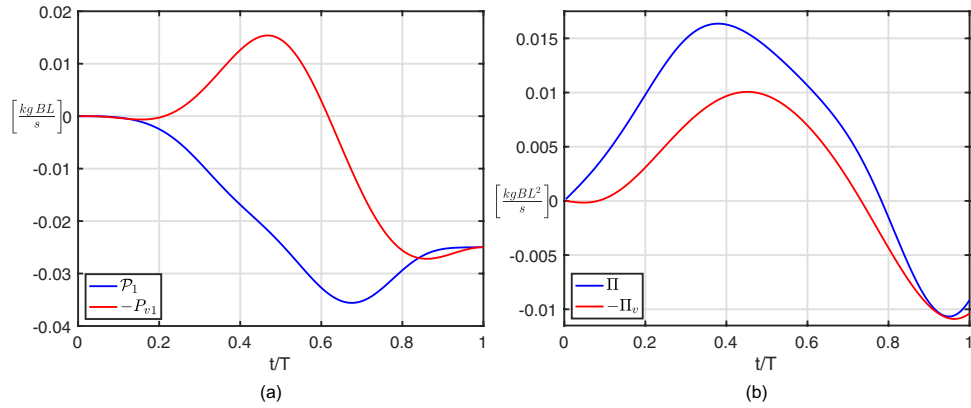
Figure 3. Fluid impulses for C-start maneuver: (**a**) total forward impulse $\mathcal{P}_1$ and its vortical contribution P_{v1}; (**b**) total angular impulse Π and its vortical contribution Π_v.

the coupling terms given by the lateral and angular velocities times the proper added mass coefficients m_{12} and m_{13}, respectively. We may easily appreciate from Fig. 3a the very large difference between $\mathcal{P}_1$ and its vortical component, obviously covered by the left aside terms whose large impact on the maneuver clearly appears. It is interesting to evaluate the relative weight of the various terms to highlight the overwhelming predominance of the coupling term $-m_{13}\Omega$ which provides a substantial momentum transfer from the angular to the forward direction (diagrams reported in Fig. S2a). All the terms covering the above difference are shown to become negligible at the end of the propulsive phase where the deformation is over and the fish returns to its straight configuration. Actually, in this condition the total and vortical impulses $\mathcal{P}_1$ and $-P_{v1}$ perfectly coincide, hence we may assess that the value of the final swimming velocity at the end of the C-start maneuver may be obtained by accounting only for the shed vortices contribution[15]. At the same time, the vortical wake is shown to be unable to give a correct picture of the global physical phenomenon since all the other terms, in a way related to the added mass, have a dominant influence during the transient phase. By following the same reasoning, let us write the equation for the angular momentum:

$$(I_{zz} + m_{33})\Omega = \Pi \tag{2}$$

where, as before, the term Π is grouping together all the other contributions but the one containing the angular velocity Ω, while I_{zz} is the body moment of inertia and m_{33} is the proper added mass coefficient. Analogously, the difference between Π and its vortical contribution $-\Pi_v$, reported in Fig. 3b, shows again the relevance of the left aside terms on the maneuver with a special regard to the coupling ones due to added mass (reported in Fig. S2c). At this point, since we have verified the limited role of the vortical wake for understanding the C-start, we may now pass to the dynamics of the maneuver to account for the effects of the added mass variability. Namely, by taking the time derivative of Eq. ((1)), we obtain

$$\frac{dU}{dt} = \frac{1}{m + m_{11}} \frac{d\mathcal{P}_1}{dt} - \frac{U}{m + m_{11}} \frac{dm_{11}}{dt} \tag{3}$$

where the acceleration $\frac{dU}{dt}$ is split into two forcing terms. The first one depends directly on the time derivative of the forward impulse $\mathcal{P}_1$, while the second one depends on the time derivative of the added mass coefficient m_{11} along the forward direction. Both terms on the right hand side of Eq. ((3)) are divided by the sum of the body mass and of its added mass coefficient m_{11}. Hence, the added mass coefficient accounting for all the water set in motion by the body forward translation behaves like the body mass, i.e. the smaller its value, the more effective are the forcing terms on the body acceleration. Moreover, the time derivative of the added mass coefficient m_{11} appears also as a forcing term which, for a reducing value of m_{11}, may provide a boost in the body forward velocity, as highlighted by Spagnolie and Shelley[16].

By proceeding in an analogous way, similar equations may be obtained for the lateral and angular velocity components but, since the lateral velocity is much smaller and less important than the angular one, we report here only the expression for the angular acceleration:

$$\frac{d\Omega}{dt} = \frac{1}{I_{zz} + m_{33}} \frac{d\Pi}{dt} - \frac{\Omega}{I_{zz} + m_{33}} \frac{dm_{33}}{dt} \tag{4}$$

where the first term on the right hand side depends on the time derivative of the angular impulse Π, while the second one accounts for the variation of the added mass coefficient m_{33}. For an easier understanding of the effects due to the added mass variation on the forward and the angular acceleration experienced by the fish, we reported in Figs. 4a and 5a, respectively, the time history of the added mass coefficients m_{11} and m_{33} while the behaviour of all the other coefficients is reported for completeness in Fig. S3. The total forward and angular accelerations and their contributions as given by Eqs. (3) and (4) are reported in Figs. 4b and 5b. In the first one, i.e. Fig. 4b, we observe how the two combined contributions always give rise to an acceleration from right to left
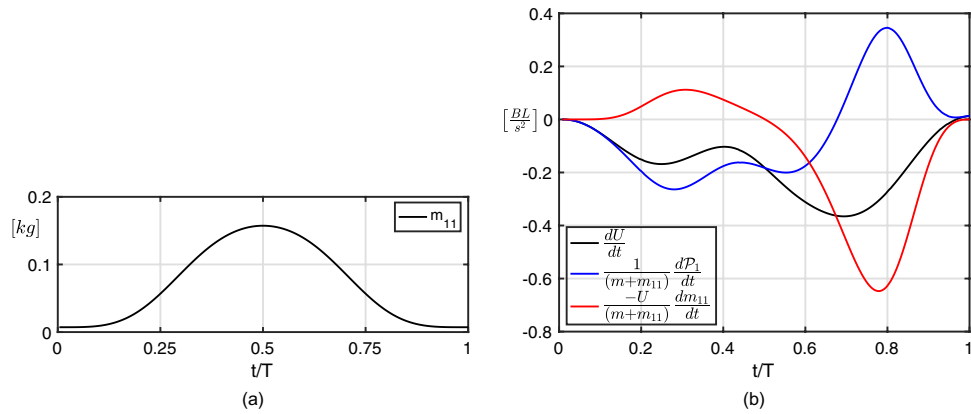
Figure 4. Time history of (**a**) the added mass coefficient m_{11} and of (**b**) the forward acceleration contributions for the C-start maneuver.
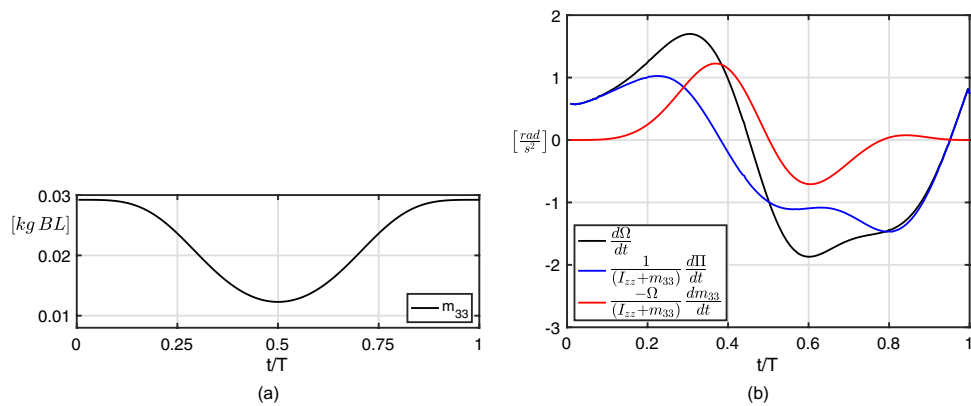

Figure 5. Time history of (**a**) the added mass coefficient m_{33} and of (**b**) the angular acceleration contributions for the C-start maneuver.

(with a negative sign in our frame of reference) until the end of the maneuver. To this regard, according also to Fig. 4a, the time history of the second term on the r.h.s. of Eq. ((3)), accounting for the added mass variation, represents the main source of acceleration in the forward direction along the propulsive phase, even though a lighter opposite acceleration, substantially a drag, is shown during the preparatory phase. At the same time, the term accounting for $\frac{d\mathcal{P}_1}{dt}$ shows a quite similar but opposite behaviour since the favorable effect appears during the preparatory phase, while the resistive effect occurs during the propulsive phase. By looking at the different components of $\frac{d\mathcal{P}_1}{dt}$ reported in the Supplementary Material (see Fig. S4a), we have a further assessment of the dominant role played by the coupling among the angular and the forward velocities. With regard to the angular acceleration reported in Fig. 5b, the term related to the variation of the added mass coefficient m_{33} goes along with the time derivative of the angular impulse $d\Pi/dt$ for most of the entire maneuver. The cooperative action of these two terms enhances the fish capability to perform quick turnings leading to a large angular velocity Ω which also has a favourable influence on the forward velocity through the coupling terms included in $\mathcal{P}_1$ as reported for completeness in Fig. S4b.

The presence of an undulatory motion cooperating with the main C-shape bending fully maintains the validity of the above reasoning about the relevance of the added mass for a good maneuverability. Indeed, the addition of a proper traveling wave is even enhancing the full deformation by leading, on the one side, to larger values of the added mass coefficients together with their time variation and, on the other side, to an increase of the angular velocity, which keeps providing the predominant forward momentum transfer. The increased deformation involving a larger amount of water to be accelerated was also mentioned by Gazzola et al.[17] as a fostering effect for the C-start performance. The snapshots in Fig. 6 and the related animation in Movie S2 give a first glance evaluation of the more efficient maneuver, while the diagrams in Fig. 7 show the larger forward and angular velocities compared with the ones without traveling wave. Further figures on this case, quite similar to the previous ones for the basic C-start, are reported in Figs. S5 and S6.

| t/T = 0 | t/T = 0.25 | t/T = 0.5 | t/T = 0.75 | t/T = 1 |
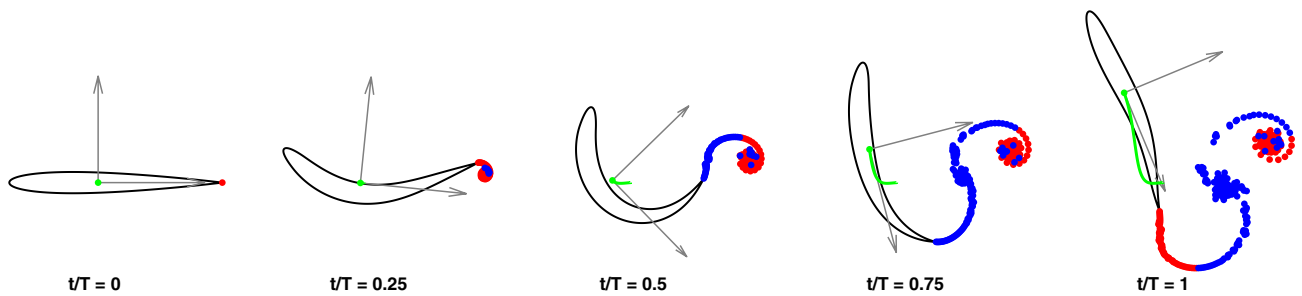
Figure 6. Snapshots of the C-start maneuver combined with a wave undulation from the numerical simulation. The relative animation is reported in the Movie S2.
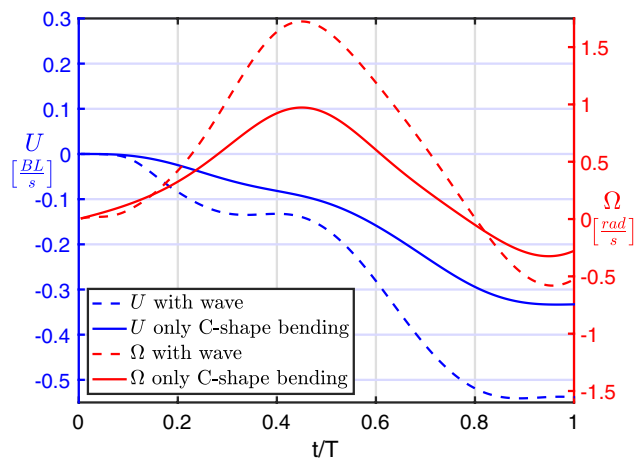
Figure 7. Comparison between forward and angular velocity components for the C-start maneuver with and without wave undulation.

Discussion

The surprising performances that fish may reach when engaged in fast start maneuvers have attracted the attention of biologists, physicists and engineers since such events are not fully understood and, even more, they are far from being reproduced by the actual more advanced technologies. It was our intention to analyze, as the most significant sample case, the C-start of a fishlike body by a simple impulse model which is instrumental to evaluate separately the various contributions for the accomplishment of the maneuver. Several previous studies[14,15,17–20] analyzed in detail position and strength of the shed vortices with the intent to draw some hints for a sound physical interpretation of the fish maneuvering performance. For instance, Epps and Techet[15] investigated the vortical wake released during the C-start and measure the complete variation of the fish linear momentum through the linear momentum of the released vortices. In other words, by evaluating the momentum associated to the vortex clusters right after the fast start, they manage to estimate the swimming velocity at the end of the maneuver. However, as suggested by many authors[21–24] and clearly stated by Zhang[25], the shed vortices behave like terrestrial footprints hence they are not telling the whole story about the fish dynamics. The debate on this point is quite subtle and we like to add a further deepening by reporting the main findings obtained by our numerical simulations. On the one hand, the vortical contributions, even though eventually dominant, are shown to be unable to explain all the intermediate steps of the maneuver. On the other hand, the added mass and its variation are proven to have, in aquatic environment, the larger impact on the extreme accelerations and on the high turning capabilities. Apart from assessing the key role of the reducing value of the coefficients m_{11} and m_{33}, we did show the prevailing action of the mutual momentum transfer between the angular and the forward direction due to the coupling terms related to the mixed coefficients. Among these terms which involve the proper recoil motions, the one associated to the angular velocity is shown to have the largest influence on the entire maneuver. No qualitative changes were observed when the C-shape bending was accompanied by a traveling wave along the fishlike body as usually observed in nature and repeatedly reported in the literature[11–14]. From a quantitative point of view, it has to be mentioned that, when a traveling wave is prescribed, the maneuver performances are even more impressive. From the above numerical results and from their analysis, we are able to draw a quite straight conclusion. In a nutshell: when considering truly unsteady motions like the fast start of a deformable body in aquatic environment, the vortical wake is not sufficient to catch the essence of the maneuver as it would be in presence of a light fluid like air, but the multiple effects associated to the added mass, though vanishing at the end of the maneuver, are prevailing for the description of the transient phase and for the realization of the maneuver itself.

Materials and methods

We study the motion of a fish $\mathcal{B}$ swimming in a quiescent fluid within an unbounded fluid domain $\mathcal{V}$. The self propelled motion is generated by the internal forces and moments exchanged between the swimming body and the surrounding fluid. These actions are expressed through the impulse formulation to avoid the convergence problems actually appearing for the momentum in unbounded fluid domains[26,27]. We consider the planar, two-dimensional motion of an impermeable, flexible body (with density ρ_b) whose bounding surface S_b is moving with velocity $\boldsymbol{u}_b$ in an incompressible flow field with density ρ and velocity $\boldsymbol{u}$ vanishing at the far field boundary. By using well known vector identities for the unbounded two-dimensional fluid volume[28–31], the linear fluid impulse is defined as

$$\mathbf{p} = \int_{\mathcal{V}} \rho\, \boldsymbol{u}\, dV = \frac{1}{N-1}\left[\int_{\mathcal{V}} \boldsymbol{x} \times \boldsymbol{\omega}\, dV + \int_{S_b} \boldsymbol{x} \times (\boldsymbol{n} \times \boldsymbol{u}^+)\, dS\right] \tag{5}$$

where N is the dimension (here $N = 2$ is assumed) and $\boldsymbol{x}$ is the position vector in the inertial frame. In Eq. (5), $\boldsymbol{\omega}$ is the vorticity, $\boldsymbol{u}^+$ stays for the limiting value of the fluid velocity on S_b and the integral over the external boundary receding to infinity has been proven to exactly vanish (Wu[28], Wu et al.[31], Noca et al.[32]). The normal $\boldsymbol{n}$ points out of the flow domain $\mathcal{V}$ which encloses all the vorticity. The right-hand side of Eq. (5) is independent of the choice of the reference frame origin[30–32].

Similarly, the angular impulse is

$$\pi = \int_{\mathcal{V}} \rho\, \boldsymbol{x} \times \boldsymbol{u}\, dV = \frac{1}{2}\left[\int_V |x|^2 \boldsymbol{\omega}\, dV + \int_{S_b} |x|^2 (\boldsymbol{n} \times \boldsymbol{u}^+)\, dS\right] \tag{6}$$

We consider here the moment with respect to a given pole, so $\boldsymbol{x}$ is the generic distance of the field point from the pole. Due to the absence of external forces the total linear and angular momenta are conserved and, by assuming null initial conditions, we have

$$\int_{\mathcal{B}} \rho_b\, \boldsymbol{u}_b\, dV + \mathbf{p} = 0 \tag{7}$$

$$\int_{\mathcal{B}} \rho_b\, \boldsymbol{x} \times \boldsymbol{u}_b\, dV + \pi = 0 \tag{8}$$

where the forces acting on the body and on the fluid are obtained by time differentiating the two terms appearing in (7), respectively. The motion of the body can be expressed as the sum of the prescribed shape deformation with velocity $\boldsymbol{u}_{sh}$ plus the translational ($\boldsymbol{u}_{cm}$) and rotational ($\boldsymbol{\Omega}$) velocity of the frame with origin in the centre-of-mass.

$$\boldsymbol{u}_b = \boldsymbol{u}_{sh} + \boldsymbol{u}_{cm} + \boldsymbol{\Omega} \times \boldsymbol{x}' \tag{9}$$

where $\boldsymbol{x}'$ is the position vector in the body frame, i.e.: $\boldsymbol{x} = \boldsymbol{x}_{cm} + \boldsymbol{x}'$. The prescribed deformation of the body has to conserve linear and angular momenta, as formally given by $\int_{\mathcal{B}} \rho_b \boldsymbol{u}_{sh}\, dV = 0$ and $\int_{\mathcal{B}} \rho_b \boldsymbol{x}' \times \boldsymbol{u}_{sh}\, dV = 0$. By combining the expression of $\boldsymbol{u}_b$ with Eqs. (7) and (8) we obtain

$$m\, \boldsymbol{u}_{cm} + \mathbf{p} = 0 \tag{10}$$

$$I_{zz}\, \Omega + \pi = 0 \tag{11}$$

where m and I_{zz} are the inertial properties of the body. We may then express $\boldsymbol{p}$ and π, via a Helmholtz decomposition, in terms of their potential and vortical contributions as $\mathbf{p} = \mathbf{p}_\phi + \mathbf{p}_v$ and $\pi = \pi_\phi + \pi_v$, where the added mass effects are embedded within the potential impulses $\mathbf{p}_\phi$ and π_ϕ while the vortical impulses $\mathbf{p}_v$ and π_v are related to the vortex sheet around the body and to the vortices shed into the wake[33–35]. A complete and detailed description of the procedure can be found in Paniccia et al.[36], where all the steps up to the final system of equations written in the body fixed frame are reported to obtain the two linear velocity components U and V and the angular velocity Ω

$$\begin{cases} (m_{11} + m)\, U + m_{12} V + m_{13}\Omega = -P_{sh1} - P_{v1} \\ m_{21} U + (m_{22} + m)V + m_{23}\Omega = -P_{sh2} - P_{v2} \\ m_{31} U + m_{32} V + (m_{33} + I_{zz})\Omega = -\Pi_{sh} - \Pi_v \end{cases} \tag{12}$$

where the added mass coefficients m_{ij}, which are usually fully embedded into the forcing terms for standard CFD simulations[37], are here easily obtained by the following definition

$$m_{ij} = -\int_{S_b} \phi_j \frac{d\phi_i}{dn}\, dS \tag{13}$$

In the above system the potential impulses have been split into some terms related to the unknown rigid body motions, which are expressed through the added mass coefficients, and other terms with the subscript sh, due to the shape deformation, which remain on the r.h.s. of the equations together with the vortical contribution. The flow solutions are obtained by an unsteady potential code for a slender body[38] while vortex shedding from the trailing edge is taken into account by a classical unsteady Kutta condition[39]. This well-known numerical

procedure has been extensively used in the literature to study rigid bodies like airfoils moving with a fully prescribed motion while we study here the free swimming of a deformable body[40,41] which presents a much larger complexity since the linear and angular rigid body velocities are now unknown. A short description of the prescribed deformation is reported in the Supplementary Material together with the specific data for the numerical simulation collected in Table S1.

Data availability

All data generated or analysed during this study are included in this published article (and its supplementary information files).

References

1. Cade, D. E., Carey, N., Domenici, P., Potvin, J. & Goldbogen, J. A. Predator-informed looming stimulus experiments reveal how large filter feeding whales capture highly maneuverable forage fish. *Proc. Natl. Acad. Sci.* **117**, 472–478, 10.1073/pnas.1911099116 (2020). https://www.pnas.org/content/117/1/472.full.pdf.
2. Bale, R., Hao, M., Bhalla, A. P. S. & Patankar, N. A. Energy efficiency and allometry of movement of swimming and flying animals. *PNAS* **111**(21), 7517–7521 (2014).
3. Paniccia, D., Padovani, L., Graziani, G. & Piva, R. The performance of a flapping foil for a self-propelled fishlike body. *Sci. Rep.* **11**, 22297. https://doi.org/10.1038/s41598-021-01730-4 (2021).
4. Domenici, P. & Blake, R. W. The kinematics and performance of fish fast-start swimming. *J. Exp. Biol.* **200**, 1165–1178 (1997).
5. Weymouth, G. D., Subramaniam, V. & Triantafyllou, M. S. Ultra-fast escape maneuver of an octopus-inspired robot. *Bioinspir. Biomim.* **10**, 016016 (2015).
6. Steele, S. C., Dahl, J. M., Weymouth, G. D. & Triantafyllou, M. S. Shape of retracting foils that model morphing bodies controls shed energy and wake structure. *J. Fluid Mech.* **805**, 355–383 (2016).
7. Steele, S. C., Weymouth, G. D. & Triantafyllou, M. S. Added mass energy recovery of octopus-inspired shape change. *J. Fluid Mech.* **810**, 155–174 (2017).
8. Lighthill, J. Aquatic animal propulsion of high hydromechanical efficiency. *J. Fluid Mech.* **44**, 265–301 (1970).
9. Maertens, A. P., Gao, A. & Triantafyllou, M. S. Optimal undulatory swimming for single fish-like body and for pair of interacting swimmers. *J. Fluid Mech.* **813**, 2 (2017).
10. Paniccia, D., Graziani, G., Lugni, C. & Piva, R. The relevance of recoil and free swimming in aquatic locomotion. *J. Fluids Struct.* **103**, 103290. https://doi.org/10.1016/j.jfluidstructs.2021.103290 (2021).
11. Jayne, B. & Lauder, G. Red and white muscle activity and kinematics of the escape response of bluegill sunfish during swimming. *J. Comp. Physiol. A* **173**, 495–508 (1993).
12. Wakeling, J. M. & Johnston, I. A. Muscle power output limits fast-start performance in fish. *J. Exp. Biol.* **201**, 1505–1526 (1998).
13. Wakeling, J. M. & Johnston, I. A. Body bending during fast-starts in fish can be explained in terms of muscle torque and hydro-dynamic resistance. *J. Exp. Biol.* **202**, 675–682 (1999).
14. Liu, G., Yu, Y. L. & Tong, B. G. Flow control by means of a traveling curvature wave in fishlike escape responses. *Phys. Rev. E* **84**, 056312 (2011).
15. Epps, B. P. & Techet, A. H. Impulse generated during unsteady maneuvering of swimming fish. *Exp Fluids* **43**, 691–700 (2007).
16. Spagnolie, S. E. & Shelley, M. J. Shape-changing bodies in fluid: Hovering, ratcheting, and bursting. *Phys. Fluids* **21**, 2 (2009).
17. Gazzola, M., van Rees, W. M. & Koumoutsakos, P. C-start: optimal start of larval fish. *J. Fluid Mech.* **698**, 5–18 (2012).
18. Borazjani, I. The functional role of caudal and anal/dorsal fins during the c-start of a bluegill sunfish. *J. Exp. Biol.* **216**, 1658–1669 (2013).
19. Triantafyllou, M. S., Weymouth, G. D. & Miao, J. M. Biomimetic survival hydrodynamics and flow sensing. *Annu. Rev. Fluid Mech* **48**, 2 (2016).
20. Akanyeti, O. *et al.* Accelerating fishes increase propulsive efficiency by modulating vortex ring geometry. *Proc. Natl. Acad. Sci.* **114**, 13828–13833 (2017).
21. Eloy, C. Optimal Strouhal number for swimming animals. *J. Fluids Struct.* **30**, 2 (2012).
22. Taylor, G. K. Simple scaling law predicts peak efficiency in oscillatory propulsion. *Proc. Natl. Acad. Sci.* **115**, 8063–8065 (2018).
23. Smits, A. Undulatory and oscillatory swimming. *J. Fluid Mech.* **874**, 1–70 (2019).
24. Floryan, D., Van Buren, T. & Smits, A. J. Swimmers wake structures are not reliable indicators of swimming performance. *Bioinspir. Biomimet.* **15**, 024002 (2020).
25. Zhang, J. Footprints of a flapping wing. *J. Fluid Mech.* **810**, 2 (2017).
26. Landau, L. D. & Lifschitz, E. M. *Fluid Mechanics*, vol. 6 (Pergamon Press, 1986), 2 edn.
27. Childress, S. *An Introduction to Theoretical Fluid Dynamics* (Courant Lecture Notes, vol. 19, AMS, 2009).
28. Wu, J. C. Theory for aerodynamic force and moment in viscous flows. *AIAA J.* **19**, 432–441 (1981).
29. Noca, F. *On the evaluation of time-dependent fluid dynamic forces on bluff bodies*. Ph.D. thesis, California Institute of Technology (1997).
30. Graziani, G. & Bassanini, P. Unsteady viscous flows about bodies: Vorticity release and forces. *Meccanica* **37**, 283–303 (2002).
31. Wu, J. Z., Ma, H. Y. & Zhou, M. D. *Vortical Flows* (Springer, 2015).
32. Noca, F., Shiels, D. & Jeon, D. A comparison of methods for evaluating time-dependent fluid dynamic forces on bodies, using only velocity fields and their derivatives. *J. Fluids Struct.* **13**, 551–578 (1999).
33. Saffman, P. G. The self-propulsion of a deformable body in a perfect fluid. *J. Fluid Mech.* **28**, 385–389 (1967).
34. Kanso, E. Swimming due to transverse shape deformations. *J. Fluid Mech.* **631**, 127–148 (2009).
35. Eldredge, J. D. A reconciliation of viscous and inviscid approaches to computing locomotion of deforming bodies. *Exp. Mech* **50**, 2 (2010).
36. Paniccia, D., Graziani, G., Lugni, C. & Piva, R. On the role of added mass and vorticity release for self propelled aquatic locomotion. *J. Fluid Mech.* **918**, A45. https://doi.org/10.1017/jfm.2021.375 (2021).
37. Limacher, E., Morton, C. & Wood, D. Generalized derivation of the added-mass and circulatory forces for viscous flows. *Phys. Rev. Fluids* **2**, 2 (2018).
38. Hess, J. L. & Smith, A. M. O. Calculation of potential flow about arbitrary bodies. *Prog. Aerosp. Sci.* **8**, 1–138 (1967).
39. Basu, B. C. & Hancock, G. J. The unsteady motion of a two-dimensional aerofoil in incompressible inviscid flow. *J. Fluid Mech.* **87**, 159–178 (1978).
40. Carling, J., Williams, T. L. & Bowtell, G. Self-propelled anguilliform swimming simultaneous solution of the two-dimensional Navier–Stokes equations and newtons laws of motion. *J. Exp. Biol.* **201**, 3143–3166 (1998).
41. Kern, S. & Koumoutsakos, P. Simulations of optimized anguilliform swimming. *J. Exp. Biol.* **209**, 4841–4857 (2006).

Acknowledgements

Author contributions

D.P., G.G, C.L. and R.P contributed equally to this work.

Competing interests

The authors declare no competing interests.

Additional information

Supplementary Information The online version contains supplementary material available at https://doi.org/10.1038/s41598-022-08923-5.

Correspondence and requests for materials should be addressed to D.P.

Reprints and permissions information is available at www.nature.com/reprints.

Publisher's note Springer Nature remains neutral with regard to jurisdictional claims in published maps and institutional affiliations.

SUPPLEMENTARY MATERIAL - The fish ability to accelerate and suddenly turn in fast maneuvers

Damiano Paniccia[1,*,+], **Giorgio Graziani**[1,+], **Claudio Lugni**[2,3,4,+], **and Renzo Piva**[1,+]

[1]Dept. of Mechanical and Aerospace Engineering, University of Rome "La Sapienza", Rome, Italy
[2]CNR-INM, Marine Technology Research Institute, Rome, Italy
[3]Institute of Marine Hydrodynamics, Harbin Engineering University, Harbin, China
[4]NTNU-AMOS, Center for Autonomous Marine Operation Systems, Trondheim, Norway
[*]damiano.paniccia@uniroma1.it
[+]these authors contributed equally to this work

Deformation and data for the numerical simulations

The C-start maneuver is mainly characterized by a C-shaped oscillatory bending through which the fish accelerates the surrounding fluid to obtain a large increase of the forward velocity and an impressive turning capability. The C bending deformation is usually accompanied by an undulatory deformation which is eventually leading to a more efficient maneuver[1-4]. In the present work we focused on the basic phenomena underlying the outstanding fish performance by means of a mathematical and a numerical model able to isolate and separate all the different physical contributions. To this purpose, we used the impulse formulation to satisfy the conservation of the total linear and angular momenta for a self-propelled deformable body and we obtained the numerical solutions by means of a two-dimensional panel method with concentrated vortex shedding through an unsteady Kutta condition. Both the mathematical and numerical models have been deeply described in Paniccia et al.[5].

The fish body is represented by a NACA0010 airfoil while its prescribed deformation is taken from Liu et al.[4] and briefly described in the following. The deformation is given by the curvature $k(s,t)$ of the airfoil midline and, in general, it is divided in two parts

$$k(s,t) = k_b(s,t) + k_w(s,t) \tag{S1}$$

where $k_b(s,t)$ is the part associated to the main C-shaped oscillatory bending and $k_w(s,t)$ is a curvature traveling wave. Specifically, the main bending is defined as

$$k_b(s,t) = \begin{cases} 0 & 0 \leq s < 0.1 \\ a_b \left(1 - \cos\left(2\pi \dfrac{t}{T} \right) \right) & s \geq 0.1 \end{cases} \tag{S2}$$

where a_b is the maximum bending amplitude and T is the time period of the entire maneuver. The curvature traveling wave is given as

$$k_w(s,t) = a_w A(s) \tau(t) \sin\left(2\pi \left(s - \dfrac{t}{T} \right) + \psi \right) \tag{S3}$$

where a_w is maximum wave amplitude and the ramp function $\tau(t)$ is assigned as

$$\tau(t) = \begin{cases} \dfrac{t}{T_r} - \dfrac{1}{2\pi} \sin\left(\dfrac{2\pi t}{T_r} \right) & 0 \leq t \leq T_r \\ 1 & t \geq T_r \end{cases} \tag{S4}$$

where T_r is the duration of the ramp and $A(s)$ is an amplitude modulation is assigned as

$$A(s) = \begin{cases} 0 & 0 \leq s < 0.1 \\ s^2 - 0.2s + 0.5 & s \geq 0.1 \end{cases} \tag{S5}$$

The values of all the different parameters used for the numerical simulations are collected in Table S1. The corresponding deformations in the body-fixed frame are reported in fig.S1 for the preparatory and the propulsive phase. To be notice the significant difference among the two phases once the undulatory deformation is considered.
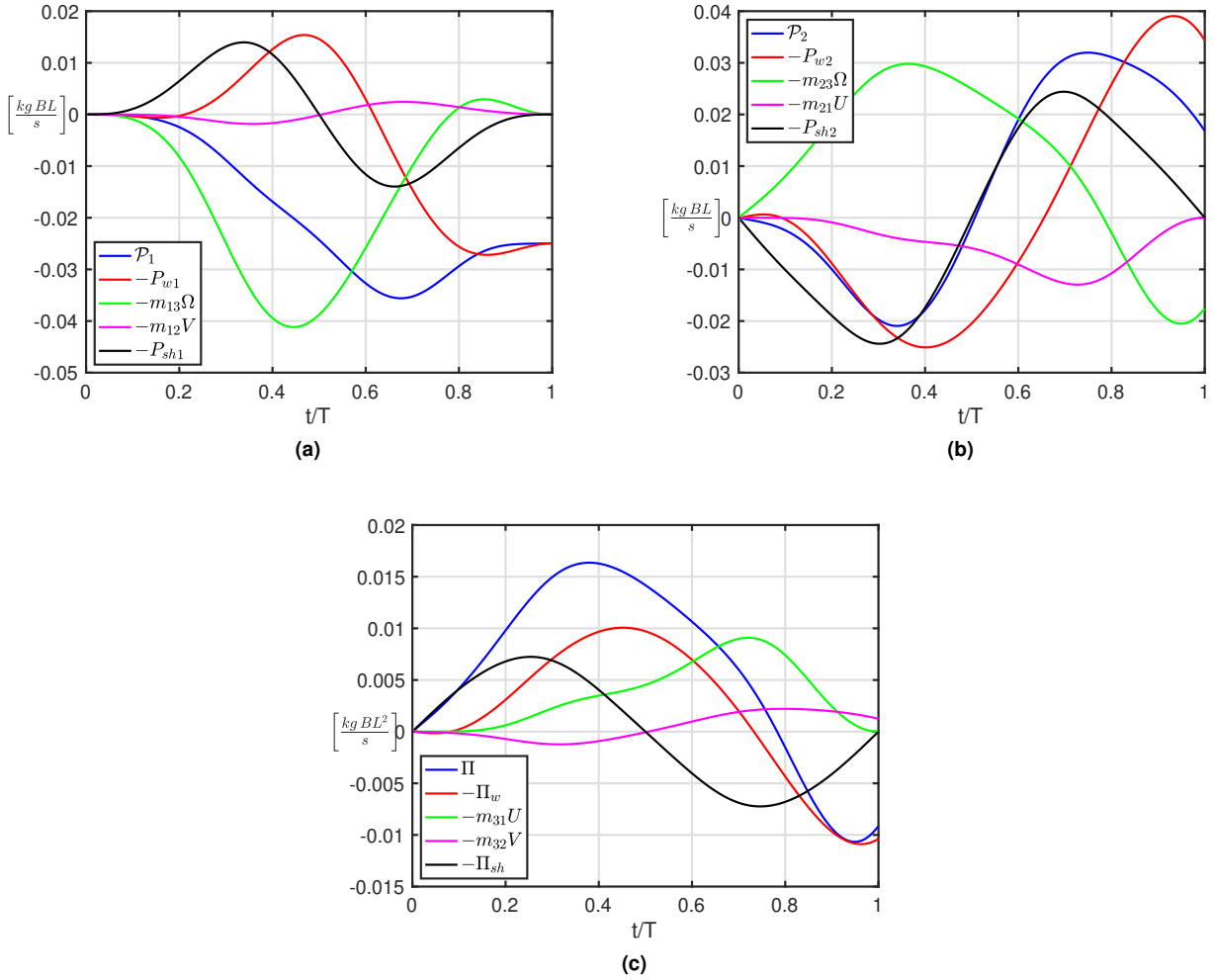
Table S1. Parameters for numerical simulations

	bending only	bending + traveling wave
a_b	0.465π	0.465π
T	2	2
a_w	0	1.4
ψ	0	π
T_r	0	0.4

(a)

(b)
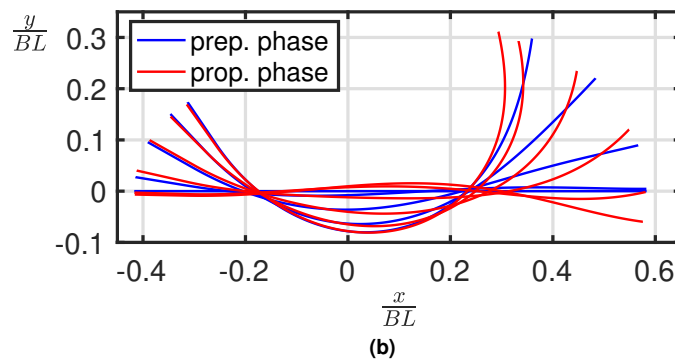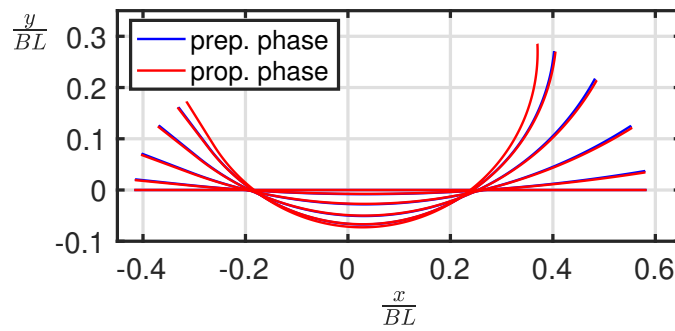
Figure S1. Midline envelope of the C-start deformation: (a) bending only and (b) bending plus traveling wave.
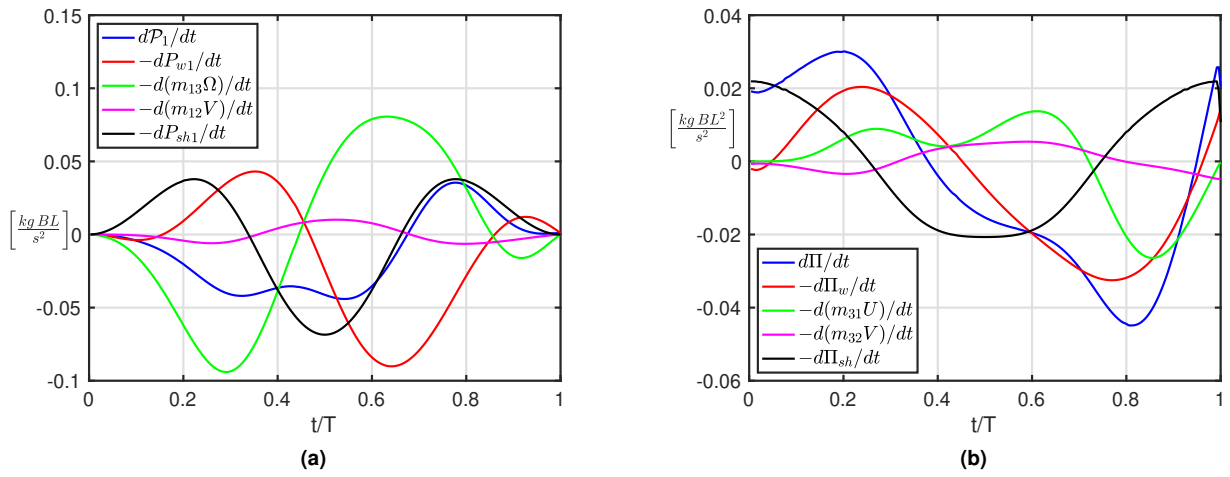
Additional Results

Figure S2. Time history of the impulses contributions for the C-start maneuver: (a) forward, (b) lateral and (c) angular direction. The blue and red curves in fig.S2a and fig.S2c, appearing also in fig.3a and fig.3b, are here compared with all the other impulse contributions not in the main text. It is worth to notice the large impact of the green curve in fig.S2a representing the momentum transfer from the angular to the forward direction discussed in the main text. With regard to the lateral impulses reported in fig.S2b, they are not mentioned in the main text due to the relatively small importance of the lateral velocity for the maneuver.
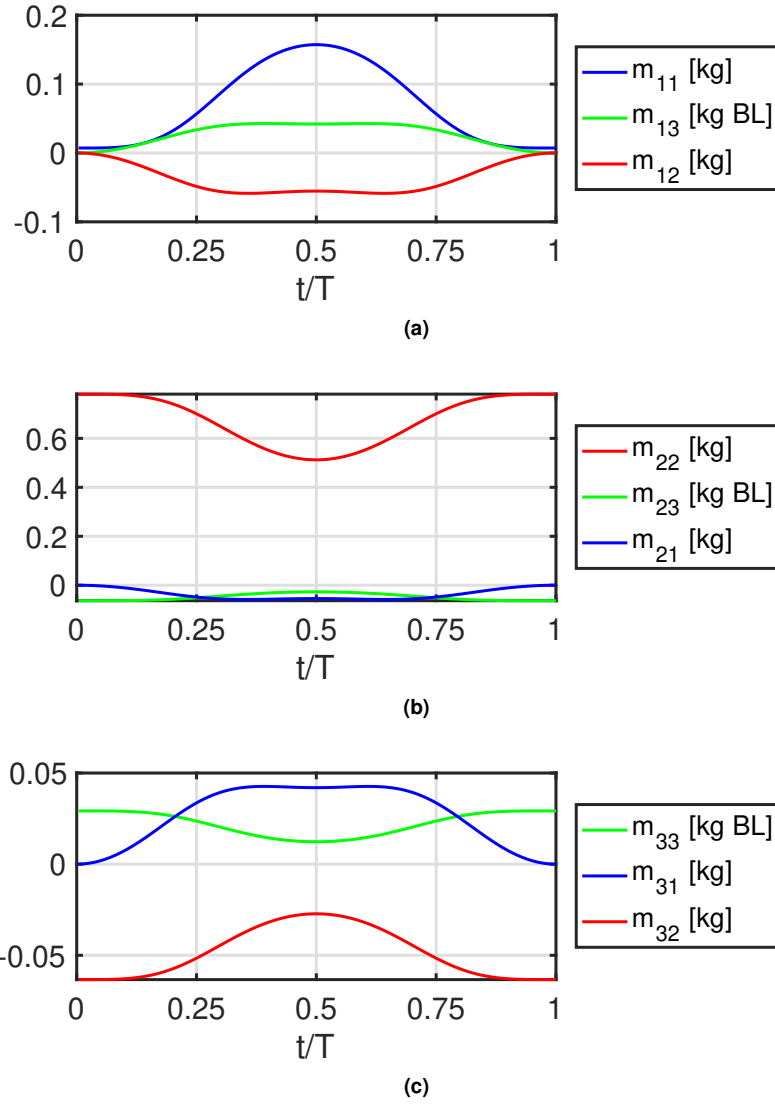
Figure S3. Time history of the added mass coefficients m_{ij} for the C-start maneuver governed by eq.(12) in the main text: (a) added mass coefficients m_{1j} appearing in the equation along the forward direction, (b) added mass coefficients m_{2j} appearing in the equation along the lateral direction and (c) added mass coefficients m_{3j} appearing in the equation along the angular direction. Notice the very large added mass coefficient m_{22} leading to a very small lateral velocity as reported in the main text.

Figure S4. Splitting of the time derivative of (a) the total forward impulse term $\mathscr{P}_1$ and (b) the total angular impulse term Π.
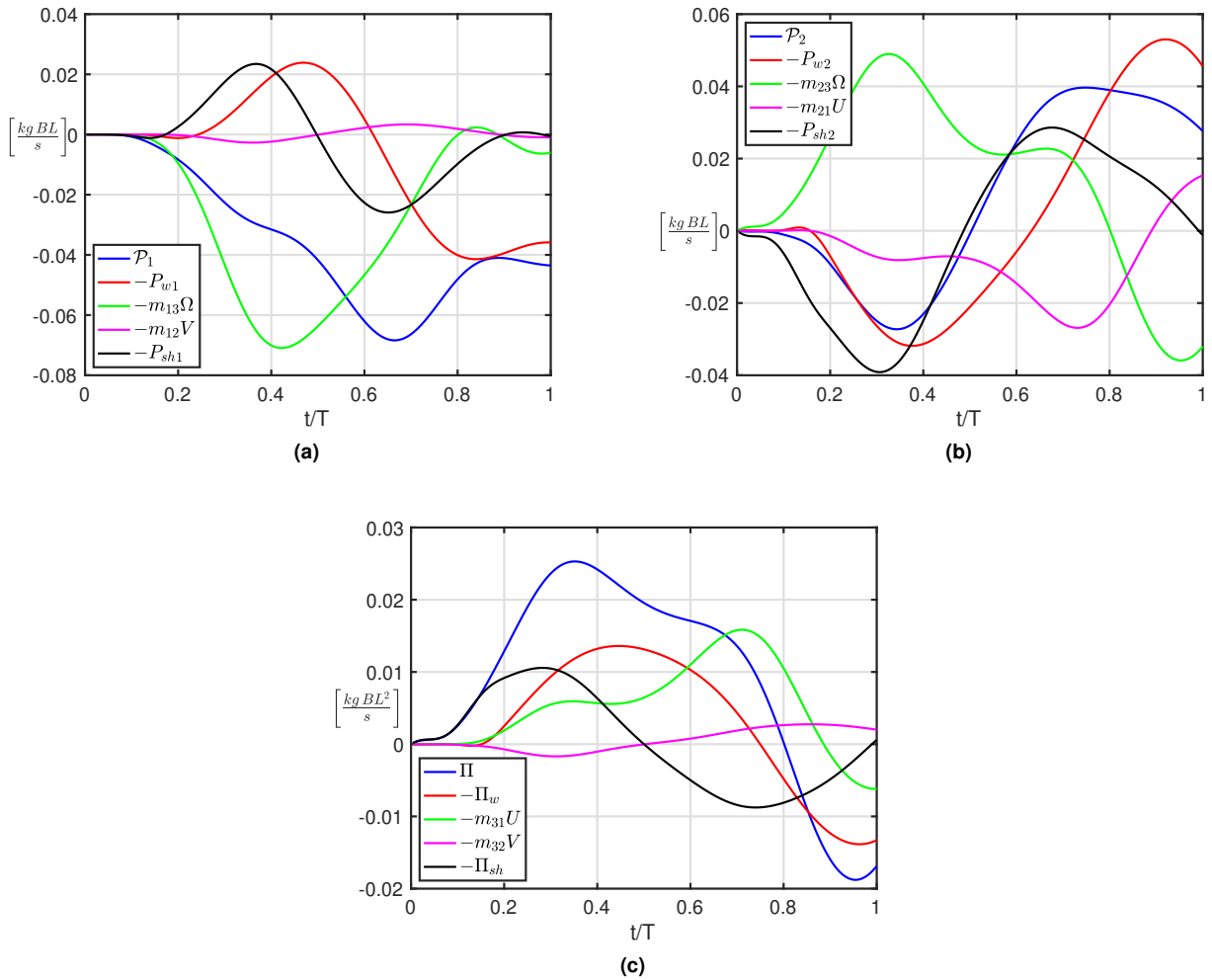
Figure S5. Time history of the impulses contributions for the C-start maneuver in presence of a traveling wave: (a) forward, (b) lateral and (c) angular direction. The curves are very similar to the ones in the absence of a traveling wave despite a certain increase in their absolute value may be appreciated.
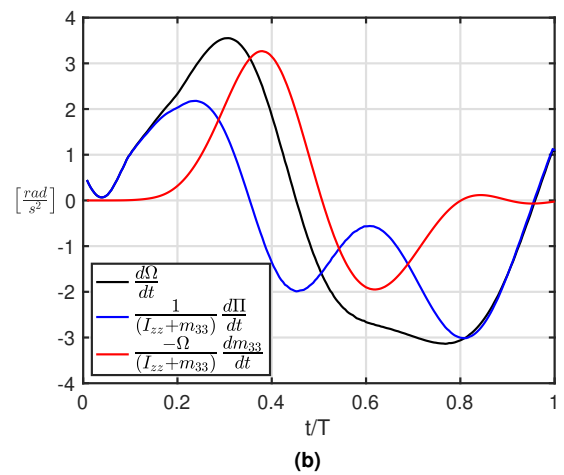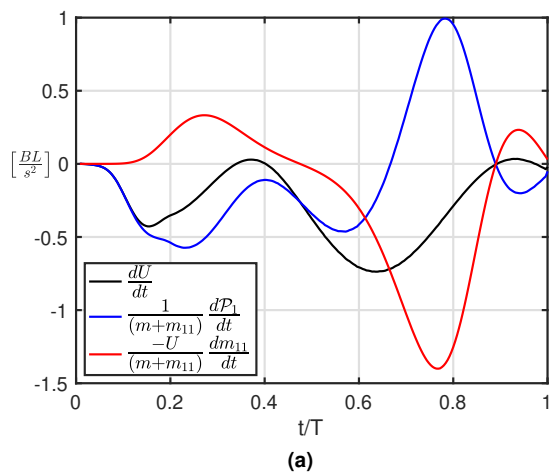
Figure S6. Time history of (a) the forward and (b) the angular acceleration contributions. The curves are very similar to the ones in the absence of a traveling wave despite a certain increase in their absolute value may be appreciated.

Supplementary Video Legends

Movie S1 Animation of the C-start maneuver for a neutrally buoyant fish from the numerical simulation.

Movie S2 Animation of the C-start maneuver with the addition of a traveling wave for a neutrally buoyant fish from the numerical simulation.

References

1. Jayne, B. & Lauder, G. Red and white muscle activity and kinematics of the escape response of bluegill sunfish during swimming. *J. Comp. Physiol. A* **173**, 495–508 (1993).

2. Wakeling, J. M. & Johnston, I. A. Muscle power output limits fast-start performance in fish. *J. Exp. Biol.* **201**, 1505–1526 (1998).

3. Wakeling, J. M. & Johnston, I. A. Body bending during fast-starts in fish can be explained in terms of muscle torque and hydrodynamic resistance. *J. Exp. Biol.* **202**, 675–682 (1999).

4. Liu, G., Yu, Y. L. & Tong, B. G. Flow control by means of a traveling curvature wave in fishlike escape responses. *Phys. Rev. E* **84**, 056312 (2011).

5. Paniccia, D., Graziani, G., Lugni, C. & Piva, R. On the role of added mass and vorticity release for self propelled aquatic locomotion. *J. Fluid Mech.* **918**, A45, DOI: 10.1017/jfm.2021.375 (2021).